

# Linking Across Data Granularity: Fitting Multivariate Hawkes Processes to Partially Interval-Censored Data

Pio Calderon, Alexander Soen, Marian-Andrei Rizoiu

**Abstract**—The multivariate Hawkes process (MHP) is widely used for analyzing data streams that interact with each other, where events generate new events within their own dimension (via self-excitation) or across different dimensions (via cross-excitation). However, in certain applications, the timestamps of individual events in some dimensions are unobservable, and only event counts within intervals are known, referred to as partially interval-censored data. The MHP is unsuitable for handling such data since its estimation requires event timestamps. In this study, we introduce the Partially Censored Multivariate Hawkes Process (PCMHP), a novel point process which shares parameter equivalence with the MHP and can effectively model both timestamped and interval-censored data. We demonstrate the capabilities of the PCMHP using synthetic and real-world datasets. Firstly, we illustrate that the PCMHP can approximate MHP parameters and recover the spectral radius using synthetic event histories. Next, we assess the performance of the PCMHP in predicting YouTube popularity and find that the PCMHP outperforms the popularity estimation algorithm Hawkes Intensity Process (HIP) [1]. Comparing with the fully interval-censored HIP, we show that the PCMHP improves prediction performance by accounting for point process dimensions, particularly when there exist significant cross-dimension interactions. Lastly, we leverage the PCMHP to gain qualitative insights from a dataset comprising daily COVID-19 case counts from multiple countries and COVID-19-related news articles. By clustering the PCMHP-modeled countries, we unveil hidden interaction patterns between occurrences of COVID-19 cases and news reporting.

**Index Terms**—temporal point process, partially observed data, popularity prediction.

## I. INTRODUCTION

THE Hawkes process, introduced by [2], is a temporal point process that exhibits the *self-exciting* property, *i.e.*, the occurrence of one event increases the likelihood of future events. The Hawkes process is widely applied in both the physical and social sciences. For example, earthquakes are known to be temporally clustered: the mainshock is often the first in a sequence of subsequent aftershocks. In online social media, tweets by influential users typically induce cascades of retweets as the message diffuses over the social network [3]. The multivariate Hawkes process (MHP) [2] extends the univariate process by allowing events to occur in multiple parallel timelines — dubbed as *dimensions*. These dimensions interact via *cross-excitation*, *i.e.*, events in one dimension can spawn events in the other dimensions. Fig. 1 schematically exemplifies the interaction between two social media platforms:

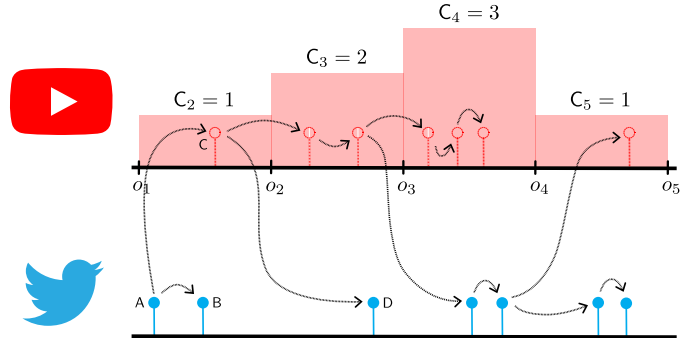


Fig. 1. **Example of multi-platform interaction** between view events on YouTube (red lollipops) and tweets on Twitter (blue lollipops). The data is partially interval-censored, as YouTube does not expose individual views, but only the view counts  $C_i$ 's over the predefined intervals  $[o_i, o_{i+1})$  (shown as red rectangles). The dashed lines show the latent branching structure between views and tweets. The red lollipops are also dashed and empty, indicating that YouTube views are not observed.

YouTube and Twitter. An initial tweet (denoted as A on the figure) spawns a retweet (B) via self-excitation and a view (C) via cross-excitation. The cross-excitation goes both ways: the view C generates the tweet D.

Given the event timestamps, we can fit the parameters of the Hawkes process using maximum likelihood estimation (MLE). However, in many practical applications, the event times are not observed, and only counts over predefined time partitions are available. We denote such data as *interval-censored*. For multivariate data, we denote the case when all dimensions are interval-censored as *completely interval-censored*. If only a subset of dimensions is interval-censored, we have *partially interval-censored* data.

One reason for interval-censoring is data availability — for epidemic data [4], we usually observe the aggregated daily counts of reported cases instead of detailed case information. Another reason is space limitations — for network traffic data [5], storing high-resolution event logs is impractical; they are stored as summaries over bins instead. A third reason is data privacy. This is the case for YouTube, as shown in the upper half of Fig. 1, where the individual views are interval-censored, and we only observe aggregated daily counts.

This paper tackles three open questions about using the MHP with partially interval-censored data. The first question relates to fitting the process to both event time and interval-censored data. When the data is presented as event times, the MHP can be fitted using MLE [6]. However, if the data

Pio Calderon and Marian-Andrei Rizoiu are with the University of Technology Sydney

Alexander Soen is with the Australian National University.

is partially or completely interval-censored, MLE cannot fit the MHP process parameters because it lacks the independent increments property [7]. Given interval-censored counts, one could approach fitting the Hawkes process naively by sampling event times uniformly over the intervals [8]. However, this quickly hits scalability issues for high interval-censored counts. For instance, the Youtube videos in our real-world dataset often have millions of views per day. For completely interval-censored univariate data, [7] proposed the Mean Behavior Poisson (MBP) — an inhomogeneous Poisson process that approximates the mean behavior of the Hawkes process — to estimate the parameters of a corresponding Hawkes process. However, a model and fitting scheme remained elusive for the partially interval-censored data. The question is, **can we devise a method to fit the MHP in the partially interval-censored setting? What are the limits to MHP parameter recovery in the partially interval-censored setting?**

The second question relates to modeling and forecasting online popularity across social media platform boundaries. Online popularity has been extensively studied within the realm of a single social media platform — see Twitter [9]–[12], YouTube [1], [13], Reddit [14] — and the self-exciting point processes are the tool of choice for modeling. However, content is often shared across multiple interacting platforms — such as YouTube and Twitter — and we need to account for cross-excitation using multivariate processes. However, YouTube only exposes view data as interval-censored, rendering it impossible to use the classical MHP. The Hawkes Intensity process (HIP) [1] proposes a workaround and treats the tweet and share counts as external stimuli for views. Its shortcoming is that it cannot model the cross-excitation from views to tweets and shares. The question is, **can we improve performance in the YouTube popularity prediction task by modeling the views, tweets, and shares through fitting on partially interval-censored data?**

The third question concerns analyzing interaction patterns across the online and offline environments, enabling us, for example, to determine whether online activity preempts or reacts to events that happen offline. Previous work has demonstrated the complex link between news and infectious disease outbreaks, notably the 2009 A/H1N1 outbreak in the Shaanxi province in China [15], the 2010 cholera outbreak in Haiti [16], and the early spread of COVID in 2020 in various provinces in China [17]. The association between media and case counts has typically been investigated by examining the cross-correlation of the news counts and case counts as paired time series and demonstrating that significant correlations exist when temporal lags are applied. [15], [17] show correlations between news and cases for both positive and negative lags, suggesting that news both had an impact and had been impacted by reported disease counts. [16] show that news typically lags behind cases; they also showcase how news counts can be used as a proxy for estimating crucial disease measures such as the basic reproduction number  $R_0$ . This highlights that the connection between news and cases is particularly relevant given that news counts can be retrieved in near real-time; in contrast, official case counts reporting is often lagging. In most previous work, uncovering time-series

cross-correlation is the focus, without building explanatory models to produce nuanced views of the interactions through interpretable parameters. The question is, **can we apply MHP on partially interval-censored data to uncover country-level differences in the interplay between recorded daily case counts of COVID-19 and the publication of COVID-19-related news articles?**

We address these three questions by introducing the Partially Censored Multivariate Hawkes Process (PCMHP)<sup>1</sup>, a novel multivariate temporal point process that operates on partially interval-censored data. We answer the first question in Section II-B, where we detail the PCMHP. The event intensity of PCMHP on the interval-censored dimensions is determined by the expected Hawkes intensity, considering the stochastic history of those dimensions conditioned on the event time dimensions. On the event time dimensions, the intensity of PCMHP corresponds to that of the respective Hawkes process. This construction allows us to fit the PCMHP to partially interval-censored data and estimate the parameters of the multivariate Hawkes process through parameter equivalence.

We address the second question in Section IV by using PCMHP to predict the popularity of YouTube videos on both YouTube and Twitter. We demonstrate that PCMHP consistently outperforms the related HIP method [1], provides quantification of prediction uncertainty and extends predictions to all dimensions — unlike HIP, which can only predict the views' dimension.

We address the third question in Section V by utilizing PCMHP to investigate the relationship between COVID-19 case incidence and news coverage. We fit a country-specific PCMHP for each of the 11 countries using a dataset consisting of reported COVID-19 cases (with interval-censored data) and the publication dates of COVID-19-related news articles during the early stage of the outbreak. We identify three distinct groupings by clustering countries using the fitted PCMHP parameters. In the first group (UK, Spain, Germany, and Brazil), we observe preemptive news coverage, where an increase in news leads to a rise in cases. The second group (China and France) exhibits reactionary news coverage, with news lagging behind the cases. No significant interaction between news and cases is found in the third group (US, Italy, Sweden, India, and the Philippines).

#### A. Related Work

A significant portion of recent literature on the Hawkes process, and on point processes in general, deals with estimation from partially observed data. This problem is nontrivial as standard MLE techniques require the complete dataset.

It was shown in [18] that a sequence of (integer-valued autoregressive time series) INAR( $\infty$ )-based family of point processes converges to the Hawkes process. Under this convergence, they concluded that the INAR( $\infty$ ) is the discrete-time version of the Hawkes process. In a follow-up, [19] presented an alternative procedure to MLE, which fits the associated bin-count sequences to the INAR( $p$ ) process. As

<sup>1</sup>Implementation available at [https://github.com/behavioral-ds/pmbp\\_implementation](https://github.com/behavioral-ds/pmbp_implementation).

the bin size goes to zero and the order  $p$  of the process goes to  $\infty$ , the INAR sequence converges to the Hawkes process and the parameter estimates converge to the Hawkes parameters. However, though fitting is performed on count data, convergence only actually occurs for small bin size.

A spectral approach to fitting the Hawkes process given interval-censored data for arbitrary bin size is presented in [20], solving the issue in [19]. Their proposed method is based on minimizing the log-spectral likelihood of the bin-count sequence instead of the usual log-likelihood of the Hawkes process. They showed that optimization converges to the Hawkes parameters under certain assumptions on the kernel.

The sample-based Monte Carlo Expectation Maximization (MC-EM) algorithm was introduced in [5] and [21] for the univariate and multivariate cases, respectively, which uses sampling to obtain proposals for the hidden event times. They showed that their approach recovers parameters more reliably than the INAR(p) estimates from [19] in synthetic experiments. Another sample-based approach, the recursive identification with sample correction (RISC) algorithm, was introduced in [22], where synthetic sample paths are iteratively generated and corrected to match the observed bin counts. Reliance on sampling makes these approaches more computationally expensive than the others.

Several modifications have been proposed to estimate the Hawkes process from daily count data in the context of modeling the spread of COVID [23]. A Hawkes process incorporating spatio-temporal covariates was estimated using an EM algorithm in [24], while the least-squares approach was utilized in [25] to model state-level differences in transmission rates in the U.S.. A discrete-time Hawkes process for country-level COVID transmission was introduced in [4] and fit using Bayesian inference.

The notion of interval-censored data is also used in other fields, most prominently in the study of time-to-event (failure time) data [26]–[28]. In these works, ‘interval-censored’ refers to situations where the precise time of an event of interest in an observational study is unknown; instead, we only know that it occurred within a certain window or follow-up period [29]. Meanwhile ‘partly interval-censored’ refers to situations where some failure times are exactly observed while others are only known to lie within certain intervals [30]. This data type is prevalent in health and clinical research [31], where exact event times may not be directly observable due to the nature of study designs. Contrary to this, our work adopts the definition of ‘interval-censored’ as outlined in [7], [32], where event times are inaccessible and we instead observe event counts over predefined time intervals, as exemplified by Youtube views in Fig. 1. Furthermore, in this work, we define partial censoring of a multivariate process as the censoring of specific dimensions, with the rest being observed as point processes.

## II. MODEL

For convenience, the list of notation that we use in this work is provided in Table I.

TABLE I  
IMPORTANT NOTATION USED IN THIS PAPER.

Symbol	Meaning
$\alpha$	Hawkes branching matrix
$\rho(\alpha)$	spectral radius of $\alpha$
$f^{ij}(t)$	exponential kernel from dimension $j$ to $i$
$\theta$	exponential kernel decay parameter matrix
$\mu(t)$	deterministic background intensity
$\varphi(t)$	Hawkes kernel, where $\varphi^{ij}(t) = \alpha^{ij} f^{ij}(t)$
$\lambda(t)$	MHP conditional intensity
$\xi(t)$	MBP conditional intensity
$D$	overall set of dimensions for PCMHP ( $d, e$ )
$E$	set of MBP dimensions for PCMHP ( $d, e$ )
$E^c$	set of Hawkes dimensions for PCMHP ( $d, e$ )
$\mathcal{H}_{t-}^j$	event sequence history on dimension $j \in D$
$\mathcal{H}_{t-}^A$	union of event sequence histories on $A \subset D$
$\xi_E(t)$	conditional intensity for PCMHP ( $d, e$ )
$\Xi_E(t)$	compensator for PCMHP ( $d, e$ )
$\Theta$	parameter set for PCMHP ( $d, e$ )
$T$	terminal time
$\mathcal{L}(\Theta; T)$	log-likelihood function for PCMHP ( $d, e$ )
$\mathcal{L}_\Theta(\Theta; T)$	gradient of log-likelihood function for PCMHP ( $d, e$ )
$\Delta^P$	time axis partition length for numerical convolution
$\gamma^h$	convergence threshold for infinite sum truncation

### A. Background

A temporal point process can be specified by its conditional intensity function. In this work, we consider *simple point processes*, where no two events can occur simultaneously. Let  $\mathbf{N}(t)$  represent the number of events that occurred up until time  $t$  and  $\mathcal{H}_{t-}^j$  be the set of all events that occur in dimension  $j$  up until  $t$ , for  $j \in \{1, \dots, d\}$ . We further denote the union of all history dimensions as  $\mathcal{H}_{t-} := \bigcup_{j=1}^d \mathcal{H}_{t-}^j$ . The  $d$ -dimensional conditional intensity function  $\lambda(t | \mathcal{H}_{t-})$  is defined as

$$\lambda^j(t | \mathcal{H}_{t-}) = \lim_{h \rightarrow 0^+} \frac{1}{h} \mathbb{P} \{ N^j(t+h) - N^j(t) = 1 \mid \mathcal{H}_{t-} \},$$

which gives the instantaneous probability of a dimension  $j$  event occurring in the increment  $[t, t+dt)$ , conditioned on all events that happen before  $t$ . For brevity and whenever it is clear from context, we drop the explicit conditioning on the history  $\mathcal{H}_{t-}$  and write  $\lambda(t) := \lambda(t | \mathcal{H}_{t-})$ .

**Hawkes Process:** The univariate Hawkes process is a type of temporal point process that models a sequence of events on a single dimension exhibiting a *self-exciting* behavior. Given  $d$  types of events, the corresponding  $d$ -dimensional multivariate Hawkes process (MHP) is a point process where each dimension tracks the dynamics of each event type. In addition to being self-exciting, the MHP is *cross-exciting* among event types, *i.e.*, an event occurring in one type of event increases the probability of any type of event occurring in the near future. The conditional intensity of the  $d$ -dimensional Hawkes process is given by

$$\lambda(t) := \mu(t) + \sum_{j=1}^d \sum_{t_k^j \in \mathcal{H}_{t-}^j} \varphi^j(t - t_k^j), \quad (1)$$

where  $\mu(t)$  is the (deterministic) background intensity, a  $d$ -dimensional non-negative vector for each  $t$  controlling the arrival of external events into the system. The matrix  $\varphi(t)$  is called the Hawkes kernel, a  $d \times d$  matrix of functions that

characterizes the self- and cross-excitation across the event types representing the  $d$  dimensions. Let  $\varphi^j(t)$  represent the  $j^{\text{th}}$  column of the Hawkes kernel. The diagonal entries  $\varphi^{jj}(t)$  and off-diagonal entries  $\varphi^{ij}(t)$ ,  $i \neq j$ , represent the self- and cross-exciting components of the Hawkes kernel, respectively. Note that the Hawkes intensity  $\lambda(t)$  defined in Eq. (1) is a stochastic function dependent on the history of any particular realization  $\mathcal{H}_{t-}$ . Given a fixed  $\mathcal{H}_{t-}$ , the intensity before or equal to  $t$  is deterministically calculated using Eq. (1). On the other hand, the intensity is a random variable for any time greater than  $t$  or if the history  $\mathcal{H}_{t-}$  itself is not observable, such as in the case of interval censoring.

The Hawkes kernel is often specified in a parametric form to facilitate simple interpretability. Let  $D$  denote the index set  $\{1, \dots, d\}$ . If we assume  $\varphi^{ij}(t) = \alpha^{ij} f^{ij}(t)$ ,  $\alpha^{ij} \geq 0$ ,  $f^{ij}(t) \geq 0$ , and  $\int_0^\infty f^{ij}(t) dt = 1$  for  $(i, j) \in D \times D$ . We call  $\alpha^{ij}$  the branching factor from  $j$  to  $i$  and the matrix  $\alpha = (\alpha^{ij}) \in (\mathbb{R}^+)^{d \times d}$  the branching matrix. The branching factor  $\alpha^{ij}$  gives the expected number of offspring events in dimension  $i$  that are triggered by an event in dimension  $j$ . The function  $f^{ij}(t)$  is typically selected to be monotonically decreasing to model the empirically observed decay in the attention that online content receives over time [13]. This is explained by viewing human attention as a limited resource that online content competes for, resulting in content being forgotten over time. In this work we consider the widely used exponential kernel [7], [11], [33], which takes the form  $\varphi^{ij}(t) = \alpha^{ij} \theta^{ij} \exp(-\theta^{ij} t)$ , where  $\theta^{ij}$  controls the rate of influence decay from  $j$  to  $i$ . We choose the exponential kernel due to its simplicity, enabling efficient computation of the intensity due to its Markovian property [34], efficient sampling [35], and strong theoretical properties, as evidenced by its link to the stochastic SIR model [36]. An alternative choice of kernel is the power law, which, while yielding better model likelihood, requires significantly more time to fit and presents a more challenging estimation due to the need to fit two parameters. More prerequisite details on the MHP are provided in Sec. 1.1 of the SI [37].

**Mean Behavior Poisson Process [7]:** Consider a univariate Hawkes process with conditional intensity  $\lambda(t)$ . The Mean Behavior Poisson (MBP) process introduced by [7] is the inhomogeneous Poisson process with conditional intensity

$$\xi(t) := \mathbb{E}_{\mathcal{H}_{t-}} [\lambda(t)]. \quad (2)$$

In contrast to the stochastic Hawkes intensity  $\lambda(t|\mathcal{H}_{t-})$ , the MBP intensity  $\xi(t)$  is a deterministic function obtained by taking the expectation of the Hawkes intensity over all possible realizations  $\{\mathcal{H}_{t-}\}$ . It was shown in [7] that  $\xi(t)$  follows the self-consistent equation

$$\xi(t) = \mu(t) + (\varphi * \xi)(t), \quad (3)$$

where  $*$  denotes convolution. Furthermore, the mapping  $\mu(t) \mapsto \xi(t)$  in Eq. (3) defines a linear time-invariant (LTI) system [38], meaning that it obeys linearity ( $\mu_1(t) \mapsto \xi_1(t)$  and  $\mu_2(t) \mapsto \xi_2(t)$  imply that  $a\mu_1(t) + b\mu_2(t) \mapsto a\xi_1(t) + b\xi_2(t)$  for  $a, b \in \mathbb{R}$ ) and time invariance ( $\mu(t) \mapsto \xi(t)$  implies that  $\mu(t - t_0) \mapsto \xi(t - t_0)$  for  $t_0 > 0$ .) As an LTI system, the response  $\xi(t)$  to the input  $\mu(t)$  can be obtained by solving for

the response of the system to the Dirac impulse  $\delta(t)$ , derived in [7] to be

$$\xi(t) = \left( \delta(t) + \sum_{n=1}^{\infty} \varphi^{\otimes n}(t) \right) * \mu(t), \quad (4)$$

where  $\otimes n$  corresponds to  $n$ -time self-convolution.

Since the MBP process is a Poisson process, its increments are independent, which allows the likelihood function to be expressed as a sum of the likelihood of disjoint Poisson distributions. This enables the MBP process to be fitted in interval-censored settings via MLE. More prerequisite details are provided in Sec. 1.2 of the SI [37].

**Hawkes Intensity Process [1]:** The Hawkes intensity process (HIP), introduced in [1], is a temporal point process that can be fit to interval-censored data. It was used primarily for YouTube popularity prediction, where YouTube video views are daily-censored, and external shares and tweets that mention the video act as the exogenous intensity  $\mu(t)$ .

Given a partition  $\mathcal{P}[0, T) = \bigcup_{k=1}^m [o_{k-1}, o_k)$ , where  $o_0 = 0$  and  $o_m = T$ , and the associated view counts  $\{C_k\}_{k=1}^m$ , the HIP model  $\hat{\xi}[\cdot; \Theta]$  is fitted by finding the parameter set  $\Theta$  that minimizes the sum of squares error  $\sum_{k=1}^m (C_k - \hat{\xi}[o_k; \Theta])^2$  of the following recursive formula for  $\hat{\xi}[o_k; \Theta]$ ,

$$\hat{\xi}[o_k; \Theta] = \mu[o_k] + \sum_{s=0}^{k-1} \varphi(o_k - o_s; \Theta) \cdot \hat{\xi}[o_s; \Theta].$$

The use of brackets emphasizes that the quantities are discretized over a partition of time. It was shown in [7, Theorem 10] that HIP is a discretized approximation of the MBP process, where an implicit assumption that the observation intervals being unit length is reflected in the sum of squares error, *i.e.*,  $\hat{\xi}[o_k; \Theta] \cdot (o_k - o_{k-1})$  is approximated as  $\hat{\xi}[o_k; \Theta]$ .

### B. Partially Censored Multivariate Hawkes Process

We define the Partially Censored Multivariate Hawkes Process PCMHP( $d, e$ ) with intensity  $\xi_E(t)$  as follows. A key idea of the PCMHP( $d, e$ ) is to fix the history of different dimensions. As such we denote the history union over a subset of dimensions  $A \subset \{1 \dots d\}$  as  $\mathcal{H}_{t-}^A := \bigcup_{j \in A} \mathcal{H}_{t-}^j$ .

**Definition 1** Consider a  $d$ -dimensional Hawkes process with conditional intensity  $\lambda(t)$  as defined in Eq. (1). Given a nonnegative integer  $e \leq d$  and the index sets  $D := \{1, \dots, d\}$ ,  $E := \{1, \dots, e\}$  and  $E^c := \{e + 1, \dots, d\}$ , the Partially Censored Multivariate Hawkes Process PCMHP( $d, e$ ) is the temporal point process whose conditional intensity  $\xi_E(t)$  is the expectation of  $\lambda(t)$  conditioned on the set of event histories  $\mathcal{H}_{t-}^{E^c}$  in the  $E^c$  dimensions and averaged over the set of event histories  $\mathcal{H}_{t-}^E$  in the  $E$  dimensions. That is,

$$\xi_E(t) := \xi \left( t \mid \mathcal{H}_{t-}^{E^c} \right) = \mathbb{E}_{\mathcal{H}_{t-}^E} \left[ \lambda(t) \mid \mathcal{H}_{t-}^{E^c} \right]. \quad (5)$$

The PCMHP( $d, e$ ) intensity is a stochastic function due to its dependence on the current realization of  $\mathcal{H}_{t-}^{E^c}$ ; on the  $E$  dimensions we take the expectation over all possible realizations of  $\mathcal{H}_{t-}^E$ , similar to the MBP intensity in Eq. (2).

In practice,  $E$  would be chosen to be the set of dimensions where event times are inaccessible and only interval-censored event counts can be obtained, while  $E^c$  would be the dimensions with event time information. In Fig. 1 for instance  $E$  would be YouTube views and  $E^c$  the set of tweets.

**Is the PCMHP  $(d, e)$  Poisson?** Due to its dependence on the history of the  $E^c$  dimensions, the PCMHP  $(d, e)$  is not a Poisson process. From Eq. (5), the PCMHP  $(d, e)$  can be interpreted as a collection of  $d$  processes, where  $\xi_E^j(t)$  follows a Hawkes process for  $j \in E^c$  and follows an inhomogeneous Poisson process (conditional on the event history of the  $E^c$  dimensions) for  $j \in E$ . In fact, the PCMHP  $(d, e)$  generalizes both the MHP (by setting  $e = 0$ ) and the MBP process (by setting  $e = d$ ).

**Convolutional Formula:** Consider the kernel  $\varphi(t) = [\varphi^1(t) \dots \varphi^e(t) \varphi^{e+1}(t) \dots \varphi^d(t)]$ , setting  $\varphi^j(t)$  to be the  $j^{\text{th}}$  column of  $\varphi(t)$ .

Similarly, let  $\varphi_E(t) = [\varphi^1(t) \dots \varphi^e(t) \ 0 \dots 0]$  and  $\varphi_{E^c}(t) = [0 \dots 0 \ \varphi^{e+1}(t) \dots \varphi^d(t)]$ .

Similar to MBP,  $\xi_E(t)$  can be expressed as the response of an LTI system, which allows us to express  $\xi_E(t)$  as a convolution with the Dirac impulse  $\delta(t)$ .

**Theorem 2** *Given the Hawkes process with intensity Eq. (1) and kernel parameters satisfying  $\lim_{n \rightarrow \infty} \varphi_E^{\otimes n}(t) = 0$ , the conditional intensity of the PCMHP  $(d, e)$  is*

$$\xi_E(t) = \left[ \delta(t) + \sum_{n=1}^{\infty} \varphi_E^{\otimes n}(t) \right] * \left[ \mu(t) + \sum_{j \in E^c} \sum_{t_k^j < t} \varphi_{E^c}^j(t - t_k^j) \right] \quad (6)$$

In general,  $\xi_E(t)$  does not admit a closed form solution because of the complexity of the infinite convolution sum of  $\varphi_E(t)$  (an interpretation of which is provided in Sec. 2 of the SI [37]). However, in the special case of PCMHP(2,1) with the exponential kernel, a closed-form solution for  $\xi_E(t)$  exists, as proven in Sec. 3 of the SI.

**Regularity Conditions:** Imposing regularity conditions on the model parameters ensure process *subcriticality*, i.e. the expected number of direct and indirect offspring spawned by a single parent is finite. For instance, an MHP is subcritical if the spectral radius  $\rho$  (i.e. magnitude of the largest eigenvalue) of the branching matrix is less than one, i.e.  $\rho(\alpha) < 1$  [39]. Here we introduce the regularity conditions applicable for the PCMHP  $(d, e)$ .

Consider the following submatrices of  $\alpha$ :

$$\begin{aligned} \alpha^{EE} &= (\alpha^{ij})_{(i,j) \in E \times E}, & \alpha^{EE^c} &= (\alpha^{ij})_{(i,j) \in E \times E^c}, \\ \alpha^{E^cE} &= (\alpha^{ij})_{(i,j) \in E^c \times E}, & \alpha^{E^cE^c} &= (\alpha^{ij})_{(i,j) \in E^c \times E^c}. \end{aligned}$$

The following are three conditions which ensure subcriticality of PCMHP  $(d, e)$ .

**Theorem 3** *The PCMHP  $(d, e)$  with branching matrix  $\alpha$  is subcritical if the following conditions hold.*

$$\rho(\alpha^{EE}) < 1, \rho(\alpha^{E^cE^c}) < 1, \rho(\alpha^{E^cE}(\mathbf{I} - \alpha^{EE})^{-1}\alpha^{EE^c}) < 1.$$

We note that the regularity conditions for PCMHP  $(d, e)$  in Theorem 3 cover the MHP and the MBP as special cases.

Proofs of Theorem 2 and Theorem 3 and a discussion on the nonlinear extension of the PCMHP are provided in Sec. 4 of the SI [37].

### C. Inference

We now consider the problem of estimating the PCMHP parameter set  $\Theta$  given a partially interval-censored dataset consisting of interval-censored data on a subset of dimensions and exact event sequences on the other dimensions. Assuming a constant exogenous term  $\mu(t) = \nu$ , the PCMHP  $(d, e)$  parameter set to be estimated is given by  $\Theta = \{\nu, \alpha, \theta\}$  with size  $|\Theta| = d + 2 \cdot d^2$ .

Consider a  $d$ -dimensional dataset over the time interval  $[0, T)$  such that observations in the first  $q$  dimensions are interval-censored, and in the last  $d-q$  dimensions, we observe event times. Formally, let  $Q := \{1, \dots, q\}$  and  $Q^c := \{q+1, \dots, d\}$ . For  $j \in Q$ , we associate a set of observation points  $\sigma_0^j < \sigma_1^j < \dots < \sigma_{n_j}^j$  such that for  $\sigma_k^j$  where  $k \geq 1$ , we observe the volume  $C_k^j$  of dimension  $j$  events that occurred during the interval  $[\sigma_{k-1}^j, \sigma_k^j)$ . Meanwhile, for  $j \in Q^c$ , we observe event sequences  $\mathcal{H}_{T-}^j = \{t_1^j < t_2^j < \dots < t_{n_j}^j\}$ . In practice, the observation partition  $\bigcup_{j \in Q} \bigcup_{k=1}^{n_j} [\sigma_{k-1}^j, \sigma_k^j)$  is not a model hyperparameter but is determined by real-world dataset availability constraints. For instance, in Fig. 1 we consider a daily partitioning for Youtube views since our dataset consists of aggregated daily view counts.

We use MLE to fit the parameters of a PCMHP  $(d, e)$  process to the above-defined data using the log-likelihood function derived below. The proof is available in Sec. 5 of the SI [37].

**Theorem 4** *Given event times  $\mathcal{H}_{T-}^{Q^c}$ , event volumes  $\bigcup_{j \in Q} \{C_k^j\}_{k=1}^{n_j}$ , and a PCMHP  $(d, e)$  model such that  $E \supseteq Q$ , the negative log-likelihood of parameter set  $\Theta$  can be written as*

$$\mathcal{L}(\Theta; T) = \sum_{j \in Q} \mathcal{L}_{\text{IC-LL}}^j(\Theta; T) + \sum_{j \in Q^c} \mathcal{L}_{\text{PP-LL}}^j(\Theta; T), \quad (7)$$

where

$$\mathcal{L}_{\text{IC-LL}}^j(\Theta; T) = \sum_{i=1}^{n_j} \left[ \Xi_E^j(\sigma_{i-1}^j, \sigma_i^j; \Theta) - C_i^j \log \Xi_E^j(\sigma_{i-1}^j, \sigma_i^j; \Theta) \right], \quad (8)$$

$$\mathcal{L}_{\text{PP-LL}}^j(\Theta; T) = - \sum_{t_k^j \in \mathcal{H}_{T-}^j} \log \xi_E^j(t_k^j; \Theta) + \Xi_E^j(T; \Theta), \quad (9)$$

and  $\Xi_E(t)$  represents the compensator, i.e., the intensity  $\xi_E(t)$  integrated over 0 to  $t$ .

**Choice of Likelihood:** The choice of likelihood on a given dimension  $j$  is solely dependent on the type of data on the said dimension. If  $j \in Q$  (dimension  $j$  is interval-censored), one should use  $\mathcal{L}_{\text{IC-LL}}^j(\Theta; T)$ ; if  $j \in Q^c$  (event-times) then  $\mathcal{L}_{\text{PP-LL}}^j(\Theta; T)$  should be used.

An event-time dimension ( $j \in Q^c$ ) can be modeled using either the Hawkes dynamics or the MBP dynamics. However, an interval-censored dimension ( $j \in Q$ ) can only be modeled

using MBP dynamics, as an interval-censored log-likelihood for the Hawkes dynamics does not exist. It follows that  $E \supseteq Q$ . In real-world applications, one would choose  $E = Q$  because any other choice  $E \supset Q$  leads to information loss due to the mismatch between the data generation model (*i.e.*, Hawkes) and the fitting model (MBP). We study the impact of model mismatch loss in Section III.

**Runtime Complexity:** Denote  $n^{E^c}$  and  $n^{Q^c}$  as the total number of observed event times in the  $E^c$  and  $Q^c$  dimensions, respectively; and  $n^E$  and  $n^Q$  as the total number of observation intervals in the  $E$  and  $Q$  dimensions, respectively. That is,  $n^{E^c} = \sum_{j \in E^c} |\mathcal{H}_{T^-}^j|$ ,  $n^{Q^c} = \sum_{j \in Q^c} |\mathcal{H}_{T^-}^j|$ ,  $n^E = \sum_{j \in E} n^j$ , and  $n^Q = \sum_{j \in Q} n^j$ . Let  $C$  denote a constant independent of the dimension of the PCMHP and the data. Evaluating  $\mathcal{L}(\Theta; T)$  has a runtime complexity of  $\mathcal{O}((C + n^{E^c}) \cdot (n^Q + n^{Q^c}))$  (see Sec. 5 of the SI [37] for more details). In the case  $E = Q = \emptyset$ , the runtime complexity reduces to  $\mathcal{O}((n^{E^c})^2)$ , consistent with the MHP. If  $E = Q = D$ , runtime complexity reduces to  $\mathcal{O}(n^E)$ , consistent with the MBP (*i.e.* Poisson) process.

**Numerical Considerations:** Due to the complexity of  $\sum_{n=1}^{\infty} \varphi_E^{\otimes n}(t)$  and its convolutions, a general closed-form expression for  $\xi_E(t)$  is not available, requiring us to leverage approximation techniques, *i.e.* numerical convolution and infinite series truncation, to compute  $\sum_{n=1}^{\infty} \varphi_E^{\otimes n}(t)$  and  $\xi_E(t)$ . The approximation error is controlled by two hyperparameters: (1)  $\Delta^P$ , the partition length of our time axis for the numerical convolution, and (2)  $\gamma^h$ , the max-norm convergence threshold to determine  $k^* \in \mathbb{N}$  to truncate the infinite sum, *i.e.*  $\sum_{n=1}^{k^*} \varphi_E^{\otimes n}(t) \approx \sum_{n=1}^{\infty} \varphi_E^{\otimes n}(t)$ . The smaller  $\Delta^P$  and  $\gamma^h$  are set, the tighter the approximation, albeit with a longer computation time. Full details and heuristics on hyperparameter choice are discussed in Sec. 7 of the SI [37]. We propose an alternative sampling-based technique to calculate  $\xi_E(t)$  that bypasses calculation of  $\sum_{n=1}^{\infty} \varphi_E^{\otimes n}(t)$  in Sec. 8 of the SI [37]. Finally, we demonstrate the convergence of the numerical and the sampling-based approximation techniques in Sec. 9 of the SI [37] by showing close agreement between the approximated  $\xi_E(t)$  and the closed-form  $\xi_E(t)$  of the exponential PCMHP (2,1) derived in Sec. 3 of the SI [37].

Gradient-based optimization tools – including IPOPT [40] that we use in our experiments in Section IV and Section V — usually require the gradient. To approximate  $\mathcal{L}(\Theta; T)$  and its gradient  $\mathcal{L}_{\Theta}(\Theta; T)$ , we propose a numerical scheme in Sec. 10 and 11 of the SI [37]. We show in the SI that the runtime complexity of the numerical scheme is mostly determined by how many dimensions we model as Hawkes and as MBP. Without any Hawkes dimensions ( $E^c = \emptyset$ ), the scheme scales linearly (similar to the MBP) with the number of observation intervals  $n^E$ , *i.e.*  $\mathcal{O}(n^E \cdot \lceil \frac{T}{\Delta^P} \rceil \cdot d \cdot e)$ . On the other hand, if  $E^c \neq \emptyset$ , the scheme scales quadratically (similar to the MHP) with the number of observed event times  $n^{E^c}$ , *i.e.*  $\mathcal{O}((n^E + n^{E^c} + \lceil \frac{T}{\Delta^P} \rceil) \cdot n^{E^c} \cdot d)$ . In both cases, the number of partition intervals  $\lceil \frac{T}{\Delta^P} \rceil$  only appears linearly. For partially interval-censored datasets with high frequency data, the number of observed event times  $n^{E^c}$  is the most important determinant of runtime complexity given that it appears quadratically, while the number of observation

intervals  $n^E$  and the number of partition intervals  $\lceil \frac{T}{\Delta^P} \rceil$  only appear linearly.

Lastly, for the purpose of sampling from the PCMHP ( $d, e$ ), we propose a modification of the thinning algorithm [34] detailed in Sec. 12 of the SI.

#### D. Heuristics for Partially Interval-Censored Data

The PCMHP is designed for cases where (1) the dataset is multivariate and partially interval-censored, and (2) we hypothesize events are self-exciting within and cross-exciting across dimensions. To handle partially interval-censored data, our strategy is to adapt the model (*i.e.* the PCMHP) to the data. However, we can take the reverse approach and apply heuristics to our dataset to be able to leverage pre-existing models.

- 1) To use *count-based time series models*, we transform our partially interval-censored dataset into a fully interval-censored dataset by censoring event times for each  $E^c$  dimension.
- 2) To use *point process models* (*i.e.* the MHP), we transform our partially interval-censored dataset into a fully time-stamped dataset by sampling event times to match the interval-censored counts, for each dimension in  $E$ .

There are three arguments against the first heuristic. First, artificially censoring the dataset leads to loss of timing information by hiding self- and cross-exciting interactions between events, particularly if the time scale of the interactions is less than the censor window length. Second, commonly used time series models (such as the Poisson autoregressive model [41] or the discrete-time Hawkes process [4]) assume evenly spaced data [42]. If the censor intervals within or across dimensions do not line up, we would need to perform further data alteration, such as interpolation [43], to attain evenly spaced data. The PCMHP does not require evenly spaced intervals. Third, using time series models on the artificially obtained interval-censored dataset requires additional model choices. For instance, we would have to set the censor window length for each dimension in  $E$  when transforming to a fully interval-censored dataset, and for autoregressive models decide up to what lag  $p$  to include. The PCMHP requires no adaptation as it was designed for partially interval-censored data.

The main deterrent against the second heuristic, artificial event sampling, is the significant addition to computation time, since evaluating the Hawkes likelihood is  $\mathcal{O}((n^{E^c})^2)$ . This is particularly infeasible in applications involving high event volumes, such as Youtube views on a viral video, which typically have view counts of the order  $10^6$  or more. If we use the PCMHP, these dimensions with high event volumes can be modeled as event counts and placed in  $E$  instead of  $E^c$ , significantly reducing computation time. Second, artificially sampling points — when only aggregated counts have been given — has the potential to produce spurious event interactions across dimensions, particularly for wide censor intervals.

### III. SYNTHETIC PARAMETER RECOVERY

In this section, we test on synthetic data the MHP parameter recovery by PCMHP( $d, e$ ). We use the setting of partial

interval-censoring with a constant exogenous term  $\mu(t) = \nu$ . We sample realizations from a  $d$ -dimensional MHP, interval-censor  $e$  dimensions using increasingly wide observation window lengths, and fit the PCMHP( $d, e$ ) model on the obtained partially interval-censored data. We inspect the recovery of parameters when varying  $d$  and  $e$ . We perform convergence analysis on the PCMHP( $d, e$ ) parameter estimates for various hyperparameter configurations in Sec. 14.2 of the SI [37],

Throughout this section, we refer to  $\{\alpha, \theta, \nu\}$  and  $\{\hat{\alpha}, \hat{\theta}, \hat{\nu}\}$  as the true (MHP) and estimated parameter sets, respectively. We first discuss the two types of information loss, then we introduce the synthetic datasets and the likelihood functions. Lastly, we present the recovery results for the individual parameters  $\{\alpha, \theta, \nu\}$ .

**Sources of Information Loss in Fitting:** We identify two sources of information loss when fitting in the partially interval-censored setup: (1) the mismatch between the data-generation model (*i.e.*, the  $d$ -dimensional MHP) and the fitting model (the PCMHP( $d, e$ )); and (2) the interval-censoring of the timestamped MHP data. Since the intensity  $\xi_E(t)$  of the PCMHP ( $d, e$ ) has to be estimated numerically (see Section II-C), numerical approximation error also contributes to type (1) information loss. The numerical approximation error is minimal for sufficiently small  $\Delta^P$  and  $\gamma^h$  (see Sec. 9 of the SI [37]) and vanishes if  $\Delta^P, \gamma^h \rightarrow 0$ .

When we estimate MHP parameters using PCMHP fit on partially interval-censored data, information losses of both types (1) and (2) occur. We disentangle between the two types of error by also fitting PCMHP( $d, e$ ) on the timestamp dataset (*i.e.*, the actual realizations sampled from the MHP, see below). Any information loss in this setup is only due to the model mismatch, the information loss of type (1). Note that the likelihood function used for fitting PCMHP depends on the employed version of the dataset (see later in this section).

We can quantify the individual effects of model mismatch and interval-censoring by comparing the parameter estimates on the two dataset versions.

**Synthetic Dataset:** Given ( $d, e$ ), we construct two synthetic datasets: the *timestamp dataset* and the *partially interval-censored dataset*. The timestamp dataset consists of samples from a  $d$ -dimensional MHP. The partially interval-censored dataset is obtained from the timestamp dataset by interval-censoring the  $E$  dimensions while leaving the  $E^c$  dimensions unchanged. In this experiment, we focus on the case  $d = 2$  and  $e = 1$ .

We consider a 2-dimensional MHP with  $\rho(\alpha) = 0.75$  and parameters  $\alpha^{11} = 0.32$ ,  $\alpha^{12} = 0.5$ ,  $\alpha^{21} = 0.3$ ,  $\alpha^{22} = 0.4$ ,  $\theta^{11} = 0.5$ ,  $\theta^{12} = 1.0$ ,  $\theta^{21} = 0.5$ ,  $\theta^{22} = 1.25$  and  $\nu^1 = \nu^2 = 0.1$ . We set  $\rho(\alpha) \in \{0.5, 0.75, 0.9\}$ . We also test another parameter combination with  $\rho(\alpha) = 0.5$  (*i.e.* subcritical) and  $\rho(\alpha) = 0.9$  (*i.e.* approaching the critical regime) in Sec. 14.1 of the SI [37].

For a given MHP parameter set, we sample 2500 event sequences  $\mathcal{H}_{100}^1 \cup \mathcal{H}_{100}^2$  over the time interval  $[0, 100)$  using the MHP thinning algorithm [34]. Following a procedure similar to prior literature [7], we partition the 2500 event sequences into 50 groups of 50 sequences.

We construct the partially interval-censored dataset by interval-censoring  $\mathcal{H}_{100}^1$ , the first dimension of each realization in the timestamp dataset. Given a partition of  $[0, 100)$ , we count the number of events on dimension 1 that fall on each subinterval. We experiment with five observation window lengths to quantify the information loss of type (2) – intuitively, longer intervals lead to more significant information loss. We consider interval lengths of 1, 2, 5, 10 and 20. For instance, with interval length of 2 we tally event counts in the partition  $\{[0, 2), [2, 4), \dots, [98, 100)\}$ .

**PCMHP Log-Likelihood Functions:** We fit the parameters of the PCMHP( $d, e$ ) model using two different versions of the likelihood function dependent on which dataset we use:

- *timestamp dataset:* we use the point-process log-likelihood on all dimensions, defined in Eq. (9):  $\sum_{j=1}^d \mathcal{L}_{PP-LL}^j(\Theta; T)$ .
- *partially interval-censored dataset:* we use the interval-censored log-likelihood on the  $E$  dimensions and the point-process log-likelihood on the  $E^c$  dimensions (see Eq. (7)):  $\sum_{j=1}^e \mathcal{L}_{IC-LL}^j(\Theta; T) + \sum_{j=e+1}^d \mathcal{L}_{PP-LL}^j(\Theta; T)$ .

In what follows, we specify as PCMHP( $d, e$ )-PP and PCMHP( $d, e$ )-IC the PCMHP( $d, e$ ) model fit on the timestamp dataset and the partially interval-censored dataset, respectively. For brevity and whenever it is clear from context, we drop the dimensionalities ( $d, e$ ), and refer to the model fits as PCMHP-PP and PCMHP-IC. Also, for the PCMHP-IC fits, we specify  $k$  – the length of the observation window – as PCMHP-IC[ $k$ ].

**Inference:** We infer a single  $\Theta$  for each group of sequences using a joint fitting procedure. Since there are 50 groups in total, this process yields 50 estimates of  $\Theta$ . For each group of 50 sequences, we obtain  $\Theta$  that minimizes the joint negative log-likelihood, which is defined as  $\mathcal{L}(\Theta, T) = \sum_{i=1}^{50} \mathcal{L}_i(\Theta, T)$ , where  $\mathcal{L}_i(\Theta, T)$  represents the negative log-likelihood for the  $i^{\text{th}}$  event sequence.

**Metrics:** We evaluate parameter recovery error with four error metrics: the root-mean-squared error (RMSE) of each PCMHP parameter type  $\{\hat{\alpha}, \hat{\theta}, \hat{\nu}\}$  concerning the generating MHP parameters  $\{\alpha, \theta, \nu\}$  and the signed deviation  $\Delta\rho = \rho(\hat{\alpha}) - \rho(\alpha)$  of the spectral radius.

**Parameter Recovery Results:** Fig. 2 shows RMSE( $\alpha$ ), RMSE( $\theta$ ), RMSE( $\nu$ ) and  $\Delta\rho$  across model fits. Each boxplot represents the distribution of errors calculated from 50 estimates of  $\Theta$ , each obtained from a different group of 50 sequences in the synthetic dataset. Within each subplot we have seven boxplots. The leftmost boxplot is the MHP fit, followed by the PCMHP-PP fit (*i.e.*, the PCMHP fit on the timestamp dataset). The next five boxplots contain PCMHP-IC fits of increasingly wider observation windows 1, 2, 5, 10 and 20. Note that the MHP fit represents the case where we do not have either model mismatch and interval censoring error.

In each subplot of Fig. 2, the gap between the first two boxplots (*i.e.* MHP vs. PCMHP(2, 1) fitted on timestamp data) indicates model mismatch error; the gap between the second and third boxplots (*i.e.* PCMHP(2, 1) fitted on timestamp data vs. partially interval-censored data) indicates interval censoring error. The gaps between succeeding boxplots indicate the effect of wider observation windows.



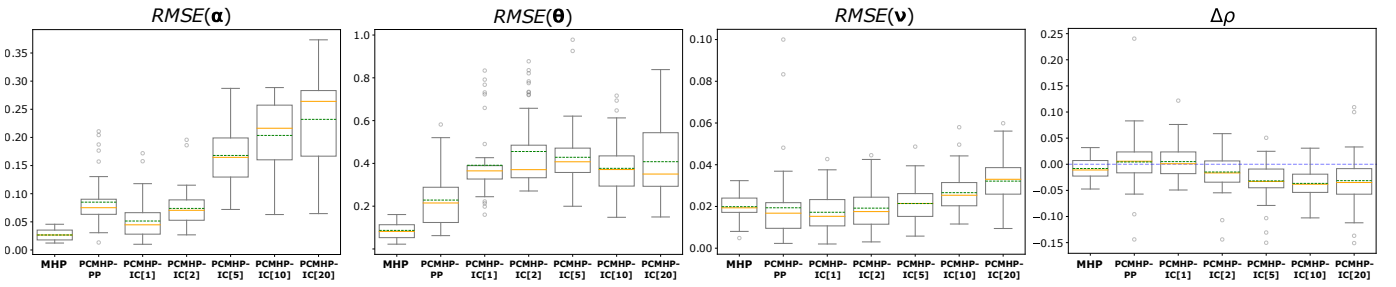


Fig. 2. Comparison of performance metrics in the parameter recovery experiment across model fits: MHP (*i.e.* the data-generating process), PCMHP-PP and PCMHP-IC for varying interval sizes (1, 2, 5, 10 and 20). (left to right) RMSE for each parameter type  $\{\alpha, \theta, \nu\}$  and spectral radius estimation error  $\Delta\rho$ . Samples are drawn from a 2-dimensional MHP with spectral radius  $\rho(\alpha) = 0.75$ . Each boxplot represents the distribution of errors calculated from 50 estimates of  $\Theta$ , each obtained from a different group in the synthetic dataset. The mean and median estimates are indicated by the dashed green lines and solid orange lines, respectively.

Fig. 2 shows three conclusions. First, model mismatch and interval censoring errors contribute to information loss relative to the MHP fit. Second, the approximation quality degrades as the observation window widens, indicating an increasing information loss of type (2). Third, for parameters  $\alpha$  and  $\nu$ , the model mismatch error appears negligible; it is only for higher values of the observation window length ( $\geq 5$ ) that the performance starts degrading due to information loss error. Both error types are present for  $\theta$ . See Sec. 14.1 of the SI for individual parameter fits.

Though we observe that the generating parameters are not always correctly recovered, we see in the rightmost subplot of Fig. 2 that, interestingly, the spectral radius estimation error  $\Delta\rho$  is close to zero regardless of model mismatch and exhibits only slight underestimation for wide observation windows. This is particularly relevant, as  $\rho(\alpha)$  is a meaningful quantity relating to information spread virality (for social media diffusions), disease infectiousness (for epidemiology), or local seismicity (in seismology). The result indicates that even when individual parameter fits are inaccurate, the MHP regime is correctly identified.

**Behavior of  $\Delta\rho$  in Higher Dimensions:** We further study the behavior of  $\Delta\rho$  for varying MBP dimensions  $e$  and model dimensionality  $d$ . We fix  $T = 100$  and  $\rho(\alpha) = 0.92$ . Results for other error metrics are in Sec. 14.2 of the SI.

In the left subplot of Fig. 3, we fix  $d = 5$  and observe how the spectral radius error  $\Delta\rho$  varies with the number of MBP dimensions  $e$ . Note that the leftmost boxplot represents the MHP fit (*i.e.*,  $e = 0$ ). Interestingly, we see that all PCMHP(5,  $e$ ),  $e < 5$  flavors except the fully MBP case (*i.e.*,  $e = d = 5$ ) can estimate the spectral radius as well as the MHP. The gap between the estimated spectral radii and the generating value (blue dashed line) is attributable to the difficulty of recovering MHP parameters in higher dimensions.

In the right subplot of Fig. 3, we fix  $e = 1$  and observe how the spectral radius error  $\Delta\rho$  varies with the dimensionality  $d$  of the PCMHP( $d, 1$ ). The recovery error is generally low (except for  $d = 1$ ). However, we see that the magnitude of the error  $\Delta\rho$  increases with increasing dimensionality starting from  $d = 2$ , which is not surprising since the number of parameters increases quadratically as we increase the dimensionality of the process. We also see that fitting with a fully MBP model ( $d = 1$ ) does not show good recovery performance due to

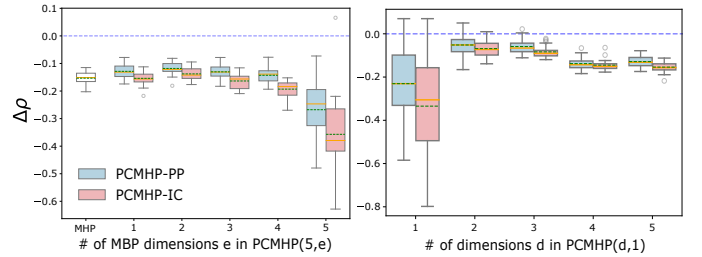


Fig. 3. (Left) Relating the spectral radius estimation error  $\Delta\rho$  of PCMHP(5,  $e$ ) and the number of MBP dimensions  $e$ . Note that PCMHP(5, 0) is the MHP (*i.e.* the data-generating process). (Right) Relating the spectral radius estimation error  $\Delta\rho$  of PCMHP( $d, 1$ ) and the model dimensionality  $d$ . In both plots, samples are drawn from a  $d$ -dimensional MHP with spectral radius  $\rho(\alpha) = 0.92$ . Hyperparameters are  $T = 100$ ,  $N_{sequences} = 20$  and  $intervalsize = 1$ . We fit two models for each PCMHP column: PCMHP-PP (*i.e.* PCMHP fit on timestamp data on all dimensions) and PCMHP-IC (*i.e.* PCMHP fit on interval-censored data on the first  $e$  dimensions and timestamp data on the last  $d - e$  dimensions). The mean and median estimates are indicated by the dashed green lines and solid orange lines, respectively.

information loss, implying the necessity of having at least one cross-exciting dimension (*i.e.*,  $d - e \neq 0$ ).

#### IV. YOUTUBE POPULARITY PREDICTION

In this section, we evaluate PCMHP( $d, e$ )'s performance in predicting the popularity of YouTube videos. For each video, we capture information about three dimensions – *views*, *external shares* and *tweets* linking to the videos – over the time period  $[0, T^{train})$ . We measure time in days relative to the time of posting on Youtube. The first two dimensions (the *views* and *shares*) are observed as daily counts, *i.e.*,  $E = \{views, shares\}$ . The third dimension (*tweets*) is provided as event times, *i.e.*  $E^c = \{tweets\}$ . Given this data setup, we use PCMHP(3, 2) to predict the daily counts of views and shares and the timestamp of the tweets posted over the period  $[T^{train}, T^{test})$ .

**Interval-Censored Forecasting with PCMHP:** To each YouTube video corresponds a partially interval-censored Hawkes realization. A straightforward approach to predict the unfolding of the realization during  $[T^{train}, T^{test})$  is to sample timestamps from PCMHP(3, 2) on each of the three dimensions, conditioned on data before  $T^{train}$ ; we then interval-censor the first two dimensions. In practice, sampling



individual views takes considerable computational effort due to their high background rates, sometimes in the order of millions of views per day, and usually at least an order of magnitude larger than shares and tweets.

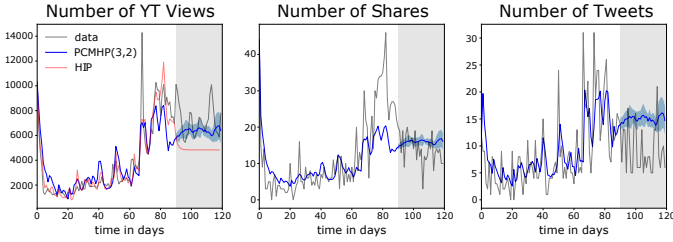


Fig. 4. Comparison of fits and predictions of our proposal PCMHP(3, 2) and the baseline HIP [1] for views (left), shares (center) and tweets (right) for a sample video from ACTIVE: a trailer for the 2014 movie Whiplash (id  $7d\_jQycdQGo$ ). The first 90 days are used to fit model parameters, while the next 30 days (indicated by the gray shaded area) are unseen by the model and used for evaluation. HIP does not predict the share and tweet counts, as it treats these as exogenous inputs. The blue shaded area shows prediction uncertainty computed for the PCMHP(3, 2) fits.

Below is an efficient procedure to calculate expected counts that leverages the compensator  $\Xi_E$  and requires sampling only the  $E^c$  dimensions (i.e., tweets). Let  $\mathcal{P}[T^{train}, T^{test}] = \bigcup_{i=1}^{P-1} [o_i, o_{i+1})$ , where  $o_1 = T^{train}$  and  $o_P = T^{test}$ , be a partition of  $[T^{train}, T^{test})$ .

- 1) Sample only the  $E^c$  dimensions on  $[T^{train}, T^{test})$ .
- 2) Compute expected counts on  $\mathcal{P}[T^{train}, T^{test})$  as  $\{\Xi_E(o_{i+1}) - \Xi_E(o_i) \mid i \in 1 \dots P - 1\}$ .
- 3) Compute the average of  $\{\Xi_E(o_{i+1}) - \Xi_E(o_i) \mid i \in 1 \dots P - 1\}$  across samples.

More details of this scheme and a comparison with the standard method of sampling both  $E^c$  and  $E$  dimensions are provided in Sec. 13 of the SI [37].

**Dataset, Experimental Setup and Evaluation:** We use two subsets of the ACTIVE dataset [1] for model fitting and evaluation. The first subset – dubbed ACTIVE 20% – contains a 20% random sample of the ACTIVE dataset [1], i.e., 2, 834 videos published between 2014-05-29 and 2014-12-26. The second subset – dubbed DYNAMIC VIDEOS – contains videos with which users engage significantly during the test period. It is known that users’ attention to YouTube videos decays with time [13], [44]; therefore, the daily views of most ACTIVE videos hover around zero more than 90 days after their upload. We select the 585 dynamic videos with the standard deviations of the views, tweets, and shares counts on days 21 – 90 higher than the median values on each of the three measures. Technical details of the filtering are in Sec. 15.1 of the SI [37].

For each video, we tune PCMHP hyperparameters and parameters using the first 90 days of daily view counts, share count to external platforms, and the timestamps of tweets that mention each video ( $T^{train} = 90$ ). It is known that generative models are suboptimal for prediction [11] and have to be adapted to the prediction task for better performance. Similar to HIP, we implement dimension weighting and parameter regularization in the likelihood. Full technical details of the fitting procedure are provided in Sec. 15.2 of the SI.

The days 91 – 120 are used for evaluation ( $T^{test} = 120$ ). We measure prediction performance using the Absolute Percentile

TABLE II  
PERFORMANCE COMPARISON OF PCMHP(3, 3), PCMHP(3, 2) AND HIP ON (A) A RANDOM SAMPLE THAT COMPRISES 20% OF THE VIDEOS IN ACTIVE, AND (B) THE SET OF DYNAMIC VIDEOS FROM ACTIVE: MEAN, MEDIAN, AND STANDARD DEVIATION OF THE PERCENTILE ERRORS FOR EACH MODEL. BEST-PERFORMING SCORE IN BOLD.

	ACTIVE20% (n=2834)			DYNAMIC (n=585)		
	PCMHP (3,3)	PCMHP (3,2)	HIP	PCMHP (3,3)	PCMHP (3,2)	HIP
Mean	<b>4.82</b>	7.36	8.12	10.86	<b>7.28</b>	9.31
Median	<b>2.55</b>	4.69	4.96	4.82	<b>3.79</b>	4.73
StdDev	<b>7.13</b>	8.34	9.89	14.24	<b>9.58</b>	11.89

Error (APE) metric [1], which accounts for the long-tailness of online popularity – e.g., the impact of an error of 10,000 views is very different for a video getting 20,000 views per day compared to a video getting 2 million views a day. We first compute the percentile scale of the number of views accumulated between days 91 and 120. APE is defined as:

$$APE = |\text{Per}(\hat{N}_{120}) - \text{Per}(N_{120})|$$

where  $\hat{N}_{120}$  and  $N_{120}$  are the predicted and observed number of views between days 91 and 120; the function  $\text{Per}(\cdot)$  returns the percentile of the argument on the popularity scale.

**Models and Baseline:** We consider two 3-dimensional PCMHP models: PCMHP(3, 2) and PCMHP(3, 3). The former treats the tweets as a Hawkes dimension (see Theorem 1) and is thus susceptible to computational explosion for high tweet counts given the quadratic complexity of computing cross- and self-excitation. The latter is an inhomogeneous Poisson process with no self- or cross-exciting dimension. We, therefore, fit PCMHP(3, 2) solely on videos that have less than 1000 tweets on days 1 – 90; we fit PCMHP(3, 3) on all videos.

We use as a baseline the Hawkes Intensity Process (HIP) [1], a parametric popularity prediction model discussed in Section II-A. HIP, however, is designed for use in a forecasting setup. That is, HIP requires the actual counts of tweets and shares in the prediction window  $[T^{train}, T^{test})$  to get forecasts for the view counts on  $[T^{train}, T^{test})$ . To adapt HIP for the prediction setup (i.e., the tweets and shares are not available at test time), we feed HIP for each of the days 91-120 the time-weighted average of the daily tweet and share counts on 1–90, i.e.  $\frac{1}{\sum_{t=1}^{90} t} \sum_{t=1}^{90} t \cdot \#tweets(t)$  and  $\frac{1}{\sum_{t=1}^{90} t} \sum_{t=1}^{90} t \cdot \#shares(t)$ , which assigns a higher weight to more recent counts.

**Results:** Fig. 4 illustrates the fits of PCMHP(3, 2) and the baseline HIP [1] for a sample video from ACTIVE. Visibly, we see that PCMHP(3, 2) and HIP have comparable fits of the popularity dynamics (left column) during the training period (unshaded area), but PCMHP(3, 2) outputs a much tighter fit during the test period (gray shaded area). We also observe two advantages of PCMHP. First, being a multivariate process that captures endogenous dynamics across its dimensions, PCMHP(3, 2) provides a prediction for future share and tweet counts (center and left columns), in addition to the number of views. In contrast, HIP treats views (i.e. popularity) as exogenously driven by tweets and shares and thus can only predict the views’ dimension. Second, PCMHP can quantify

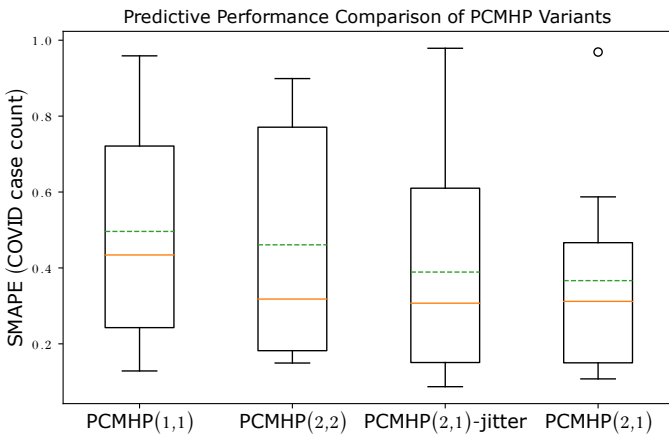


Fig. 5. Performance comparison of PCMHP(1,1), PCMHP(2,2), PCMHP(2,1)-jitter and PCMHP(2,1) on the COVID case count prediction task over our sample of 11 countries. The dashed line and solid line indicate the mean and median estimates, respectively.

the uncertainty of the popularity prediction by sampling multiple unfoldings of a realization and computing the variance of the samples (shown as the blue shaded area in Fig. 4).

In Table II, we tabulate the mean, median and standard deviation of percentile errors for PCMHP(3,3), PCMHP(3,2), and HIP on ACTIVE 20% and DYNAMIC VIDEOS. We observe that the PCMHP flavors consistently outperform the baseline HIP on both datasets. Visibly, on ACTIVE 20%, PCMHP(3,3) outperforms PCMHP(3,2). This is because most videos in ACTIVE 20% do not exhibit much activity during the test period. Consequently, as a nonhomogeneous Poisson process with no self-excitation, PCMHP(3,3) fits better such flat trends than the self-exciting PCMHP(3,2) and HIP models. On DYNAMIC VIDEOS we see a reversal of performance ranking: PCMHP(3,2) performs best, followed by HIP and PCMHP(3,3). This result corroborates our claim in Section II-D that applying the heuristic of censoring event times leads to information loss. We see that PCMHP(3,2) (trained on tweet times) can better capture the popularity dynamics of the most complex videos (which are also the most interesting) compared to PCMHP(3,3) (trained on tweet counts).

## V. INTERACTION BETWEEN COVID-19 CASES AND NEWS

In the previous section we have validated the predictive power of the PCMHP. Here, we shift our attention to the interpretability of PCMHP-fitted parameters. We showcase how PCMHP can link online and offline streams of events by learning the interaction between the COVID-19 daily case counts and publication dates of COVID-19-related news articles for 11 different countries during the early stage of the pandemic.

**Dataset:** We curate and align two data sources.

The first dataset contains COVID daily case counts from the Johns Hopkins University [45]. The dataset is a set of date-indexed spreadsheets containing COVID reported case counts split by country and region. We focus on the following 11 countries: UK, USA, Brazil, China, France, Germany, India,

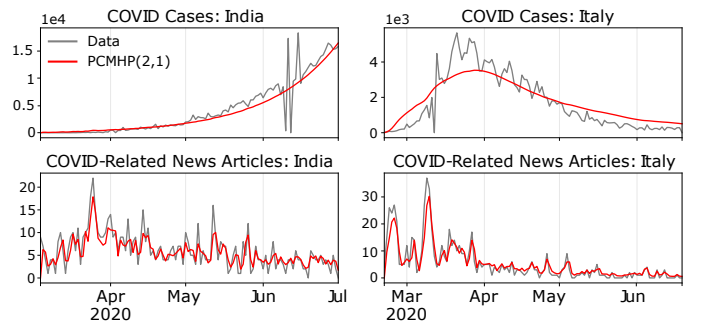


Fig. 6. Observed and PCMHP(2,1)-fitted daily COVID-19 case counts (top row) and COVID-19-related news articles (bottom row) for India (left column) and Italy (right) during the early stage of the outbreak.

Italy, Spain, Sweden, and the Philippines. We select the same countries as [4], to which we add the Philippines.

The second dataset contains timestamps of COVID-19-related news articles provided by the NLP startup Aylien [46]. This dataset is a dump of COVID-related English news articles from 440 major sources from November 2019 to July 2020. We filter the Aylien dataset for news articles that mention the selected 11 countries in the headline. To improve relevancy, for China, we also use several COVID-related keywords (such as *coronavirus*, *covid* and *virus*). Lastly, we only select articles from popular news sites with an Alexa rank of less than 150. Such news sources include Google News and Yahoo! News.

For each country, we fit PCMHP(2,1) with  $E = \{cases\}$  and  $E^c = \{news\}$ . We consider as  $t = 0$  the first day on which a minimum of 10 cases were recorded. Except for China, which had cases as early as January 2020, the initial time for each country in our sample lies between February and March 2020. We only consider data until  $t = 120$ , with time measured in days.

**Incorporating News Information:** To demonstrate the utility of news information in modeling COVID case counts, we compare the predictive performance of PCMHP(2,1) with three variants that leverage different granularities of news information. First, we compare with PCMHP(1,1) which does not use news information at all. Second, we compare with PCMHP(2,2) that uses daily aggregated news counts. Lastly, to test whether exact timing of news is important, we disaggregate daily news counts by adding a uniform jitter to each time, similar to what is done in [8], and fit PCMHP(2,1) to this dataset. We call this baseline PCMHP(2,1)-jitter.

Similar to Section IV, we split our timeframe into a training period  $[0, T^{train} = 90)$  and a testing period  $[T^{train}, T^{test} = 120)$ . In our training period, we fit the models and perform hyperparameter tuning; in our testing period, we sample from the fitted models and evaluate performance. We measure performance using the Symmetric Mean Absolute Percentage Error (SMAPE), given by  $SMAPE = \frac{1}{n} \sum_{t=1}^n \frac{|F_t - A_t|}{|A_t| + |F_t|}$ , where  $F_t$  and  $A_t$  are the forecasted and actual values at time  $t$ , respectively.

Across our sample of 11 countries, we see in Fig. 5 that PCMHP(2,1) has the best performance compared to the three baselines and incorporating more granular news information leads to better predictive performance. We observe

TABLE III  
 $K$ -MEANS CLUSTER CENTROIDS ON THE PARAMETERS OBTAINED BY FITTING PCMHP(2, 1) ON THE CASE COUNT AND NEWS ARTICLE DATASET.

Cluster	$\theta^{11}$	$\theta^{12}$	$\theta^{21}$	$\theta^{22}$	$\alpha^{11}$	$\alpha^{12}$	$\alpha^{21}$	$\alpha^{22}$	$\nu^1$	$\nu^2$
UK, German, Spain	0.76	0.12	1.82	1.84	0.79	3.60	0.02	0.42	0.03	0.28
Brazil	0.13	0.01	1.89	2.46	1.08	5.48	0	0.38	0	1.47
China, France	0.62	4	1.70	3.55	0.68	0.73	0.3	0.39	0	0.05
US, Italy, Sweden	0.67	0.22	1.61	1.51	0.93	0.73	0.006	0.65	0.29	0.59
India, Philippines	0.12	2.28	2.15	1.88	1.35	0.54	0.007	0.58	0.08	0.66

that the news-agnostic PCMHP(1, 1) and the day aggregated PCMHP(2, 2) models do not fit the data well and cannot capture the complex COVID case count dynamics. This supports our claim in Section II-D that application of data-altering heuristics leads to loss of information. However, by incorporating timestamped news information, we see significant performance improvement and we can match the trend in the case time series. We also see subtle performance improvement by incorporating exact news times (PCMHP(2, 1)-jitter vs. PCMHP(2, 1)).

**Results:** Fig. 6 shows the daily COVID-19 case counts and daily news article volume of the PCMHP(2, 1) fits for India and Italy. We show the plots for the other countries, the table of parameter estimates, and the goodness-of-fit analysis in Sec. 16 of the SI [37]. Visible from Fig. 6, PCMHP(2, 1) captures well the dynamics of both countries. Based on the sample-based fit score introduced in the SI, the actual COVID-19 case counts for India and Italy fall within the model’s prediction interval for 97% and 61% of the time, respectively.

**Cluster countries based on model fittings:** The parameters capture different aspects of the interaction between news and cases. Here, we cluster the fitted parameter sets across countries to identify groups that have similar diffusion profiles. To render the scale of parameters comparable across countries, we rescale the maximum daily number of cases for each country over the considered timeframe to be 100, fit the PCMHP(2, 1) on this scaled data, and perform  $K$ -means clustering on the resulting parameter sets.

The  $k = 5$  clusters are shown in Table III and visualized in Fig. 7 using t-SNE [47]. The first cluster (the UK, Germany, Spain) has high  $\alpha^{12}$  and low  $\alpha^{11}$ . The second cluster – made solely of Brazil – has both a high  $\alpha^{12}$  and a very high  $\alpha^{11}$ . With high  $\alpha^{12}$ , the two clusters contain countries where *news strongly preempts cases*. The third cluster (China and France) has a high  $\alpha^{21}$  indicative of *news playing a reactive role to cases*. The fourth cluster (US, Italy, Sweden) and fifth cluster (India, Philippines) both have low  $\alpha^{12}$  and  $\alpha^{21}$ , indicating *little interaction between news and cases*. We notice that COVID infectiousness is much higher in the fifth cluster (India, Philippines), with  $\alpha^{11}$  greater than one (each case generates more than one case) and  $\theta^{11}$  lowest across all clusters (slow decay, therefore long influence from cases to cases). Our fits indicate that India and the Philippines are countries particularly affected by COVID-19 in the early days.

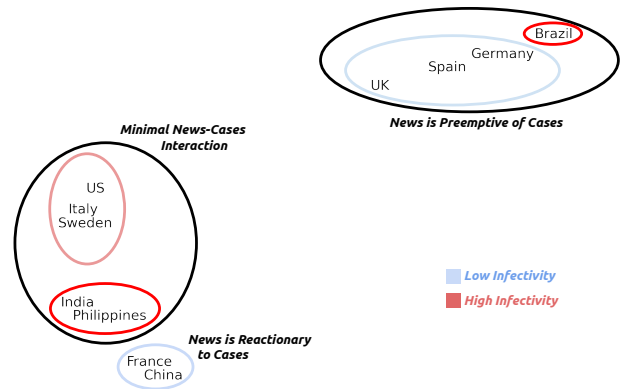


Fig. 7. Labeled tSNE visualization of the clusters obtained from the fitted PCMHP(2, 1) parameters across the 11 countries we consider.

## VI. SUMMARY AND FUTURE WORK

This work introduces the Partially Censored Multivariate Hawkes Process (PCMHP), a generalization of the MHP where we take the conditional expectation of a subset of dimensions over the stochastic history of the process. The PCMHP is motivated by the fact that the MHP cannot directly be fit to partially interval-censored data; the PCMHP can be used to approximate MHP parameters via a correspondence of parameters.

In this paper, we derive the conditional intensity function of the PCMHP by considering the impulse response to the associated LTI system. Additionally, we derive its regularity conditions which leads to a subcritical process; which we find generalizes regularity conditions of the multivariate Hawkes process and the previously proposed MBP process. The MLE loss function is also derived for the partially interval-censored setting. To test the practicality of our proposed approach, we consider three empirical experiments.

First, we test the capability of the PCMHP in recovering multivariate Hawkes process parameters in the partially interval-censored setting. By using synthetic data, we investigate the information loss from model mismatch and the interval-censoring of the timestamped data. Our results show that the fitted PCMHP can approximate the parameters and recover the spectral radius of the original multivariate Hawkes process used to generate the data.

Second, we demonstrate the predictive capability of the PCMHP model by applying it to YouTube popularity prediction and showing that it outperforms the popularity estimation algorithm Hawkes Intensity Process [1].

Third, to demonstrate interpretability of the PCMHP parameters, we fit the process to a curated dataset of COVID-19 cases and COVID-19-related news articles during the early stage of the outbreak in a sample of countries. By inspecting the country-level parameters, we show that there is a demonstrable clustering of countries based on how news predominantly played its role: whether it was reactionary, preemptive, or neutral to the rising level of cases.

**Limitations and Future Work:** The number of parameters estimated with the PCMHP( $d, e$ ) increases quadratically

with the process dimension  $d$ , meaning the curse of dimensionality applies. However, since the primary use case for  $\text{PCMHP}(d, e)$  is in popularity prediction across social media platforms (i.e., where the dimensions represent platforms), which is a low-dimensional scenario, the curse of dimensionality is not a significant concern. Difficulties would arise, however, if  $\text{PCMHP}(d, e)$  were applied at the user level (i.e., where the dimensions correspond to individual users). In such cases, future work would be required to extend  $\text{PCMHP}$  by employing scalable variants of the Hawkes process. These approaches generally reduce the  $d$  dimensions into a more compact  $r$ -dimensional space ( $r \ll d$ ) through factorization of the interaction matrix [48], [49]. This is a direction for future research.

There are three other areas where future work can be explored. First, theoretical analysis on the approximation error of the model mismatch (i.e., fitting Hawkes data to the  $\text{PCMHP}$  model) should be performed, since we only performed an empirical evaluation in this work. Second, methods to approximate the conditional intensity should be investigated, as the current solution relies on the computationally heavy discrete convolution approximation. Lastly, given that the  $\text{PCMHP}(d, e)$ , by construction, is not self- and cross-exciting in the  $E$  dimensions, an open research question is whether we can construct a process that retains the self- and cross-exciting properties in all dimensions whilst also being flexible enough to be used in the partially interval-censored setting.

## VII. ACKNOWLEDGMENTS

The work was partially supported by the National Science Centre, Poland, under Grant 2021/41/B/HS6/02798.

## REFERENCES

- [1] M. A. Rizoïu, L. Xie, S. Sanner, M. Cebrian, H. Yu, and P. Van Henteryck, "Expecting to be HIP: Hawkes intensity processes for social media popularity," *WWW 2017*, pp. 735–744, 2017.
- [2] A. G. Hawkes, "Spectra of some self-exciting and mutually exciting point processes," *Biometrika*, vol. 58, no. 1, pp. 83–90, 1971.
- [3] M.-A. Rizoïu, Y. Lee, S. Mishra, and L. Xie, *A Tutorial on Hawkes Processes for Events in Social Media*. Frontiers of Multimedia Research, 12 2017, pp. 191–218.
- [4] R. Browning, D. Sulem, K. Mengersen, V. Rivovirard, and J. Rousseau, "Simple discrete-time self-exciting models can describe complex dynamic processes: A case study of covid," *PLoS ONE*, pp. 1–28, 2021.
- [5] L. Shlomovich, E. A. Cohen, N. Adams, and L. Patel, "Parameter estimation of binned Hawkes processes," *Journal of Computational and Graphical Statistics*, vol. 31, no. 4, pp. 990–1000, 2022.
- [6] D. Daley and D. Vere-Jones, *An introduction to the theory of point processes. Vol. 1*, 2nd ed., ser. Probability and its Applications (New York). New York: Springer-Verlag, 2003.
- [7] M.-A. Rizoïu, A. Soen, S. Li, P. Calderon, L. Dong, A. K. Menon, and L. Xie, "Interval-censored Hawkes processes," *Journal of Machine Learning Research*, vol. 23, no. 338, pp. 1–84, 2022.
- [8] H. J. T. Unwin, I. Routledge, S. Flaxman, M.-A. Rizoïu, S. Lai, J. Cohen, D. J. Weiss, S. Mishra, and S. Bhatt, "Using Hawkes Processes to model imported and local malaria cases in near-elimination settings," *PLOS Computational Biology*, vol. 17, no. 4, Apr. 2021.
- [9] Q. Zhao, M. A. Erdogdu, H. Y. He, A. Rajaraman, and J. Leskovec, "Seismic: A self-exciting point process model for predicting tweet popularity," in *SIGKDD 2015*, 2015, pp. 1513–1522.
- [10] R. Kobayashi and R. Lambiotte, "Tideh: Time-dependent Hawkes process for predicting retweet dynamics," in *ICWSM 2016*, pp. 191–200.
- [11] S. Mishra, M. A. Rizoïu, and L. Xie, "Feature driven and point process approaches for popularity prediction," *CIKM 2016*, pp. 1069–1078.
- [12] A. Zadeh and R. Sharda, "How can our tweets go viral? point-process modelling of brand content," *Information & Management*, vol. 59, no. 2, p. 103594, 2022.
- [13] R. Crane and D. Sornette, "Robust dynamic classes revealed by measuring the response function of a social system," *PNAS*, vol. 105, no. 41, pp. 15 649–15 653, 2008.
- [14] R. Krohn and T. Wenginger, "Modelling online comment threads from their start," in *2019 IEEE International Conference on Big Data*, 2019, pp. 820–829.
- [15] Q. Yan, S. Tang, S. Gabriele, and J. Wu, "Media coverage and hospital notifications: Correlation analysis and optimal media impact duration to manage a pandemic," *Journal of Theoretical Biology*, vol. 390, pp. 1–13, Feb. 2016.
- [16] R. Chunara, J. R. Andrews, and J. S. Brownstein, "Social and News Media Enable Estimation of Epidemiological Patterns Early in the 2010 Haitian Cholera Outbreak," *The American Journal of Tropical Medicine and Hygiene*, vol. 86, no. 1, pp. 39–45, Jan. 2012.
- [17] Q. Yan, Y. Tang, D. Yan, J. Wang, L. Yang, X. Yang, and S. Tang, "Impact of media reports on the early spread of COVID-19 epidemic," *Journal of Theoretical Biology*, vol. 502, p. 110385, Oct. 2020.
- [18] M. Kirchner, "Hawkes and  $\text{INAR}(\infty)$  processes," *Stochastic Processes and their Applications*, vol. 126, no. 8, pp. 2494–2525, Aug. 2016.
- [19] —, "An estimation procedure for the Hawkes process," *Quantitative Finance*, vol. 17, no. 4, pp. 571–595, Apr. 2017.
- [20] F. Cheysson and G. Lang, "Spectral estimation of Hawkes processes from count data," *The Annals of Statistics*, vol. 50, no. 3, pp. 1722 – 1746, 2022.
- [21] L. Shlomovich, E. A. K. Cohen, and N. Adams, "A parameter estimation method for multivariate binned Hawkes processes," *Statistics and Computing*, vol. 32, no. 6, p. 98, Oct. 2022.
- [22] P. J. Schneider and T. A. Weber, "Estimation of self-exciting point processes from time-censored data," *Physical Review E*, vol. 108, no. 1, p. 015303, Jul. 2023.
- [23] A. L. Bertozzi, E. Franco, G. Mohler, M. B. Short, and D. Sledge, "The challenges of modeling and forecasting the spread of COVID-19," *PNAS*, vol. 117, no. 29, pp. 16 732–16 738, Jul. 2020.
- [24] W.-H. Chiang, X. Liu, and G. Mohler, "Hawkes process modeling of COVID-19 with mobility leading indicators and spatial covariates," *International Journal of Forecasting*, vol. 38, no. 2, pp. 505–520, 2022.
- [25] F. Schoenberg, "Estimating Covid-19 transmission time using Hawkes point processes," *The Annals of Applied Statistics*, vol. 17, no. 4, 2023.
- [26] J. Sun, *The statistical analysis of interval-censored failure time data*. Springer, 2006, vol. 3, no. 1.
- [27] D.-G. D. Chen, J. Sun, and K. E. Peace, *Interval-censored time-to-event data: methods and applications*. CRC Press, 2012.
- [28] K. Bogaerts, A. Komarek, and E. Lesaffre, *Survival analysis with interval-censored data: a practical approach with examples in R, SAS, and BUGS*. Chapman and Hall/CRC, 2017.
- [29] M. Du and J. Sun, "Statistical analysis of interval-censored failure time data," *Chinese Journal of Applied Probability and Statistics*, vol. 37, no. 6, pp. 627–654, 2021.
- [30] L.-P. Chen and B. Qiu, "Analysis of length-biased and partly interval-censored survival data with mismeasured covariates," *Biometrics*, vol. 79, no. 4, pp. 3929–3940, 2023.
- [31] L. Ma, Y. Feng, D.-G. D. Chen, and J. Sun, "Interval-censored time-to-event data and their applications in clinical trials," *Clinical Trial Biostatistics and Biopharmaceutical Applications*, vol. 307, 2014.
- [32] Q. Kong, P. Calderon, R. Ram, O. Boichak, and M.-A. Rizoïu, "Interval-censored transformer Hawkes: Detecting information operations using the reaction of social systems," in *ACM Web Conference*, 2023.
- [33] H. Shen, D. Wang, C. Song, and A.-L. Barabási, "Modeling and predicting popularity dynamics via reinforced Poisson processes," in *AAAI*, vol. 28, no. 1, 2014.
- [34] Y. Ogata, "On Lewis' simulation method for point processes," *IEEE Transactions on Information Theory*, vol. 27, no. 1, pp. 23–31, 1981.
- [35] A. Dassios and H. Zhao, "Exact simulation of Hawkes process with exponentially decaying intensity," 2013.
- [36] M.-A. Rizoïu, S. Mishra, Q. Kong, M. Carman, and L. Xie, "Sir-hawkes: Linking epidemic models and Hawkes processes to model diffusions in finite populations," in *Proceedings of the 2018 World Wide Web Conference*, 2018, pp. 419–428.
- [37] "Appendix: Linking across data granularity: Fitting multivariate Hawkes processes to partially interval-censored data," 2024, <https://bit.ly/3UAKpt6>.
- [38] C. L. Phillips, J. M. Parr, E. A. Riskin, and T. Prabhakar, *Signals, systems, and transforms*. Prentice Hall Upper Saddle River, 2003.

- [39] Y. Ogata, "The asymptotic behaviour of maximum likelihood estimators for stationary point processes," *Annals of the Institute of Statistical Mathematics*, vol. 30, no. 2, pp. 243–261, Dec. 1978.
- [40] A. Wächter and L. T. Biegler, "On the implementation of an interior-point filter line-search algorithm for large-scale nonlinear programming," *Mathematical Programming*, vol. 106, no. 1, pp. 25–57, Mar. 2006.
- [41] K. Fokianos, A. Rahbek, and D. Tjøstheim, "Poisson autoregression," *Journal of the American Statistical Association*, vol. 104, no. 488, pp. 1430–1439, 2009.
- [42] E. Erdogan, S. Ma, A. Beygelzimer, and I. Rish, *Statistical Models for Unequally Spaced Time Series*, pp. 626–630.
- [43] K. Rehfeld, N. Marwan, J. Heitzig, and J. Kurths, "Comparison of correlation analysis techniques for irregularly sampled time series," *Nonlinear Processes in Geophysics*, vol. 18, no. 3, pp. 389–404, 2011.
- [44] S. Wu, M.-A. Rizoïu, and L. Xie, "Estimating Attention Flow in Online Video Networks," *ACM HCI*, vol. 3, no. CSCW, pp. 1–25, nov 2019.
- [45] E. Dong, H. Du, and L. Gardner, "An interactive web-based dashboard to track COVID-19 in real time," *The Lancet Infectious Diseases*, vol. 20, no. 5, pp. 533–534, May 2020.
- [46] Aylien, "AYLIEN Coronavirus Dataset," 2020.
- [47] L. van der Maaten and G. Hinton, "Visualizing data using t-sne," *Journal of Machine Learning Research*, vol. 9, no. 86, pp. 2579–2605, 2008.
- [48] R. Lemonnier, K. Scaman, and A. Kalogeratos, "Multivariate hawkes processes for large-scale inference," in *Proceedings of the AAAI conference on artificial intelligence*, vol. 31, no. 1, 2017.
- [49] M. Nickel and M. Le, "Modeling sparse information diffusion at scale via lazy multivariate hawkes processes," in *Proceedings of the Web Conference 2021*, 2021, pp. 706–717.

# Contents

<b>1</b>	<b>Background Material</b>	<b>2</b>
1.1	Multivariate Hawkes Process . . . . .	2
1.2	Mean Behavior Poisson Process . . . . .	6
<b>2</b>	<b>Interpretation of <math>\mathbf{h}_E</math></b>	<b>7</b>
<b>3</b>	<b>Closed Form <math>\xi_E(t)</math> for the PCMHP(2,1) Process</b>	<b>8</b>
<b>4</b>	<b>Additional Results and Proofs for Section II.B</b>	<b>18</b>
4.1	Convolutional Formula . . . . .	19
4.2	Regularity Conditions . . . . .	30
<b>5</b>	<b>Additional Results and Proofs for Section II.C</b>	<b>40</b>
<b>6</b>	<b>Convexity Analysis of the PCMHP(2,1) Likelihood</b>	<b>42</b>
<b>7</b>	<b>Approximating the Conditional Intensity <math>\xi_E(t)</math></b>	<b>49</b>
7.1	Numerical Convolution . . . . .	49
7.2	Infinite Series Truncation . . . . .	52
7.3	Algorithm to Approximate $\xi_E(t)$ . . . . .	52
<b>8</b>	<b><math>\xi_E(t)</math> as a Conditional Expectation over MHP Samples</b>	<b>54</b>
<b>9</b>	<b>Comparison of <math>\xi_E(t)</math> Evaluation Methods</b>	<b>57</b>
<b>10</b>	<b>Numerical Scheme to Calculate PCMHP Likelihood</b>	<b>58</b>
<b>11</b>	<b>Gradient <math>\mathcal{L}_{\Theta}(\Theta; T)</math> Calculations</b>	<b>60</b>



<b>12 Sampling from PCMHP</b>	<b>63</b>
12.1 Thinning Algorithm . . . . .	64
12.2 Derivation of Thinning Upper Bounds for PCMHP( $d, e$ ) . . . . .	66
<b>13 Prediction of Expected Counts with PCMHP(<math>d, e</math>)</b>	<b>71</b>
<b>14 Additional Results for Section III</b>	<b>73</b>
14.1 Individual Parameter Estimates . . . . .	74
14.2 Convergence Analysis . . . . .	77
<b>15 Additional Details for Section IV</b>	<b>82</b>
15.1 Technical Details for Fitting . . . . .	82
15.2 Filtering for Dynamic Videos . . . . .	85
15.3 Performance Comparison of PCMHP and HIP . . . . .	86
<b>16 Additional Results for Section V</b>	<b>86</b>
16.1 Goodness-of-Fit Tests . . . . .	86
16.2 Interpreting Individual Country Fits . . . . .	88

# 1 Background Material

## 1.1 Multivariate Hawkes Process

**Alternative view of conditional intensity.** The conditional intensity can be viewed as the mean number of events occurring in an infinitesimal interval, conditioned on the past. A simple multivariate extension of the result in Rasmussen (2018) gives

$$\lambda^*(t)dt = \mathbb{E} [d\mathbf{N}(t)|\mathcal{H}_t^D]. \quad (1)$$

**Compensator.** By integrating the conditional intensity, we obtain another important measure: the compensator  $\Lambda(t)$  of the process.

**Definition 1** Given a temporal point process with conditional intensity  $\lambda^*(t)$ , the compensator  $\Lambda(t)$  is defined as

$$\Lambda(t) = \int_0^t \lambda^*(\tau) d\tau. \quad (2)$$

where  $0 \leq s \leq t$ .

**Remark 2** The compensator  $\Lambda(t)$  can be interpreted as the expected number of events over  $[0, t)$  given  $\mathcal{H}_t^D$ . This follows by integrating Eq. (1) over  $[0, t)$ ,

By integrating  $\lambda^*(t)$ , we obtain an explicit form for the compensator  $\Lambda(t)$  of the  $d$ -dimensional Hawkes process:

$$\Lambda(t) = \mathbf{M}(t) + \sum_{j=1}^d \sum_{t_k^j < t} \Phi^j(t - t_k^j), \quad (3)$$

where

$$\mathbf{M}(t) = \int_0^t \boldsymbol{\mu}(s) ds, \quad (4)$$

$$\Phi(t) = \int_0^t \boldsymbol{\varphi}(s) ds. \quad (5)$$

**Regularity condition.** A univariate Hawkes process is *subcritical* if the expected number of direct and indirect offsprings (*i.e.*, the progeny) spawned by a single parent is finite. In this case, the Hawkes process is expected to die out as  $t \rightarrow \infty$ . The intuition for the multivariate Hawkes process is similar, but in this case we have to consider that any event in one dimension is capable of producing events in any other dimension by cross-excitation. A multivariate Hawkes process is subcritical if the progeny resulting from a single event of dimension  $j$  to dimension  $i$  is finite for every pair  $(i, j) \in D \times D$ .

**Definition 3** Let  $\lambda^1, \dots, \lambda^d$  be the eigenvalues of the branching matrix  $\boldsymbol{\alpha}$ . The spectral radius  $\rho(\boldsymbol{\alpha})$  of  $\boldsymbol{\alpha}$  is defined as

$$\rho(\boldsymbol{\alpha}) = \max\{|\lambda^1|, \dots, |\lambda^d|\}. \quad (6)$$

For a one-dimensional Hawkes process, the spectral radius is exactly the branching factor, the expected number of secondary events triggered by a parent event. If the branching factor is less than one, the Hawkes process is **subcritical**. If the branching factor is greater than one, the process is **supercritical**, and the progeny of a single parent event is expected to have an infinite number of offspring events as  $t \rightarrow \infty$ . In this case the Hawkes process is also called **explosive**.

The following proposition is a standard result that characterizes the convergence of a geometric series of matrices. We use the following to obtain a closed-form expression of the total progeny produced by events in every dimension for the MHP.

**Proposition 4 (Hubbard & Hubbard (2002))** If  $\rho(\boldsymbol{\alpha}) < 1$ ,  $\sum_{n=0}^{\infty} \boldsymbol{\alpha}^n$  converges and is equal to  $(\mathbf{I} - \boldsymbol{\alpha})^{-1}$ .

The subcriticality condition for a multivariate Hawkes process is given by the following.

**Theorem 5** A Hawkes process with branching matrix  $\boldsymbol{\alpha}$  is subcritical if  $\rho(\boldsymbol{\alpha}) < 1$ .

**Proof** Let  $\rho(\boldsymbol{\alpha}) < 1$ . Suppose we have one parent event in dimension  $j \in D$ . Let us consider the offsprings of this parent event.

The expected number of direct (*i.e.*, first-generation) offsprings in dimension  $i$  is  $\alpha^{ij}$ . The expected number of second-generation offsprings in dimension  $i$  is  $\sum_{k=1}^d \alpha^{ik} \alpha^{kj} = (\boldsymbol{\alpha}^2)^{ij}$ , which is intuitively the dimension  $i$  offsprings of the first-generation offsprings of the dimension  $j$  parent event. By the same argument, the number of  $m^{\text{th}}$  generation offsprings would then be  $(\boldsymbol{\alpha}^m)^{ij}$ . Thus, it follows that the  $(i, j)$  element of  $\sum_{n=1}^m \boldsymbol{\alpha}^n$  tracks the

total number of dimension  $i$  offsprings up to the  $m^{\text{th}}$  generation produced a single parent event in dimension  $j$ . In the limit  $m \rightarrow \infty$ , we can conclude by Proposition 4 that the Hawkes process is subcritical. Furthermore, the expected number of dimension  $i$  offsprings of a dimension  $j$  parent event is given by the  $(i, j)$  element of  $(\mathbf{I} - \boldsymbol{\alpha})^{-1} - \mathbf{I}$ . ■

**Parameter estimation.** Suppose that we are given a set of observed events  $\mathcal{H}_{T-}^D$  up until some maximum time  $T > 0$ . Our task is to find the parameter set  $\Theta$  that best fits this given set of observations. The standard approach is maximum likelihood estimation (MLE), where we find  $\Theta$  that maximizes the probability of observing the data given the point process model. Equivalently, we can minimize the negative log-likelihood function  $\mathcal{L}(\Theta; \bigcup_{j=1}^d \mathcal{H}_{T-}^j)$  of the parameter set  $\Theta$ .

For the  $d$ -dimensional Hawkes process (and in general, for a  $d$ -dimensional point process with intensity  $\boldsymbol{\lambda}^*(t)$ ), the negative log-likelihood function is given by

$$\begin{aligned} \mathcal{L}_{\text{PP-LL}}(\Theta; \mathcal{H}_{T-}^D) &:= -\log \mathbb{P} \left\{ \mathcal{H}_{T-}^D \mid \Theta \right\} \\ &= -\sum_{j=1}^d \left[ \sum_{t_k^j \in \mathcal{H}_{T-}^j} \log \lambda^j(t_k^j; \Theta) - \Lambda^j(T; \Theta) \right]. \end{aligned} \quad (7)$$

We add the subscript PP-LL (Point-Process Log-Likelihood) to emphasize that the likelihood is evaluated with respect to event timestamps.

**Sampling.** Given an MHP, the standard approach to sample event sequences is via the thinning algorithm discussed in Ogata (1981). This technique converts the task of sampling a Hawkes process into the significantly simpler task of sampling a homogeneous Poisson process. The rate of this Poisson process is obtained as an upper bound to the Hawkes conditional intensity and is recomputed every time a new event is accepted. Proposed events

from the procedure are ‘thinned’ out with rejection sampling using the Hawkes conditional intensity. Algorithm 1 shows how to sample event sequences from a  $d$ -dimensional Hawkes process given a constant background intensity.

## 1.2 Mean Behavior Poisson Process

**Regularity condition.** The sufficient condition for the subcriticality of the MBP process is  $\alpha < 1$ . This condition ensures that the infinite sum  $\sum_{n=1}^{\infty} \varphi^{\otimes n}(t)$  in the MBP intensity  $\xi(t)$  converges to zero as  $t \rightarrow \infty$ .

**Parameter estimation in interval-censored settings.** Since the MBP process is a Poisson process, its increments are independent, which allows the likelihood function to be expressed as a sum of the likelihood of disjoint Poisson distributions. This enables the MBP process to be fitted in interval-censored settings via maximum likelihood estimation.

Suppose instead of observing the sequence of events  $\mathcal{H}_{T-}$ , we observe interval-censored counts over a given partition of  $[0, T)$ , which we denote as  $\mathcal{P}[0, T)$ . Furthermore, assume that the partition is subdivided into  $m$  subintervals, so that  $\mathcal{P}[0, T) = \bigcup_{k=1}^m [o_{k-1}, o_k)$ , where  $o_0 = 0$  and  $o_m = T$ . For each subinterval  $[o_{k-1}, o_k)$ , we are given the count  $\mathbf{C}_k$  of events that occur. In this setting and given the MBP process, the negative log-likelihood function  $\mathcal{L}(\Theta; \{\mathbf{C}_k\}_{k=1}^m)$  can be obtained with the following result.

**Proposition 6 (Rizoïu et al. (2022))** *Suppose we are given interval-censored counts  $\{\mathbf{C}_k\}_{k=1}^m$  over the partition  $\mathcal{P}[0, T) = \bigcup_{k=1}^m [o_{k-1}, o_k)$ , where  $o_0 = 0$  and  $o_m = T$ . The negative log-likelihood function of an MBP process with intensity  $\xi(t)$  and compensator  $\Xi(t)$  is given*

by

$$\begin{aligned} \mathcal{L}_{\text{IC-LL}}(\Theta; \{\mathbf{C}_k\}_{k=1}^m) &= -\log \mathbb{P} \left\{ \bigcup_{k=1}^m \{\Xi(o_{k-1}, o_k) = \mathbf{C}_k\} \mid \Theta \right\} \\ &\propto \sum_{k=1}^m [\Xi(o_{k-1}, o_k; \Theta) - \mathbf{C}_k \log \Xi(o_{k-1}, o_k; \Theta)], \end{aligned} \quad (8)$$

where we add the subscript IC-LL (Interval-Censored Log Likelihood) to make explicit the fact that we are calculating the likelihood with respect to interval-cen

## 2 Interpretation of $\mathbf{h}_E$

The function  $\mathbf{h}_E(t) = \sum_{n=1}^{\infty} \varphi_E^{\otimes n}(t)$  appearing in Main Text Equation 5 can be expressed term-by-term as

$$\mathbf{h}_E(t) = \varphi_E(t) + \varphi_E^{\otimes 2}(t) + \varphi_E^{\otimes 3}(t) + \dots \quad (9)$$

Given a Hawkes kernel of the form  $\varphi(t) = \boldsymbol{\alpha} \odot \mathbf{f}(t)$ , where  $\odot$  denotes elementwise multiplication, Eq. (9) can be written as

$$\mathbf{h}_E(t) = \boldsymbol{\alpha}_E \odot \mathbf{f}_E(t) + \boldsymbol{\alpha}_E^2 \odot \mathbf{f}_E^{\otimes 2}(t) + \boldsymbol{\alpha}_E^3 \odot \mathbf{f}_E^{\otimes 3}(t) + \dots \quad (10)$$

Consider the  $i, j$  entry of the  $n^{\text{th}}$  term of the sum:

$$(\boldsymbol{\alpha}_E^n \odot \mathbf{f}_E^{\otimes n}(t))^{ij} = (\boldsymbol{\alpha}_E^n)^{ij} \odot (\mathbf{f}_E^{\otimes n}(t))^{ij}$$

This expression can be interpreted as follows:

- $(\boldsymbol{\alpha}_E^n)^{ij}$  is the expected number of  $n^{\text{th}}$  generation offspring events of type  $i$  produced by a single parent of type  $j$  in a  $d$ -dimensional branching process where only the  $E$  dimensions can produce offsprings.
- $(\mathbf{f}_E^{\otimes n}(t))^{ij}$  is the density of  $n^{\text{th}}$  generation type  $i$  offspring events at time  $t$  produced by a single parent of type  $j$  at time 0.



- The product  $(\boldsymbol{\alpha}_E^n)^{ij} \odot (\mathbf{f}_E^{\otimes n}(t))^{ij}$  can be interpreted as the expected intensity contribution at time  $t$  from  $n^{\text{th}}$  generation type  $i$  offspring events produced by a single parent of type  $j$ .

Thus  $h_E^{ij}(t)$ , given by

$$\mathbf{h}_E^{ij}(t) = \underbrace{(\boldsymbol{\alpha}_E \odot \mathbf{f}_E(t))^{ij}}_{\text{first generation}} + \underbrace{(\boldsymbol{\alpha}_E^2 \odot \mathbf{f}_E^{\otimes 2}(t))^{ij}}_{\text{second generation}} + \underbrace{(\boldsymbol{\alpha}_E^3 \odot \mathbf{f}_E^{\otimes 3}(t))^{ij}}_{\text{third generation}} + \cdots,$$

is the expected type- $i$  intensity at time  $t$  from a single parent event of type  $j$ , over the entire progeny of offsprings.

Fig. 1 shows the nonzero entries of  $\mathbf{h}_E(t)$  for a PCMHP(3, 2) process with parameter set  $\boldsymbol{\theta} = [1, 0.1, 0, 1, 1, 0, 1, 1, 0]$ ,  $\boldsymbol{\alpha} = [0.2, 0.2, 0, 0.2, 0.2, 0, 0.2, 0.2, 0]$ . In the plot we show the contributions of the first to the fifth generation to  $\mathbf{h}_E(t)$ . As we can see, the contributions of succeeding generations become increasingly smaller as every  $\alpha^{ij} < 1$ . The contributions all go to zero asymptotically as  $t \rightarrow \infty$ . In addition, we see that the mode of each generation's contribution is shifted to the right as the generation index increases. Intuitively, a delay exists because offspring events in generation  $n + 1$  are produced by generation  $n$  events. The extent of the delay is controlled by  $\boldsymbol{\theta}$ .

### 3 Closed Form $\boldsymbol{\xi}_E(t)$ for the PCMHP(2, 1) Process

Given a PCMHP(2, 1) process, the conditional intensity function  $\boldsymbol{\xi}_E(t)$  is given by

$$\xi_1^1(t | \mathcal{H}_t^2) = \mu^1 + \sum_{t_k^2 < t} \varphi^{12}(t - t_k^2) + (\varphi^{11} * \xi_1^1)(t)$$

$$\xi_1^2(t | \mathcal{H}_t^2) = \mu^2 + \sum_{t_k^2 < t} \varphi^{22}(t - t_k^2) + (\varphi^{21} * \xi_1^1)(t).$$

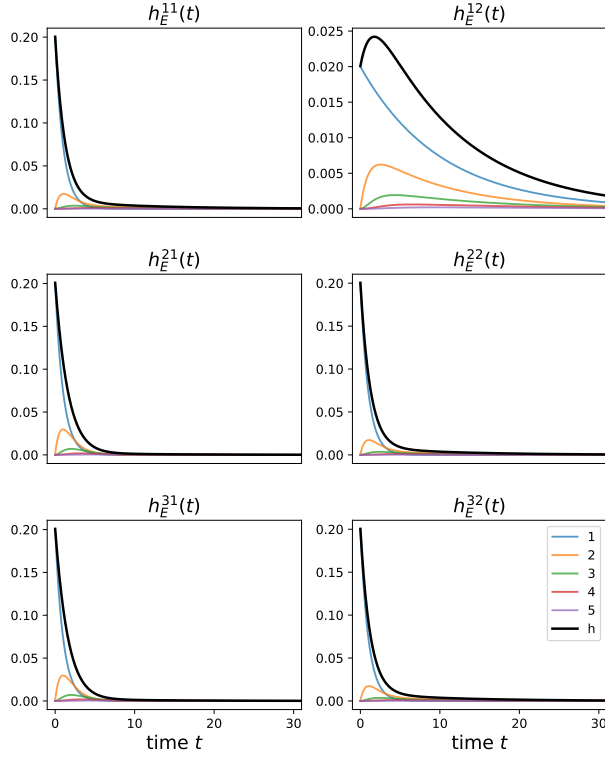


Figure 1: Nonzero entries of  $\mathbf{h}_E(t)$  for a PCMHP(3,2) process with parameter set  $\boldsymbol{\theta} = [1, 0.1, 0, 1, 1, 0, 1, 1, 0]$ ,  $\boldsymbol{\alpha} = [0.2, 0.2, 0, 0.2, 0.2, 0, 0.2, 0.2, 0]$ . Colored lines correspond to the contribution of the first up to the fifth generation offsprings to  $\mathbf{h}_E(t)$ . The black line ( $\mathbf{h}_E(t)$ ) is the total contribution of the progeny.

Given a fixed event sequence for dimension 2  $\{t_1^2 < t_2^2 < \dots < t_N^2\}$  prior to time  $t$ , the intensity function given by  $\xi_1^1(t \mid \mathcal{H}_t^1)$  can be interpreted as a univariate MBP process. Assuming an exponential kernel, the intensity function in this case can be expressed in closed form using the impulse response function.

Suppose that  $\varphi^{ij}(x) = \alpha^{ij}\theta^{ij} \exp(-\theta^{ij}x)$ . The impulse response for  $\xi_1^1(t \mid \mathcal{H}_t^2)$  is given by:

$$E_1(t) = \delta(t) + h(t), \tag{11}$$

where

$$h(t) = \alpha^{11}\theta^{11} \exp((\alpha^{11} - 1)\theta^{11}t) \cdot \llbracket t \geq 1 \rrbracket. \tag{12}$$

Setting  $\hat{s}(t) = \left[ \mu^1 + \sum_{t_k^2 < t} \alpha^{12} \theta^{12} \exp(-\theta^{12}(t - t_k^2)) \right]$ ,

$$\xi_1^1(t | \mathcal{H}_t^2) = (E_1 * \hat{s})(t) = \hat{s}(t) + (h * \hat{s})(t). \quad (13)$$

$$\begin{aligned} & (h * \hat{s})(t) \\ &= \int_1^t h(t - \tau) \cdot \hat{s}(\tau) d\tau \\ &= \int_1^t \alpha^{11} \theta^{11} \exp((\alpha^{11} - 1)\theta^{11}(t - \tau)) \cdot \hat{s}(\tau) d\tau \\ &= \int_1^t \alpha^{11} \theta^{11} \exp((\alpha^{11} - 1)\theta^{11}(t - \tau)) \cdot \left[ \mu^1 + \sum_{t_k^2 < \tau} \alpha^{12} \theta^{12} \exp(-\theta^{12}(\tau - t_k^2)) \right] d\tau \\ &= \mu^1 \int_1^t \alpha^{11} \theta^{11} \exp((\alpha^{11} - 1)\theta^{11}(t - \tau)) d\tau \\ &\quad + \int_1^t \alpha^{11} \theta^{11} \exp((\alpha^{11} - 1)\theta^{11}(t - \tau)) \cdot \left[ \sum_{t_k^2 < \tau} \alpha^{12} \theta^{12} \exp(-\theta^{12}(\tau - t_k^2)) \right] d\tau \\ &= \mu^1 \alpha^{11} \theta^{11} \int_1^t \exp((\alpha^{11} - 1)\theta^{11}(t - \tau)) d\tau \\ &\quad + \alpha^{11} \theta^{11} \alpha^{12} \theta^{12} \int_1^t \exp((\alpha^{11} - 1)\theta^{11}(t - \tau)) \cdot \left[ \sum_{t_k^2 < \tau} \exp(-\theta^{12}(\tau - t_k^2)) \right] d\tau. \end{aligned}$$

We calculate each of the integral terms separately:

$$\begin{aligned} & \int_1^t \exp((\alpha^{11} - 1)\theta^{11}(t - \tau)) d\tau \\ &= -\frac{1}{(\alpha^{11} - 1)\theta^{11}} \exp((\alpha^{11} - 1)\theta^{11}(t - \tau)) \Big|_{\tau=1}^{\tau=t} \\ &= \frac{1}{(\alpha^{11} - 1)\theta^{11}} [\exp((\alpha^{11} - 1)\theta^{11}t) - 1]. \end{aligned}$$

And,

$$\begin{aligned}
& \int_1^t \exp((\alpha^{11} - 1)\theta^{11}(t - \tau)) \cdot \left[ \sum_{t_k^2 < \tau} \exp(-\theta^{12}(\tau - t_k^2)) \right] d\tau \\
&= \sum_{k=1}^N \int_{t_k^2}^t \exp((\alpha^{11} - 1)\theta^{11}(t - \tau)) \cdot \exp(-\theta^{12}(\tau - t_k^2)) d\tau \\
&= \sum_{k=1}^N \int_{t_k^2}^t \exp((\alpha^{11} - 1)\theta^{11}t) \cdot \exp(-(\alpha^{11} - 1)\theta^{11}\tau) \cdot \exp(-\theta^{12}\tau) \cdot \exp(\theta^{12}t_k^2) d\tau \\
&= \sum_{i=1}^N \exp((\alpha^{11} - 1)\theta^{11}t) \cdot \exp(\theta^{12}t_k^2) \cdot \int_{t_k^2}^t \exp(-(\alpha^{11} - 1)\theta^{11}\tau) \cdot \exp(-\theta^{12}\tau) d\tau \\
&= \sum_{i=1}^N \exp((\alpha^{11} - 1)\theta^{11}t) \cdot \exp(\theta^{12}t_k^2) \cdot \int_{t_k^2}^t \exp(-[(\alpha^{11} - 1)\theta^{11} + \theta^{12}]\tau) d\tau \\
&= \sum_{i=1}^N \frac{\exp((\alpha^{11} - 1)\theta^{11}t) \cdot \exp(\theta^{12}t_k^2)}{(\alpha^{11} - 1)\theta^{11} + \theta^{12}} \\
&\quad \cdot [\exp(-[(\alpha^{11} - 1)\theta^{11} + \theta^{12}]t_k^2) - \exp(-[(\alpha^{11} - 1)\theta^{11} + \theta^{12}]t)] \\
&= \sum_{i=1}^N \frac{\exp((\alpha^{11} - 1)\theta^{11}(t - t_k^2)) - \exp(-\theta^{12}(t - t_k^2))}{(\alpha^{11} - 1)\theta^{11} + \theta^{12}}
\end{aligned}$$

Together we have,

$$\begin{aligned}
(h * \hat{s})(t) &= \frac{\mu^1 \alpha^{11}}{\alpha^{11} - 1} [\exp((\alpha^{11} - 1)\theta^{11}t) - 1] \\
&\quad + \sum_{k=1}^N \frac{\alpha^{11} \theta^{11} \alpha^{12} \theta^{12}}{(\alpha^{11} - 1)\theta^{11} + \theta^{12}} [\exp((\alpha^{11} - 1)\theta^{11}(t - t_k^2)) - \exp(-\theta^{12}(t - t_k^2))].
\end{aligned}$$

This gives the MBP intensity function for dimension 1 as

$$\begin{aligned}
\xi_1^1(t | \mathcal{H}_t^2) &= \mu^1 + \sum_{t_k^2 < t} \alpha^{12} \theta^{12} \exp(-\theta^{12}(t - t_k^2)) + \frac{\mu^1 \alpha^{11}}{\alpha^{11} - 1} [\exp((\alpha^{11} - 1)\theta^{11}t) - 1] \\
&\quad + \sum_{t_k^2 < t} \frac{\alpha^{11} \theta^{11} \alpha^{12} \theta^{12}}{(\alpha^{11} - 1)\theta^{11} + \theta^{12}} [\exp((\alpha^{11} - 1)\theta^{11}(t - t_k^2)) - \exp(-\theta^{12}(t - t_k^2))].
\end{aligned} \tag{14}$$

To calculate the MBP intensity function  $\xi_1^2$  for dimension 2, we would need to calculate

$$(\varphi^{21} * \xi_1^1)(t) = \alpha^{21} \theta^{21} \int_1^t \exp(-\theta^{21}(t - \tau)) \xi_1^1(\tau | \mathcal{H}_\tau^2) d\tau.$$

We expand the integrand above using the expression for  $\xi_1^1$  in Eq. (15) and calculate the integral term-by-term.

$$\begin{aligned}
\int_1^t \exp(-\theta^{21}(t-\tau))\mu^1 d\tau &= \mu^1 \int_1^t \exp(-\theta^{21}(t-\tau))d\tau \\
&= -\frac{\mu^1}{\theta^{21}} \exp(-\theta^{21}(t-\tau)) \Big|_{\tau=1}^{\tau=t} \\
&= \frac{\mu^1}{\theta^{21}} [2 - \exp(-\theta^{21}(t))].
\end{aligned}$$

$$\begin{aligned}
&\int_2^t \exp(-\theta^{21}(t-\tau))\frac{\mu^1\alpha^{11}}{\alpha^{11}-1} [\exp((\alpha^{11}-1)\theta^{11}\tau) - 1] d\tau \\
&= \frac{\mu^1\alpha^{11}}{\alpha^{11}-1} \int_1^t \exp(-\theta^{21}(t-\tau)) [\exp((\alpha^{11}-1)\theta^{11}\tau) - 1] d\tau \\
&= \frac{\mu^2\alpha^{11}}{\alpha^{11}-1} \exp(-\theta^{21}t) \int_1^t \exp(\theta^{21}\tau) [\exp((\alpha^{11}-1)\theta^{11}\tau) - 1] d\tau \\
&= \frac{\mu^1\alpha^{11}}{\alpha^{11}-1} \exp(-\theta^{21}t) \left[ \int_1^t \exp((\theta^{21} + (\alpha^{11}-1)\theta^{11})\tau)d\tau - \int_1^t \exp(\theta^{21}\tau)d\tau \right] \\
&= \frac{\mu^1\alpha^{11}}{\alpha^{11}-1} \exp(-\theta^{21}t) \left[ \frac{\exp((\theta^{21} + (\alpha^{11}-1)\theta^{11})t) - 1}{\theta^{21} + (\alpha^{11}-1)\theta^{11}} - \frac{\exp(\theta^{21}t) - 1}{\theta^{21}} \right].
\end{aligned}$$

For the remaining two terms in the integral, we need to consider two cases:  $\theta^{21} = \theta^{12}$  and  $\theta^{21} \neq \theta^{12}$ .

Case 1:  $\theta^{21} = \theta^{12}$ .

$$\begin{aligned}
& \int_1^t \exp(-\theta^{21}(t-\tau)) \sum_{t_k^2 < t} \alpha^{12} \theta^{12} \exp(-\theta^{12}(\tau-t_k^2)) d\tau \\
&= \alpha^{12} \theta^{12} \int_1^t \exp(-\theta^{21}(t-\tau)) \sum_{t_k^2 < t} \exp(-\theta^{12}(\tau-t_k^2)) d\tau \\
&= \alpha^{12} \theta^{12} \sum_{k=1}^N \int_{t_k^2}^t \exp(-\theta^{21}(t-\tau)) \exp(-\theta^{12}(\tau-t_k^2)) d\tau \\
&= \alpha^{12} \theta^{12} \sum_{k=1}^N \exp(\theta^{12}t_k^2 - \theta^{21}t) \int_{t_k^2}^t \exp((\theta^{21} - \theta^{12})\tau) d\tau \\
&= \alpha^{12} \theta^{12} \sum_{k=1}^N \exp(\theta^{12}t_k^2 - \theta^{21}t) \int_{t_k^2}^t d\tau \\
&= \alpha^{12} \theta^{12} \sum_{k=1}^N \exp(\theta^{12}t_k^2 - \theta^{21}t) (t - t_k^2)
\end{aligned}$$



$$\begin{aligned}
& \int_1^t \exp(-\theta^{21}(t-\tau)) \sum_{t_k^2 < \tau} \frac{\alpha^{11}\theta^{11}\alpha^{12}\theta^{12}}{(\alpha^{11}-1)\theta^{11} + \theta^{12}} \\
& \quad \left[ \exp((\alpha^{11}-1)\theta^{11}(\tau-t_k^2)) - \exp(-\theta^{12}(\tau-t_k^2)) \right] d\tau \\
&= \frac{\alpha^{11}\theta^{11}\alpha^{12}\theta^{12}}{(\alpha^{11}-1)\theta^{11} + \theta^{12}} \int_1^t \exp(-\theta^{21}(t-\tau)) \\
& \quad \sum_{t_k^2 < \tau} \left[ \exp((\alpha^{11}-1)\theta^{11}(\tau-t_k^2)) - \exp(-\theta^{12}(\tau-t_k^2)) \right] d\tau \\
&= \frac{\alpha^{11}\theta^{11}\alpha^{12}\theta^{12}}{(\alpha^{11}-1)\theta^{11} + \theta^{12}} \int_1^t \sum_{t_k^2 < \tau} \exp(-\theta^{21}(t-\tau)) \\
& \quad \left[ \exp((\alpha^{11}-1)\theta^{11}(\tau-t_k^2)) - \exp(-\theta^{12}(\tau-t_k^2)) \right] d\tau \\
&= \frac{\alpha^{11}\theta^{11}\alpha^{12}\theta^{12}}{(\alpha^{11}-1)\theta^{11} + \theta^{12}} \sum_{k=1}^N \exp(-\theta^{21}t) \int_{t_k^2}^t \exp(\theta^{21}\tau) \\
& \quad \left[ \exp((\alpha^{11}-1)\theta^{11}(\tau-t_k^2)) - \exp(-\theta^{12}(\tau-t_k^2)) \right] d\tau \\
&= \frac{\alpha^{11}\theta^{11}\alpha^{12}\theta^{12}}{(\alpha^{11}-1)\theta^{11} + \theta^{12}} \sum_{k=1}^N \exp(-\theta^{21}t) \\
& \quad \left[ \exp(-(\alpha^{11}-1)\theta^{11}t_k^2) \int_{t_k^2}^t \exp(\theta^{21}\tau) \exp((\alpha^{11}-1)\theta^{11}\tau) d\tau \right. \\
& \quad \left. - \exp(\theta^{12}t_k^2) \int_{t_k^2}^t \exp(\theta^{21}\tau) \exp(-\theta^{12}\tau) d\tau \right] \\
&= \frac{\alpha^{11}\theta^{11}\alpha^{12}\theta^{12}}{(\alpha^{11}-1)\theta^{11} + \theta^{12}} \sum_{k=1}^N \exp(-\theta^{21}t) \\
& \quad \left[ \exp(-(\alpha^{11}-1)\theta^{11}t_k^2) \int_{t_k^2}^t \exp((\theta^{21} + (\alpha^{11}-1)\theta^{11})\tau) d\tau \right. \\
& \quad \left. - \exp(\theta^{12}t_k^2) \int_{t_k^2}^t \exp((\theta^{21} - \theta^{12})\tau) d\tau \right] \\
&= \frac{\alpha^{11}\theta^{11}\alpha^{12}\theta^{12}}{(\alpha^{11}-1)\theta^{11} + \theta^{12}} \sum_{k=1}^N \exp(-\theta^{21}t) \\
& \quad \left[ \exp(-(\alpha^{11}-1)\theta^{11}t_k^2) \int_{t_k^2}^t \exp((\theta^{21} + (\alpha^{11}-1)\theta^{11})\tau) d\tau - \exp(\theta^{12}t_k^2) \int_{t_k^2}^t d\tau \right] \\
&= \frac{\alpha^{11}\theta^{11}\alpha^{12}\theta^{12}}{(\alpha^{11}-1)\theta^{11} + \theta^{12}} \sum_{k=1}^N \left[ \frac{\exp((\alpha^{11}-1)\theta^{11}(t-t_k^2))}{\theta^{21} + (\alpha^{11}-1)\theta^{11}} - \frac{\exp(-\theta^{21}(t-t_k^2))}{\theta^{21} + (\alpha^{11}-1)\theta^{11}} \right. \\
& \quad \left. - \exp(\theta^{12}t_k^2 - \theta^{21}t)(t-t_k^2) \right]. \quad 14
\end{aligned}$$

Case 2:  $\theta^{21} \neq \theta^{12}$ .

$$\begin{aligned}
& \int_1^t \exp(-\theta^{21}(t-\tau)) \sum_{t_k^2 < t} \alpha^{12} \theta^{12} \exp(-\theta^{12}(\tau-t_k^2)) d\tau \\
&= \alpha^{12} \theta^{12} \int_1^t \exp(-\theta^{21}(t-\tau)) \sum_{t_k^2 < t} \exp(-\theta^{12}(\tau-t_k^2)) d\tau \\
&= \alpha^{12} \theta^{12} \sum_{k=1}^N \int_{t_k^2}^t \exp(-\theta^{21}(t-\tau)) \exp(-\theta^{12}(\tau-t_k^2)) d\tau \\
&= \alpha^{12} \theta^{12} \sum_{k=1}^N \exp(\theta^{12}t_k^2 - \theta^{21}t) \int_{t_k^2}^t \exp((\theta^{21} - \theta^{12})\tau) d\tau \\
&= \frac{\alpha^{12} \theta^{12}}{\theta^{21} - \theta^{12}} \sum_{k=1}^N \exp(\theta^{12}t_k^2 - \theta^{21}t) [\exp((\theta^{21} - \theta^{12})t) - \exp((\theta^{21} - \theta^{12})t_k^2)] \\
&= \frac{\alpha^{12} \theta^{12}}{\theta^{21} - \theta^{12}} \sum_{k=1}^N [\exp(-\theta^{12}(t-t_k^2)) - \exp(-\theta^{21}(t-t_k^2))] .
\end{aligned}$$

$$\begin{aligned}
& \int_1^t \exp(-\theta^{21}(t-\tau)) \sum_{t_k^2 < \tau} \frac{\alpha^{11}\theta^{11}\alpha^{12}\theta^{12}}{(\alpha^{11}-1)\theta^{11} + \theta^{12}} \left[ \exp((\alpha^{11}-1)\theta^{11}(\tau-t_k^2)) - \exp(-\theta^{12}(\tau-t_k^2)) \right] d\tau \\
&= \frac{\alpha^{11}\theta^{11}\alpha^{12}\theta^{12}}{(\alpha^{11}-1)\theta^{11} + \theta^{12}} \int_1^t \exp(-\theta^{21}(t-\tau)) \sum_{t_k^2 < \tau} \left[ \exp((\alpha^{11}-1)\theta^{11}(\tau-t_k^2)) - \exp(-\theta^{12}(\tau-t_k^2)) \right] d\tau \\
&= \frac{\alpha^{11}\theta^{11}\alpha^{12}\theta^{12}}{(\alpha^{11}-1)\theta^{11} + \theta^{12}} \int_1^t \sum_{t_k^2 < \tau} \exp(-\theta^{21}(t-\tau)) \left[ \exp((\alpha^{11}-1)\theta^{11}(\tau-t_k^2)) - \exp(-\theta^{12}(\tau-t_k^2)) \right] d\tau \\
&= \frac{\alpha^{11}\theta^{11}\alpha^{12}\theta^{12}}{(\alpha^{11}-1)\theta^{11} + \theta^{12}} \sum_{k=1}^N \int_{t_i^1}^t \exp(-\theta^{21}(t-\tau)) \left[ \exp((\alpha^{11}-1)\theta^{11}(\tau-t_k^2)) - \exp(-\theta^{12}(\tau-t_k^2)) \right] d\tau \\
&= \frac{\alpha^{11}\theta^{11}\alpha^{12}\theta^{12}}{(\alpha^{11}-1)\theta^{11} + \theta^{12}} \sum_{k=1}^N \exp(-\theta^{21}t) \int_{t_k^2}^t \exp(\theta^{21}\tau) \left[ \exp((\alpha^{11}-1)\theta^{11}(\tau-t_k^2)) - \exp(-\theta^{12}(\tau-t_k^2)) \right] d\tau \\
&= \frac{\alpha^{11}\theta^{11}\alpha^{12}\theta^{12}}{(\alpha^{11}-1)\theta^{11} + \theta^{12}} \sum_{k=1}^N \exp(-\theta^{21}t) \left[ \exp(-(\alpha^{11}-1)\theta^{11}t_k^2) \int_{t_k^2}^t \exp(\theta^{21}\tau) \exp((\alpha^{11}-1)\theta^{11}\tau) d\tau \right. \\
&\quad \left. - \exp(\theta^{12}t_k^2) \int_{t_k^2}^t \exp(\theta^{21}\tau) \exp(-\theta^{12}\tau) d\tau \right] \\
&= \frac{\alpha^{11}\theta^{11}\alpha^{12}\theta^{12}}{(\alpha^{11}-1)\theta^{11} + \theta^{12}} \sum_{k=1}^N \exp(-\theta^{21}t) \left[ \exp(-(\alpha^{11}-1)\theta^{11}t_k^2) \int_{t_k^2}^t \exp((\theta^{21} + (\alpha^{11}-1)\theta^{11})\tau) d\tau \right. \\
&\quad \left. - \exp(\theta^{12}t_k^2) \int_{t_k^2}^t \exp((\theta^{21} - \theta^{12})\tau) d\tau \right] \\
&= \frac{\alpha^{11}\theta^{11}\alpha^{12}\theta^{12}}{(\alpha^{11}-1)\theta^{11} + \theta^{12}} \sum_{k=1}^N \exp(-\theta^{21}t) \left[ \frac{\exp(-(\alpha^{11}-1)\theta^{11}t_k^2)}{\theta^{21} + (\alpha^{11}-1)\theta^{11}} \left[ \exp((\theta^{21} + (\alpha^{11}-1)\theta^{11})t) \right. \right. \\
&\quad \left. \left. - \exp((\theta^{21} + (\alpha^{11}-1)\theta^{11})t_k^2) \right] - \frac{\exp(\theta^{12}t_k^2)}{\theta^{21} - \theta^{12}} \left[ \exp((\theta^{21} - \theta^{12})t) - \exp((\theta^{21} - \theta^{12})t_k^2) \right] \right] \\
&= \frac{\alpha^{11}\theta^{11}\alpha^{12}\theta^{12}}{(\alpha^{11}-1)\theta^{11} + \theta^{12}} \sum_{k=1}^N \left[ \frac{\exp((\alpha^{11}-1)\theta^{11}(t-t_k^2))}{\theta^{21} + (\alpha^{11}-1)\theta^{11}} - \frac{\exp(-\theta^{21}(t-t_k^2))}{\theta^{21} + (\alpha^{11}-1)\theta^{11}} - \frac{\exp(-\theta^{12}(t-t_k^2))}{\theta^{21} - \theta^{12}} \right. \\
&\quad \left. + \frac{\exp(-\theta^{21}(t-t_k^2))}{\theta^{21} - \theta^{12}} \right].
\end{aligned}$$

Therefore, if  $\theta^{21} = \theta^{12}$ ,

$$\begin{aligned}
\xi_1^2(t | \mathcal{H}_t^2) &= \mu^2 + \sum_{k=1}^N \alpha^{22} \theta^{22} \exp(-\theta^{22}(t - t_k^2)) + \mu^1 \alpha^{21} [2 - \exp(-\theta^{21}(t))] \\
&+ \alpha^{12} \theta^{12} \alpha^{21} \theta^{21} \sum_{k=1}^N \exp(\theta^{12} t_k^2 - \theta^{21} t)(t - t_k^2) \\
&+ \frac{\mu^1 \alpha^{11} \alpha^{21} \theta^{21}}{\alpha^{11} - 1} \left[ \frac{\exp((\alpha^{11} - 1)\theta^{11} t) - \exp(-\theta^{21} t)}{\theta^{21} + (\alpha^{11} - 1)\theta^{11}} - \frac{2 - \exp(-\theta^{21} t)}{\theta^{21}} \right] \\
&+ \frac{\alpha^{11} \theta^{11} \alpha^{12} \theta^{12} \alpha^{21} \theta^{21}}{(\alpha^{11} - 1)\theta^{11} + \theta^{12}} \sum_{k=1}^N \left[ \frac{\exp((\alpha^{11} - 1)\theta^{11}(t - t_k^2))}{\theta^{21} + (\alpha^{11} - 1)\theta^{11}} \right. \\
&\quad \left. - \frac{\exp(-\theta^{21}(t - t_k^2))}{\theta^{21} + (\alpha^{11} - 1)\theta^{11}} - \exp(\theta^{12} t_k^2 - \theta^{21} t)(t - t_k^2) \right].
\end{aligned}$$

If  $\theta^{21} \neq \theta^{12}$ ,

$$\begin{aligned}
\xi_1^2(t | \mathcal{H}_t^2) &= \mu^2 + \sum_{k=1}^N \alpha^{22} \theta^{22} \exp(-\theta^{22}(t - t_k^2)) + \mu^1 \alpha^{21} [2 - \exp(-\theta^{21}(t))] \\
&+ \frac{\alpha^{12} \theta^{12} \alpha^{21} \theta^{21}}{\theta^{21} - \theta^{12}} \sum_{k=1}^N [\exp(-\theta^{12}(t - t_k^2)) - \exp(-\theta^{21}(t - t_k^2))] \\
&+ \frac{\mu^1 \alpha^{11} \alpha^{21} \theta^{21}}{\alpha^{11} - 1} \left[ \frac{\exp((\alpha^{11} - 1)\theta^{11} t) - \exp(-\theta^{21} t)}{\theta^{21} + (\alpha^{11} - 1)\theta^{11}} - \frac{2 - \exp(-\theta^{21} t)}{\theta^{21}} \right] \\
&+ \frac{\alpha^{11} \theta^{11} \alpha^{12} \theta^{12} \alpha^{21} \theta^{21}}{(\alpha^{11} - 1)\theta^{11} + \theta^{12}} \sum_{k=1}^N \left[ \frac{\exp((\alpha^{11} - 1)\theta^{11}(t - t_k^2))}{\theta^{21} + (\alpha^{11} - 1)\theta^{11}} \right. \\
&\quad \left. - \frac{\exp(-\theta^{21}(t - t_k^2))}{\theta^{21} + (\alpha^{11} - 1)\theta^{11}} - \frac{\exp(-\theta^{12}(t - t_k^2))}{\theta^{21} - \theta^{12}} + \frac{\exp(-\theta^{21}(t - t_k^2))}{\theta^{21} - \theta^{12}} \right].
\end{aligned}$$

Integrating  $\xi_1^1(t | \mathcal{H}_t^2)$  and  $\xi_1^2(t | \mathcal{H}_t^2)$  over the interval  $[1, T]$ , we obtain the compensator

as (Take note that integrals over the exponentials are from  $t_2^k$  to  $t$ )

$$\begin{aligned}
\Xi_1^1(t | \mathcal{H}_t^2) &= \mu^1 t + \sum_{t_k^2 < t} \alpha^{12} (2 - \exp(-\theta^{12}(t - t_k^2))) \\
&+ \frac{\mu^1 \alpha^{11}}{\alpha^{11} - 1} \left[ \frac{1}{(\alpha^{11} - 1)\theta^{11}} (\exp((\alpha^{11} - 1)\theta^{11} t) - 1) - t \right] \\
&+ \sum_{t_k^2 < t} \frac{\alpha^{11} \theta^{11} \alpha^{12} \theta^{12}}{(\alpha^{11} - 1)\theta^{11} + \theta^{12}} \left[ \frac{\exp((\alpha^{11} - 1)\theta^{11}(t - t_k^2)) - 1}{(\alpha^{11} - 1)\theta^{11}} - \frac{2 - \exp(-\theta^{12}(t - t_k^2))}{\theta^{12}} \right]. \quad (15)
\end{aligned}$$

If  $\theta^{21} = \theta^{12}$ ,

$$\begin{aligned}
\Xi_1^2(t | \mathcal{H}_t^2) &= \mu^2 t + \sum_{k=1}^N \alpha^{22} (2 - \exp(-\theta^{22}(t - t_2^k))) + \mu^1 \alpha^{21} \left[ t - \frac{1}{\theta^{21}} (2 - \exp(-\theta^{21}t)) \right] \\
&+ \frac{\alpha^{12} \theta^{12} \alpha^{21}}{\theta^{21}} \sum_{k=1}^N \exp(\theta^{12} t_k^2 - \theta^{21}(t_k^2 + t)) \left[ \exp(\theta^{21} t_k^2) (\theta^{21} t_k^2 - \theta^{21} t - 1) + \exp(\theta^{21} t) \right] \\
&+ \frac{\mu^1 \alpha^{11} \alpha^{21} \theta^{21}}{\alpha^{11} - 1} \left[ \frac{1}{\theta^{21} + (\alpha^{11} - 1) \theta^{11}} \left( \frac{\exp(((\alpha^{11} - 1) \theta^{11})t) - 2}{(\alpha^{11} - 1) \theta^{11}} + \frac{\exp(-\theta^{21}t) - 1}{\theta^{21}} \right) \right. \\
&\quad \left. - \left( \frac{t}{\theta^{21}} + \frac{\exp(-\theta^{21}t) - 1}{(\theta^{21})^2} \right) \right] \\
&+ \frac{\alpha^{11} \theta^{11} \alpha^{12} \theta^{12} \alpha^{21} \theta^{21}}{(\alpha^{11} - 1) \theta^{11} + \theta^{12}} \sum_{k=1}^N \left[ \frac{\exp((\alpha^{11} - 1) \theta^{11}(t - t_2^k)) - 2}{(\theta^{21} + (\alpha^{11} - 1) \theta^{11})(\alpha^{11} - 1) \theta^{11}} \right. \\
&\quad \left. + \frac{\exp(-\theta^{21}(t - t_2^k)) - 2}{(\theta^{21} + (\alpha^{11} - 1) \theta^{11}) \theta^{21}} - \frac{1}{(\theta^{21})^2} \exp(\theta^{12} t_k^2 - \theta^{21}(t_k^2 + t)) \right. \\
&\quad \left. \left[ \exp(\theta^{21} t_k^2) (\theta^{21} t_k^2 - \theta^{21} t - 1) + \exp(\theta^{21} t) \right] \right].
\end{aligned}$$

If  $\theta^{21} \neq \theta^{12}$ ,

$$\begin{aligned}
\Xi_1^2(t | \mathcal{H}_t^2) &= \mu^2 t + \sum_{k=1}^N \alpha^{22} (2 - \exp(-\theta^{22}(t - t_2^k))) + \mu^1 \alpha^{21} \left[ t - \frac{1}{\theta^{21}} (2 - \exp(-\theta^{21}t)) \right] \\
&+ \frac{\alpha^{12} \theta^{12} \alpha^{21} \theta^{21}}{\theta^{21} - \theta^{12}} \sum_{k=1}^N \left[ \frac{2 - \exp(-\theta^{12}(t - t_2^k))}{\theta^{12}} - \frac{2 - \exp(-\theta^{21}(t - t_2^k))}{\theta^{21}} \right] \\
&+ \frac{\mu^1 \alpha^{11} \alpha^{21} \theta^{21}}{\alpha^{11} - 1} \left[ \frac{1}{\theta^{21} + (\alpha^{11} - 1) \theta^{11}} \left( \frac{\exp(((\alpha^{11} - 1) \theta^{11})t) - 2}{(\alpha^{11} - 1) \theta^{11}} \right. \right. \\
&\quad \left. \left. + \frac{\exp(-\theta^{21}t) - 1}{\theta^{21}} \right) - \left( \frac{t}{\theta^{21}} + \frac{\exp(-\theta^{21}t) - 1}{(\theta^{21})^2} \right) \right] \\
&+ \frac{\alpha^{11} \theta^{11} \alpha^{12} \theta^{12} \alpha^{21} \theta^{21}}{(\alpha^{11} - 1) \theta^{11} + \theta^{12}} \sum_{k=1}^N \left[ \frac{\exp((\alpha^{11} - 1) \theta^{11}(t - t_2^k)) - 2}{(\theta^{21} + (\alpha^{11} - 1) \theta^{11})(\alpha^{11} - 1) \theta^{11}} \right. \\
&\quad - \frac{2 - \exp(-\theta^{21}(t - t_2^k))}{(\theta^{21} + (\alpha^{11} - 1) \theta^{11}) \theta^{21}} - \frac{1}{\theta^{21} - \theta^{12}} \left[ \frac{2 - \exp(-\theta^{12}(t - t_2^k))}{\theta^{12}} \right. \\
&\quad \left. \left. - \frac{2 - \exp(-\theta^{21}(t - t_2^k))}{\theta^{21}} \right] \right].
\end{aligned}$$

## 4 Additional Results and Proofs for Section II.B

## 4.1 Convolutional Formula

**Lemma 7** Consider  $\text{PCMHP}(d, e)$  with conditional intensity  $\boldsymbol{\xi}_E(t)$  and  $\mathbf{N}(t)$  be the counting process of the corresponding  $d$ -dimensional Hawkes process. The following holds:

$$\boldsymbol{\xi}_E(s)ds = \mathbb{E}_{\mathcal{H}_{s^-}^E} \left[ d\mathbf{N}(s) \middle| \mathcal{H}_{s^-}^{E^c} \right]. \quad (16)$$

**Proof** Taking the conditional expectation over  $\mathcal{H}_{s^-}^E$  of both sides of Eq. (1), we get

$$\mathbb{E}_{\mathcal{H}_{s^-}^E} \left[ \boldsymbol{\lambda}^*(s)ds \middle| \mathcal{H}_{s^-}^{E^c} \right] = \mathbb{E}_{\mathcal{H}_{s^-}^E} \left[ \mathbb{E} \left[ d\mathbf{N}(s) \middle| \mathcal{H}_{s^-}^D \right] \middle| \mathcal{H}_{s^-}^{E^c} \right]$$

Pulling out the infinitesimal  $ds$  out of the expectation on the left-hand side, we get

$$\mathbb{E}_{\mathcal{H}_{s^-}^E} \left[ \boldsymbol{\lambda}^*(s) \middle| \mathcal{H}_{s^-}^{E^c} \right] ds = \mathbb{E}_{\mathcal{H}_{s^-}^E} \left[ \mathbb{E} \left[ d\mathbf{N}(s) \middle| \mathcal{H}_{s^-}^D \right] \middle| \mathcal{H}_{s^-}^{E^c} \right]$$

Notice that the left-hand side is exactly  $\boldsymbol{\xi}_E(t)$ , as defined in Main Text Equation 4. For the right-hand side, note that  $\mathcal{H}_{s^-}^D = (\mathcal{H}_{s^-}^E) \cup (\mathcal{H}_{s^-}^{E^c})$ . Applying the tower property of conditional expectation, we average out the inner conditioning over  $\mathcal{H}_{s^-}^E$  and arrive at the desired result:

$$\boldsymbol{\xi}_E(s)ds = \mathbb{E}_{\mathcal{H}_{s^-}^E} \left[ d\mathbf{N}(s) \middle| \mathcal{H}_{s^-}^{E^c} \right].$$

■

**Remark 8** Lemma 7 extends the result in Eq. (1) for the  $d$ -dimensional Hawkes process, to the partial multivariate case considered by the  $\text{PCMHP}(d, e)$  process. To go from Eq. (1) to Eq. (16), we simply replace the total expectation with the conditional expectation over event histories in the  $E$  dimensions.

The following theorem provides an expression for the conditional intensity  $\boldsymbol{\xi}_E(t)$  of a  $\text{PCMHP}(d, e)$  process in terms of the Hawkes kernel  $\boldsymbol{\varphi}(t)$  and the background intensity  $\boldsymbol{\mu}(t)$ .

**Theorem 9** *Given the Hawkes process with the kernel  $\varphi(t)$  and the background intensity  $\boldsymbol{\mu}(t)$ , the conditional intensity of its corresponding PCMHP( $d, e$ ) process is given by*

$$\boldsymbol{\xi}_E(t) = \boldsymbol{\mu}(t) + (\boldsymbol{\varphi}_E * \boldsymbol{\xi}_E)(t) + \sum_{j \in E^c} \sum_{t_k^j < t} \boldsymbol{\varphi}^j(t - t_k^j). \quad (17)$$

**Proof** Starting from the PCMHP definition (Eq. (4) in the main text), we expand  $\boldsymbol{\lambda}^*(t)$  as shown below.

$$\boldsymbol{\xi}_E(t) = \mathbb{E}_{\mathcal{H}_{t^-}^E} \left[ \boldsymbol{\mu}(t) + \int_0^{t^-} \boldsymbol{\varphi}(t-s) \cdot d\mathbf{N}(s) \middle| \mathcal{H}_{t^-}^{E^c} \right].$$

The exogenous term  $\boldsymbol{\mu}(t)$  is independent of the conditioning and may be taken out. We then use the decomposition of  $\boldsymbol{\varphi}$  as  $\boldsymbol{\varphi}_E + \boldsymbol{\varphi}_{E^c}$ . We then have

$$\boldsymbol{\xi}_E(t) = \boldsymbol{\mu}(t) + \mathbb{E}_{\mathcal{H}_{t^-}^E} \left[ \int_0^{t^-} \boldsymbol{\varphi}_E(t-s) \cdot d\mathbf{N}(s) + \int_0^{t^-} \boldsymbol{\varphi}_{E^c}(t-s) \cdot d\mathbf{N}(s) \middle| \mathcal{H}_{t^-}^{E^c} \right].$$

Given that the conditioning assumes that events in  $\mathcal{H}_{t^-}^{E^c}$  are observed, we can write the integral involving  $\boldsymbol{\varphi}_{E^c}$  as a sum of events in the  $E^c$  dimensions. We then have the following sequence of calculations.

$$\begin{aligned} \boldsymbol{\xi}_E(t) &= \boldsymbol{\mu}(t) + \mathbb{E}_{\mathcal{H}_{t^-}^E} \left[ \int_0^{t^-} \boldsymbol{\varphi}_E(t-s) \cdot d\mathbf{N}(s) + \sum_{j \in E^c} \sum_{t_k^j < t} \boldsymbol{\varphi}_{E^c}(t-t_k^j) \middle| \mathcal{H}_{t^-}^{E^c} \right] \\ &\stackrel{(a)}{=} \boldsymbol{\mu}(t) + \mathbb{E}_{\mathcal{H}_{t^-}^E} \left[ \int_0^{t^-} \boldsymbol{\varphi}_E(t-s) \cdot d\mathbf{N}(s) \middle| \mathcal{H}_{t^-}^{E^c} \right] + \sum_{j \in E^c} \sum_{t_k^j < t} \boldsymbol{\varphi}_{E^c}(t-t_k^j) \\ &\stackrel{(b)}{=} \boldsymbol{\mu}(t) + \int_0^{t^-} \boldsymbol{\varphi}_E(t-s) \cdot \mathbb{E}_{\mathcal{H}_{t^-}^E} \left[ d\mathbf{N}(s) \middle| \mathcal{H}_{t^-}^{E^c} \right] + \sum_{j \in E^c} \sum_{t_k^j < t} \boldsymbol{\varphi}_{E^c}(t-t_k^j) \\ &\stackrel{(c)}{=} \boldsymbol{\mu}(t) + \int_0^{t^-} \boldsymbol{\varphi}_E(t-s) \cdot \boldsymbol{\xi}_E(s) ds + \sum_{j \in E^c} \sum_{t_k^j < t} \boldsymbol{\varphi}_{E^c}(t-t_k^j) \\ &= \boldsymbol{\mu}(t) + (\boldsymbol{\varphi}_E * \boldsymbol{\xi}_E)(t) + \sum_{j \in E^c} \sum_{t_k^j < t} \boldsymbol{\varphi}_{E^c}(t-t_k^j). \end{aligned}$$

In (a), we take out the event intensity contributed by events in the dimensions in  $E^c$ , as these are observed in  $\mathcal{H}_{t^-}^{E^c}$ . In (b), we reverse the order of the integral over time and the

conditional expectation. In (c), we use Lemma 7. ■

**Proof** [of Main Text Theorem 2.] Our starting point is Section 4.1. First, note that the input-output map  $\boldsymbol{\mu}(t) \stackrel{\heartsuit}{\Rightarrow} \boldsymbol{\xi}_E(t)$  does not correspond to an LTI system (see the succeeding proof). However, if we define the effective input as

$$\mathbf{s}(t) := \boldsymbol{\mu}(t) + \sum_{j \in E^c} \sum_{t_k^j < t} \boldsymbol{\varphi}_{E^c}^j(t - t_k^j), \quad (18)$$

then the map  $\mathbf{s}(t) \stackrel{\heartsuit}{\Rightarrow} \boldsymbol{\xi}_E(t)$  given by

$$\boldsymbol{\xi}_E(t) = \mathbf{s}(t) + (\boldsymbol{\varphi}_E * \boldsymbol{\xi}_E)(t) \quad (19)$$

corresponds to an LTI system.

Let  $i \in D$  and  $\boldsymbol{\xi}_E(t)$  be the corresponding impulse response under  $\mathbf{s}(t) \stackrel{\heartsuit}{\Rightarrow} \boldsymbol{\xi}_E(t)$ . Suppose that  $\mathbf{E}^i(t)$  is the system's response to  $\boldsymbol{\delta}^i(t)$ , the unit impulse in dimension  $i$  given by the  $i^{\text{th}}$  column of the diagonal matrix  $\boldsymbol{\delta}(t)$ .

Applying Eq. (19) on the input-output pair  $(\boldsymbol{\delta}^i(t), \mathbf{E}^i(t))$ ,

$$\mathbf{E}^i(t) = \boldsymbol{\delta}^i(t) + (\boldsymbol{\varphi}_E * \mathbf{E}^i)(t). \quad (20)$$

Observe that Eq. (20) is a recursive equation in  $\mathbf{E}^i(t)$ . Substituting  $\mathbf{E}^i(t)$  back into itself, we get

$$\begin{aligned} \mathbf{E}^i(t) &= \boldsymbol{\delta}^i(t) + \boldsymbol{\varphi}_E(t) * [\boldsymbol{\delta}^i(t) + (\boldsymbol{\varphi}_E * \mathbf{E}^i)(t)] \\ &= \boldsymbol{\delta}^i(t) + \boldsymbol{\varphi}_E^i(t) + (\boldsymbol{\varphi}_E^{\otimes 2} * \mathbf{E}^i)(t) \\ &= \boldsymbol{\delta}^i(t) + \boldsymbol{\varphi}_E^i(t) + [\boldsymbol{\varphi}_E^{\otimes 2}]^i(t) + (\boldsymbol{\varphi}_E^{\otimes 3} * \mathbf{E}^i)(t) \\ &\vdots \\ &= \boldsymbol{\delta}^i(t) + \sum_{n=1}^{\infty} [\boldsymbol{\varphi}_E^{\otimes n}]^i(t) + \lim_{n \rightarrow \infty} (\boldsymbol{\varphi}_E^{\otimes n} * \mathbf{E}^i)(t). \end{aligned} \quad (21)$$



Note that  $\mathbf{s}(t)$  can be expressed as

$$\mathbf{s}(t) = \sum_{i=1}^d (\boldsymbol{\delta}^i * s^i)(t). \quad (22)$$

Since  $\mathbf{s}(t) \overset{\heartsuit}{\mapsto} \boldsymbol{\xi}_E(t)$  is LTI, we have

$$\boldsymbol{\xi}_E(t) = \sum_{i=1}^d (\mathbf{E}^i * s^i)(t). \quad (23)$$

Substituting Eq. (21) into Eq. (23), we then have

$$\boldsymbol{\xi}_E(t) = \sum_{i=1}^d \left[ \boldsymbol{\delta}^i(t) + \sum_{n=1}^{\infty} [\boldsymbol{\varphi}_E^{\otimes n}]^i(t) + \lim_{n \rightarrow \infty} (\boldsymbol{\varphi}_E^{\otimes n} * \mathbf{E}^i)(t) \right] * s^i(t). \quad (24)$$

We consider each convolution of the term in the right-hand side parenthesis separately.

The first term is precisely  $\mathbf{s}(t)$  in Eq. (22).

With some algebra (see succeeding proof), the second term can be written as

$$\sum_{i=1}^d \sum_{n=1}^{\infty} [\boldsymbol{\varphi}_E^{\otimes n}]^i(t) * s^i(t) = (\mathbf{h}_E * \mathbf{s})(t). \quad (25)$$

By commutativity of convolution, the third term can be written as

$$\sum_{i=1}^d \lim_{n \rightarrow \infty} (\boldsymbol{\varphi}_E^{\otimes n} * \mathbf{E}^i)(t) * s^i(t) = \lim_{n \rightarrow \infty} \boldsymbol{\varphi}_E^{\otimes n}(t) * \left[ \sum_{i=1}^d (\mathbf{E}^i * s^i)(t) \right] = \lim_{n \rightarrow \infty} (\boldsymbol{\varphi}_E^{\otimes n} * \boldsymbol{\xi}_E)(t),$$

where we made use of Eq. (23) to arrive at the last equality.

By combining the three terms, Eq. (24) can be written as

$$\boldsymbol{\xi}_E(t) = \mathbf{s}(t) + (\mathbf{h}_E * \mathbf{s})(t) + \lim_{n \rightarrow \infty} (\boldsymbol{\varphi}_E^{\otimes n} * \boldsymbol{\xi}_E)(t).$$

Imposing on the previous equation the assumption  $\lim_{n \rightarrow \infty} \boldsymbol{\varphi}_E^{\otimes n}(t) \rightarrow 0$ , we have

$$\boldsymbol{\xi}_E(t) = \mathbf{s}(t) + \left( \sum_{i=1}^d \boldsymbol{\varphi}_E^{\otimes n} * \mathbf{s} \right)(t). \quad (26)$$

Lastly, applying the specific form of  $\mathbf{s}(t)$  in Eq. (18), we obtain the desired formula. ■

**Proof** [in Proof of Main Text Theorem 2, that  $\boldsymbol{\mu}(t) \overset{\circ}{\Rightarrow} \boldsymbol{\xi}_E(t)$  is not LTI, but  $\mathbf{s}(t) \overset{\heartsuit}{\Rightarrow} \boldsymbol{\xi}_E(t)$  is.] Let  $c \in \mathbb{R}$ . Define  $\boldsymbol{\mu}'(t) = c\boldsymbol{\mu}(t)$  and  $\boldsymbol{\xi}'_E(t) = c\boldsymbol{\xi}_E(t)$ .

If the system were LTI, then linearity  $\boldsymbol{\mu}'(t) \overset{\circ}{\Rightarrow} \boldsymbol{\xi}'_E(t)$  must hold. That is, Eq. (17) tells us

$$\boldsymbol{\xi}'_E(t) = \boldsymbol{\mu}'(t) + (\boldsymbol{\varphi}_E * \boldsymbol{\xi}'_E)(t) + \sum_{j \in E^c} \sum_{t_k^j < t} \boldsymbol{\varphi}^j(t - t_k^j), \quad (27)$$

However, if we multiply both sides of Eq. (17) by  $c$ , we see that

$$\begin{aligned} c\boldsymbol{\xi}_E(t) &= c\boldsymbol{\mu}(t) + c(\boldsymbol{\varphi}_E * \boldsymbol{\xi}_E)(t) + c \sum_{j \in E^c} \sum_{t_k^j < t} \boldsymbol{\varphi}^j(t - t_k^j) \\ \Leftrightarrow \boldsymbol{\xi}'_E(t) &= \boldsymbol{\mu}'(t) + (\boldsymbol{\varphi}_E * \boldsymbol{\xi}'_E)(t) + c \sum_{j \in E^c} \sum_{t_k^j < t} \boldsymbol{\varphi}^j(t - t_k^j) \end{aligned} \quad (28)$$

Unless  $c = 1$  (trivial case) or  $d = e$ , Eq. (27) and Eq. (28) cannot hold simultaneously because of the summation over  $E^c$ .

Thus,  $\boldsymbol{\mu}(t) \overset{\circ}{\Rightarrow} \boldsymbol{\xi}_E(t)$  is not LTI unless  $e = d$ , which is the special case of an MBP process.

Now consider the system  $\mathbf{s}(t) \overset{\heartsuit}{\Rightarrow} \boldsymbol{\xi}_E(t)$  as defined in Eq. (18). The proof of this system being LTI is a straightforward multivariate extension of the proof of Theorem 2 in Rizoïu et al. (2022), but we present it here for completeness.

(Linearity) This follows simply by multiplying both sides of Eq. (17) by a constant  $c$ .

(Time invariance) The response of  $\mathbf{s}(t - t_0)$  under  $\mathbf{s}(t) \xrightarrow{\heartsuit} \boldsymbol{\xi}_E(t)$  is

$$\begin{aligned}
& \mathbf{s}(t - t_0) + \int_0^t \boldsymbol{\varphi}_E(t - t_0 - s) \cdot \boldsymbol{\xi}_E(s) ds \\
&= \mathbf{s}(t - t_0) + \int_0^{t'+t_0} \boldsymbol{\varphi}_E(t' - s) \cdot \boldsymbol{\xi}_E(s) ds \\
&\stackrel{(a)}{=} \mathbf{s}(t - t_0) + \int_0^{t'} \boldsymbol{\varphi}_E(t' - s) \cdot \boldsymbol{\xi}_E(s) ds + \int_{t'}^{t'+t_0} \boldsymbol{\varphi}_E(t' - s) \cdot \boldsymbol{\xi}_E(s) ds \\
&= \mathbf{s}(t - t_0) + (\boldsymbol{\varphi}_E * \boldsymbol{\xi}_E)(t - t_0) \\
&= \boldsymbol{\xi}_E(t - t_0),
\end{aligned}$$

where in (a) we used the fact that  $\boldsymbol{\varphi}_E(s) = 0$  if  $s < 0$ . Thus  $\mathbf{s}(t) \rightarrow \boldsymbol{\xi}_E(t)$  is LTI. ■

**Proof** [in Proof of Main Text Theorem 2, that  $\sum_{i=1}^d \sum_{n=1}^{\infty} [\boldsymbol{\varphi}_E^{\otimes n}]^i(t) * s^i(t) = \left( \sum_{i=1}^d \boldsymbol{\varphi}_E^{\otimes n}(t) * \mathbf{s} \right)(t)$ ]

$$\begin{aligned}
\sum_{i=1}^d \sum_{n=1}^{\infty} [\varphi_E^{\otimes n}]^i(t) * s^i(t) &= \sum_{n=1}^{\infty} \sum_{i=1}^d ([\varphi_E^{\otimes n}]^i * s^i)(t) \\
&= \sum_{n=1}^{\infty} \left[ \begin{pmatrix} [\varphi_E^{\otimes n}]^{11}(t) \\ \vdots \\ [\varphi_E^{\otimes n}]^{d1}(t) \end{pmatrix} * s^1(t) + \cdots + \begin{pmatrix} [\varphi_E^{\otimes n}]^{1d}(t) \\ \vdots \\ [\varphi_E^{\otimes n}]^{dd}(t) \end{pmatrix} * s^d(t) \right] \\
&= \sum_{n=1}^{\infty} \begin{pmatrix} [\varphi_E^{\otimes n}]^{11}(t) * s^1(t) & \cdots & [\varphi_E^{\otimes n}]^{1d}(t) * s^d(t) \\ \vdots & \ddots & \vdots \\ [\varphi_E^{\otimes n}]^{d1}(t) * s^1(t) & \cdots & [\varphi_E^{\otimes n}]^{dd}(t) * s^d(t) \end{pmatrix} \\
&= \sum_{n=1}^{\infty} \begin{pmatrix} [\varphi_E^{\otimes n}]^{11}(t) & \cdots & [\varphi_E^{\otimes n}]^{1d}(t) \\ \vdots & \ddots & \vdots \\ [\varphi_E^{\otimes n}]^{d1}(t) & \cdots & [\varphi_E^{\otimes n}]^{dd}(t) \end{pmatrix} * \begin{pmatrix} s^1(t) \\ \vdots \\ s^d(t) \end{pmatrix} \\
&= \sum_{n=1}^{\infty} (\varphi_E^{\otimes n} * \mathbf{s})(t) \\
&= \left( \sum_{n=1}^{\infty} \varphi_E^{\otimes n} * \mathbf{s} \right) (t).
\end{aligned}$$

■

The additional assumption  $\lim_{n \rightarrow \infty} \varphi_E^{\otimes n}(t) = 0$  introduced in Main Text Theorem 2 is a necessary condition for the convergence of  $\sum_{n=1}^{\infty} \varphi_E^{\otimes n}(t)$ . Intuitively, what this entails is that the intensity contribution of late-generation offsprings has to asymptotically go to zero to achieve convergence of the infinite sum. This is discussed further in Section 2.

**Remark 10 (Nonlinear Hawkes)** *Consider the nonlinear Hawkes process (Brémaud &*

Massoulié 1996) with conditional intensity

$$\boldsymbol{\lambda}^*_{NL}(t) := \boldsymbol{\phi} \left( \int_0^{t^-} \boldsymbol{\varphi}(t-s) \cdot d\mathbf{N}(s) \right), \quad (29)$$

where  $\boldsymbol{\phi} : \mathbb{R}^d \rightarrow (\mathbb{R}^+)^d$ . Following Main Text Definition 1, the nonlinear PCMHP can be defined as the process with intensity

$$\boldsymbol{\xi}_{NL,E}(t) := \mathbb{E}_{\mathcal{H}_{t^-}^E} \left[ \boldsymbol{\lambda}^*_{NL}(t) \middle| \mathcal{H}_{t^-}^{E^c} \right]. \quad (30)$$

The convolution formula in Theorem 9 does not hold exactly for the nonlinear PCMHP. If  $\boldsymbol{\phi}$  is convex (concave) in all dimensions, we have an upper (lower) bound for  $\boldsymbol{\xi}_{NL,E}(t)$  (see Section 4). In either case, we can make the approximation

$$\boldsymbol{\xi}_{NL,E}(t) \approx \boldsymbol{\phi} \left( (\boldsymbol{\varphi}_E * \boldsymbol{\xi}_{NL,E})(t) + \sum_{j \in E^c} \sum_{t_k^j < t} \boldsymbol{\varphi}_{E^c}(t - t_k^j) \right), \quad (31)$$

which becomes exact for linear  $\boldsymbol{\phi}$  (i.e. Theorem 9).

Due to the nonlinearity introduced by  $\boldsymbol{\phi}$ , the linear time-invariant solution concept is inapplicable, and alternative methods must be used to solve Eq. (31) for  $\boldsymbol{\xi}_{NL,E}(t)$ . Eq. (31) can be classified as a nonlinear Volterra functional integral equation (VFIE) of the second kind (Kamont 2012). VFIEs have been solved numerically using collocation methods (Xie et al. 2011) and cubic B-spline scaling functions (Maleknejad et al. 2014), which may be applicable to solve Eq. (31). Once  $\boldsymbol{\xi}_{NL,E}(t)$  is obtained, the compensator  $\boldsymbol{\Xi}_{NL,E}(t)$  can be approximated by numerical integration.

The techniques we introduce to approximate  $\boldsymbol{\xi}_E(t)$  (Section 7) and sample PCMHP (Section 12) are not applicable for the nonlinear PCMHP as they rely on the impulse response solution for  $\boldsymbol{\xi}_E(t)$ . Fitting the the nonlinear PCMHP to data can still be done via maximum likelihood estimation using the likelihood function we introduce in Main Text Section II.C.

A more in-depth study of the nonlinear PCMHP process, including an analysis of the tightness of Eq. (31), regularity conditions, and efficient numerical schemes to solve Eq. (31), is left for future work.

**Proof** [in Remark 10, that the convolution formula Theorem 9 does not apply for the nonlinear PCMHP ] Consider the nonlinear Hawkes process and the nonlinear PCMHP with intensities defined in Eq. (29) and Eq. (30), respectively. Plugging in Eq. (29) into Eq. (30), we have

$$\boldsymbol{\xi}_{NL,E}(t) = \mathbb{E}_{\mathcal{H}_{t^-}^E} \left[ \boldsymbol{\phi} \left( \int_0^{t^-} \boldsymbol{\varphi}(t-s) \cdot d\mathbf{N}(s) \right) \middle| \mathcal{H}_{t^-}^{E^c} \right]. \quad (32)$$

Without loss of generality, assume two cases for  $\boldsymbol{\phi}$ . If  $\boldsymbol{\phi}$  is convex in all dimensions, then Jensen's inequality applied to each dimension yields

$$\begin{aligned} \boldsymbol{\xi}_{NL,E}(t) &\leq \boldsymbol{\phi} \left( \mathbb{E}_{\mathcal{H}_{t^-}^E} \left[ \int_0^{t^-} \boldsymbol{\varphi}(t-s) \cdot d\mathbf{N}(s) \middle| \mathcal{H}_{t^-}^{E^c} \right] \right) \\ &\stackrel{(a)}{=} \boldsymbol{\phi} \left( (\boldsymbol{\varphi}_E * \boldsymbol{\xi}_{NL,E})(t) + \sum_{j \in E^c} \sum_{t_k^j < t} \boldsymbol{\varphi}_{E^c}(t - t_k^j) \right) \end{aligned} \quad (33)$$

where in (a) we follow the proof of Theorem 9 to simplify the term inside  $\boldsymbol{\phi}(\cdot)$

Similarly if  $\boldsymbol{\phi}$  is concave in all dimensions,

$$\boldsymbol{\xi}_{NL,E}(t) \geq \boldsymbol{\phi} \left( (\boldsymbol{\varphi}_E * \boldsymbol{\xi}_{NL,E})(t) + \sum_{j \in E^c} \sum_{t_k^j < t} \boldsymbol{\varphi}_{E^c}(t - t_k^j) \right). \quad (34)$$

We see that equality does not hold except when  $\boldsymbol{\phi}$  is both convex and concave (*i.e.* linear), allowing us to combine Eq. (33) and Eq. (34) to obtain

$$\boldsymbol{\xi}_{NL,E}(t) = \boldsymbol{\phi} \left( (\boldsymbol{\varphi}_E * \boldsymbol{\xi}_{NL,E})(t) + \sum_{j \in E^c} \sum_{t_k^j < t} \boldsymbol{\varphi}_{E^c}(t - t_k^j) \right), \quad (35)$$

which would be the corresponding convolution formula for the nonlinear PCMHP analogous to Theorem 9.

Since Main Text Theorem 2 relies on expressing  $\xi_{NL,E}(t)$  as the solution of a linear time-invariant (LTI) system, the nonlinearity induced by  $\phi$  makes the LTI approach inapplicable. ■

**Remark 11** *Under a given effective input  $\mathbf{s}(t)$ , the system  $\mathbf{s}(t) \overset{\heartsuit}{\Rightarrow} \xi_E(t)$  returns the resulting intensity of the PCMHP process averaged over the stochastic history of the  $E$  dimensions. Given that the effective input  $\mathbf{s}(t)$  treats the intensity contribution of events in the  $E^c$  dimensions as exogenous, only events in the  $E$  dimensions are self- and cross-exciting in  $\mathbf{s}(t) \overset{\heartsuit}{\Rightarrow} \xi_E(t)$ . In other words, the associated branching process for  $\mathbf{s}(t) \overset{\heartsuit}{\Rightarrow} \xi_E(t)$  considers the scenario where only events in the  $E$  dimensions produce offsprings.*

*Under  $\mathbf{s}(t) = \delta^j(0)$ , Eq. (26) tells us that the response of the LTI system  $\mathbf{s}(t) \overset{\heartsuit}{\Rightarrow} \xi_E(t)$  in the  $i^{\text{th}}$  dimension is*

$$\xi_E^i(\tau) = h_E^{ij}(\tau), \quad (36)$$

for  $\tau > 0$ .

*Integrating both sides of Eq. (36) over  $[0, t]$ , we get*

$$\Xi_E^i(t) = \int_0^t h_E^{ij}(\tau) d\tau.$$

*Taking the limit of both sides as  $t \rightarrow \infty$ ,*

$$\Xi_E^i(\infty) = \int_0^\infty h_E^{ij}(t).$$

*We see that if the integral of the right-hand side diverges to  $\infty$ , then the expected number of events, in view of Remark 2, explodes as  $t \rightarrow \infty$ .*

*In order to have a finite expected number of events in the branching process over the  $E$  dimensions, the integral of  $\mathbf{h}_E(t)$  over  $[0, \infty)$  must be finite. Stated differently, we require  $\mathbf{h}_E \in \mathcal{L}^1(\mathbb{R}^+)^{d \times d}$ .*

**Corollary 12** *The PCMHP( $d, e$ ) compensator  $\Xi_E(t)$  is given by*

$$\Xi_E(t) = [\delta(t) + \mathbf{h}_E(t)] * \left[ \mathbf{M}(t) + \sum_{j \in E^c} \sum_{t_k^j < t} \Phi_{E^c}^j(t - t_k^j) \right], \quad (37)$$

where  $\mathbf{h}_E(t) = \sum_{n=1}^{\infty} \varphi_E^{\otimes n}(t)$  and  $\mathbf{M}(t)$  and  $\Phi(t)$  are the integral of the background intensity  $\mu(t)$  and the integral of the Hawkes kernel  $\varphi(t)$  as defined in Eq. (4) and Eq. (5), respectively.  $\Phi_{E^c}(t)$  is defined similar to  $\varphi_{E^c}(t)$ , where we zero out the columns corresponding to the  $E^c$  dimensions.

**Proof** Integrating both sides of Main Text Equation 4 over  $[0, t)$ , we get

$$\Xi_E(t) = \int_0^t \left[ [\delta(\tau) + \mathbf{h}_E(\tau)] * \left[ \mu(\tau) + \sum_{j \in E^c} \sum_{t_k^j < \tau} \varphi_{E^c}^j(\tau - t_k^j) \right] \right] d\tau.$$

For brevity, set  $\mathbf{s}(t)$  as in Eq. (18), and set  $\mathbf{S}(t) = \int_0^t \mathbf{s}(\tau) d\tau$ . Now, we focus on the  $i^{\text{th}}$  entry of both sides. Expanding the convolution, we get

$$\begin{aligned} \Xi_E^i(t) &= \int_0^t \left[ s^i(\tau) + \sum_{j=1}^d (h_E^{ij} * s^j)(\tau) \right] d\tau \\ &\stackrel{(a)}{=} \int_0^t s^i(\tau) d\tau + \sum_{j=1}^d \int_0^t [(h_E^{ij} * s^j)(\tau)] d\tau \\ &\stackrel{(b)}{=} S^i(t) + \sum_{j=1}^d \int_0^t \int_0^\tau [h_E^{ij}(v) \cdot s^j(\tau - v)] dv d\tau \\ &\stackrel{(c)}{=} S^i(t) + \sum_{j=1}^d \int_0^t \int_v^t [h_E^{ij}(v) \cdot s^j(\tau - v)] d\tau dv \\ &= S^i(t) + \sum_{j=1}^d \int_0^t h_E^{ij}(v) \int_v^t s^j(\tau - v) d\tau dv \\ &\stackrel{(d)}{=} S^i(t) + \sum_{j=1}^d \int_0^t h_E^{ij}(v) \int_0^{t-v} s^j(u) du dv \\ &= S^i(t) + \sum_{j=1}^d \int_0^t h_E^{ij}(v) \cdot S^j(t - v) dv \\ &= S^i(t) + \sum_{j=1}^d (h_E^{ij} * S^j)(t), \end{aligned}$$



where in (a) we applied the linearity of integration, (b) we used the definition of convolution, (c) reversed the order of integration, and (d) made a change of variable  $u = \tau - v$ .

Collecting the results for every dimension  $i$ , we arrive at the desired formula. ■

## 4.2 Regularity Conditions

The following theorem presents the condition on the branching matrix  $\alpha$  that ensures  $\mathcal{L}^1$ -convergence of  $\mathbf{h}_E(t) = \sum_{n=1}^{\infty} \varphi_E^{\otimes n}(t)$  appearing in the PCMHP intensity in Main Theorem Theorem 2. As discussed in Remark 11,  $\mathcal{L}^1$ -convergence of  $\mathbf{h}_E(t)$  guarantees that the dynamics under the branching process on the  $E$  dimensions is nonexplosive and that we have a finite expected number of events.

**Theorem 13** *If the branching submatrix  $\alpha^{EE}$  satisfies  $\rho(\alpha^{EE}) < 1$ , then  $\mathbf{h}_E \in \mathcal{L}^1(\mathbb{R}^+)^{d \times d}$ .*

To prove Theorem 13, we need the following result on convergence in  $\mathcal{L}^p$  spaces.

**Theorem 14 (Folland (1999))** *Let  $\mathcal{L}^p(\mathbb{R}^+)$  is the space of functions  $f : \mathbb{R}^+ \rightarrow \mathbb{R}$  that have finite  $p$ -norm. If  $1 \leq p < \infty$ , every absolutely convergent series in  $\mathcal{L}^p(\mathbb{R}^+)$  converges.*

The following preliminary result is an upper bound on the 1-norm of each entry of  $\varphi^{\otimes n}(t)$  expressed in terms of the  $n^{\text{th}}$  power of the branching matrix  $\alpha$ . We use this upper bound in the proof of Theorem 13, which identifies the condition on the branching matrix  $\alpha$  for a convergent  $\mathbf{h}_E(t)$ .

**Lemma 15** *Let  $\alpha = (\alpha^{ij}) \in (\mathbb{R}^+)^{e \times e}$  and  $\varphi(t) = (\varphi^{ij}(t)) \in (\mathbb{R}^+)^{e \times e}$  be a matrix satisfying  $\varphi^{ij}(t) = \alpha^{ij} f^{ij}(t)$ ,  $f^{ij}(t) \geq 0$  and  $\int_0^{\infty} f^{ij}(t) dt = 1$ . Then for  $n \geq 1$ ,*

$$\mathbf{b}_n \leq \alpha^n,$$

where  $\mathbf{b}_n = (b_n^{ij}) \in (\mathbb{R}^+)^{e \times e}$  and  $b_n^{ij} = \|(\varphi^{\otimes n})^{ij}\|_1$ .

**Proof** We proceed by induction. Let  $\alpha$  and  $\varphi(t)$  be as stated. Let  $(i, j) \in E \times E$ .

Suppose  $n = 1$ .

$$\begin{aligned}
 b_1^{ij} &= \|(\varphi^{\otimes 1})^{ij}\|_1 \\
 &= \|\varphi^{ij}\|_1 \\
 (a) &= \|\alpha^{ij} f^{ij}\|_1 \\
 (b) &= \alpha^{ij} \|f^{ij}\|_1 \\
 (c) &= \alpha^{ij},
 \end{aligned}$$

where (a) and (c) follow from the definitions of  $\varphi^{ij}$  and  $f^{ij}$ , and (b) follows from  $\alpha^{ij}$  being a constant. Thus,  $\mathbf{b}_n \leq \alpha^n$  holds for  $n = 1$ .

Suppose that the relation holds for  $n = k \in \mathbb{N}$ . That is,  $\mathbf{b}_k \leq \alpha^k$ . This means that for every  $(p, q) \in E \times E$ , the following holds:

$$\|(\varphi^{\otimes k})^{pq}\|_1 \leq (\alpha^k)^{pq}. \tag{38}$$

Now, we show that the relation holds for  $n = k + 1$ . We observe that

$$\begin{aligned}
b_{k+1}^{ij} &= \|(\varphi^{\otimes k+1})^{ij}\|_1 \\
&= \|(\varphi^{\otimes k} * \varphi)^{ij}\|_1 \\
&\stackrel{(a)}{=} \left\| \sum_l (\varphi^{\otimes k})^{il} * \varphi^{lj} \right\|_1 \\
&\stackrel{(b)}{\leq} \sum_l \|(\varphi^{\otimes k})^{il} * \varphi^{lj}\|_1 \\
&\stackrel{(c)}{\leq} \sum_l \|(\varphi^{\otimes k})^{il}\|_1 \|\varphi^{lj}\|_1 \\
&= \sum_l \|(\varphi^{\otimes k})^{il}\|_1 \|\alpha^{lj} f^{lj}\|_1 \\
&= \sum_l \|(\varphi^{\otimes k})^{il}\|_1 \alpha^{lj} \|f^{lj}\|_1 \\
&= \sum_l \|(\varphi^{\otimes k})^{il}\|_1 \alpha^{lj} \\
&\stackrel{(d)}{\leq} \sum_l (\alpha^k)^{il} \alpha^{lj} \\
&= (\alpha^{k+1})^{ij}
\end{aligned}$$

In (a), the definition of the matrix product was used. In (b) and (c), the Minkowski inequality and Young's convolution inequality were used, respectively. In (d), our induction hypothesis Eq. (38) was used.

By induction,  $\mathbf{b}_n \leq \alpha^n$  holds for  $n \in \mathbb{N}$ . ■

We are now ready to prove Theorem 13.

**Proof** [of Theorem 13] Let  $\rho(\alpha^{EE}) < 1$ .

If we are able to show that the series  $\mathbf{h}_E = \sum_{n=1}^{\infty} \varphi_E^{\otimes n}$  is absolutely convergent in  $\mathcal{L}^1(\mathbb{R}^+)^{d \times d}$ , then Theorem 14 tells us that  $\mathbf{h}_E \in \mathcal{L}^1(\mathbb{R}^+)^{d \times d}$ .

Our task is then to prove absolute convergence of every entry in  $\mathbf{h}_E$ . If we denote  $\mathbf{h}_E^k$

to be the  $k^{\text{th}}$  partial sum of the series  $\mathbf{h}_E$ , *i.e.*

$$\mathbf{h}_E^k(t) = \sum_{n=1}^k \varphi_E^{\otimes n}(t),$$

then what we need to show is

$$\lim_{k \rightarrow \infty} \|(h_E^k)^{ij}\|_1 < \infty,$$

for  $(i, j) \in D \times D$ .

Define  $\varphi^{EE} \in \mathcal{L}^1(\mathbb{R}^+)^{e \times e}$  and  $\varphi^{E^c E} \in \mathcal{L}^1(\mathbb{R}^+)^{(d-e) \times e}$  as the submatrices of  $\varphi$  given by

$$\varphi^{EE} = \begin{pmatrix} \alpha^{11} f^{11} & \dots & \alpha^{1e} f^{1e} \\ \vdots & \vdots & \vdots \\ \alpha^{e1} f^{e1} & \dots & \alpha^{ee} f^{ee} \end{pmatrix},$$

$$\varphi^{E^c E} = \begin{pmatrix} \alpha^{e+1,1} f^{e+1,1} & \dots & \alpha^{e+1,e} f^{e+1,e} \\ \vdots & \vdots & \vdots \\ \alpha^{d1} f^{d1} & \dots & \alpha^{de} f^{de} \end{pmatrix}.$$

$\varphi_E$  may be written in block matrix form as

$$\varphi_E = \left[ \begin{array}{c|c} \varphi^{EE} & \mathbf{0} \\ \hline \varphi^{E^c E} & \mathbf{0} \end{array} \right].$$

Convolving  $\varphi_E$  with itself, we see that  $\varphi_E^{\otimes 2}$  can be written as

$$\varphi_E^{\otimes 2} = \left[ \begin{array}{c|c} (\varphi^{EE})^{\otimes 2} & \mathbf{0} \\ \hline \varphi^{E^c E} * \varphi^{EE} & \mathbf{0} \end{array} \right].$$

Convolving  $n$  times, we arrive at

$$\varphi_E^{\otimes n} = \left[ \begin{array}{c|c} (\varphi^{EE})^{\otimes n} & \mathbf{0} \\ \hline \varphi^{E^c E} * (\varphi^{EE})^{\otimes n-1} & \mathbf{0} \end{array} \right]. \quad (39)$$

For  $(i, j) \in E \times E$ , Eq. (39) states that

$$(\varphi_E^{\otimes n})^{ij} = ((\varphi^{EE})^{\otimes n})^{ij} \quad (40)$$

Taking the 1-norm of both sides, we see that

$$\|(\varphi_E^{\otimes n})^{ij}\|_1 = \|((\varphi^{EE})^{\otimes n})^{ij}\|_1 \leq ((\boldsymbol{\alpha}^{EE})^n)^{ij}, \quad (41)$$

where the last inequality is due to Lemma 15.

Similarly, for  $(i, j) \in E^c \times E$ ,

$$\begin{aligned} \|(\varphi_E^{\otimes n})^{ij}\|_1 &= \|(\varphi^{E^c E} * (\varphi^{EE})^{\otimes n-1})^{i-e,j}\|_1 \\ (a) &= \|(\varphi^{E^c E} * (\varphi^{EE})^{\otimes n-1})^{i'j}\|_1 \\ (b) &= \left\| \sum_l (\varphi^{E^c E})^{i'l} * ((\varphi^{EE})^{\otimes n-1})^{lj} \right\|_1 \\ (c) &\leq \sum_l \left\| (\varphi^{E^c E})^{i'l} * ((\varphi^{EE})^{\otimes n-1})^{lj} \right\|_1 \\ (d) &\leq \sum_l \left\| (\varphi^{E^c E})^{i'l} \right\|_1 \left\| ((\varphi^{EE})^{\otimes n-1})^{lj} \right\|_1 \\ (e) &\leq \sum_l \left\| (\varphi^{E^c E})^{i'l} \right\|_1 ((\boldsymbol{\alpha}^{EE})^{n-1})^{lj} \\ (f) &= \sum_l (\boldsymbol{\alpha}^{E^c E})^{i'l} ((\boldsymbol{\alpha}^{EE})^{n-1})^{lj} \\ &= (\boldsymbol{\alpha}^{E^c E} (\boldsymbol{\alpha}^{EE})^{n-1})^{i'j} \end{aligned} \quad (42)$$

$$= (\boldsymbol{\alpha}^{E^c E} (\boldsymbol{\alpha}^{EE})^{n-1})^{i-e,j} \quad (43)$$

In (a), we reindex  $i' = i - e$  to start our index at 1. Lines (b), (c), (d) are applications of the definition of matrix product, Minkowski's inequality, and Young's convolution inequality, respectively. In (e), we apply Lemma 15, and in (f), we apply the definition of  $\varphi^{E^c E}$ .

Putting in Eq. (41) and Eq. (43) into Eq. (39), we see that

$$\|(\varphi_E^{\otimes n})^{ij}\|_1 \leq \left[ \begin{array}{c|c} (\alpha^{EE})^n & \mathbf{0} \\ \hline \alpha^{E^c E} (\alpha^{EE})^{n-1} & \mathbf{0} \end{array} \right]. \quad (44)$$

Taking  $\sum_{n=1}^{\infty}$  of both sides, we get

$$\begin{aligned} \sum_{n=1}^{\infty} \|(\varphi_E^{\otimes n})^{ij}\|_1 &\leq \left[ \begin{array}{c|c} \sum_{n=1}^{\infty} (\alpha^{EE})^n & \mathbf{0} \\ \hline \alpha^{E^c E} \sum_{n=1}^{\infty} (\alpha^{EE})^{n-1} & \mathbf{0} \end{array} \right] \\ &= \left[ \begin{array}{c|c} (\mathbf{I} - \alpha^{EE})^{-1} - \mathbf{I} & \mathbf{0} \\ \hline \alpha^{E^c E} (\mathbf{I} - \alpha^{EE})^{-1} & \mathbf{0} \end{array} \right]. \end{aligned} \quad (45)$$

where the previous equation follows from  $\rho(\alpha^{EE}) < 1$  and Proposition 4.

Inspecting every block of Eq. (45), it is clear that that for all  $(i, j) \in D \times D$ ,

$$\sum_{n=1}^{\infty} \|(\varphi_E^{\otimes n})^{ij}\|_1 < \infty. \quad (46)$$

Given that

$$\|(h_E^k)^{ij}\|_1 \leq \sum_{n=1}^k \|(\varphi_E^{\otimes n})^{ij}\|_1 \xrightarrow{k \rightarrow \infty} \sum_{n=1}^{\infty} \|(\varphi_E^{\otimes n})^{ij}\|_1 < \infty, \quad (47)$$

we have proven that every entry in  $\mathbf{h}_E$  is absolutely convergent in  $\mathcal{L}^1(\mathbb{R}^+)$ .  $\blacksquare$

**Proof** [of Main Text Theorem 3] Consider a PCMHP( $d, e$ ) process with conditional intensity  $\boldsymbol{\xi}_E(t)$  given by Main Text Equation 5. If  $\rho(\alpha^{EE}) < 1$ ,  $\sum_{n=1}^{\infty} \varphi_E^{\otimes n}$  is a convergent function by Theorem 13, so  $\boldsymbol{\xi}_E(t)$  is well-defined.

We proceed by noting that the intensity  $\xi_E(t)$  splits as the sum of three distinct terms:

(A) an inhomogeneous Poisson process rate:

$$\boldsymbol{\mu}(t) + \sum_{n=1}^{\infty} (\varphi_E^{\otimes n} * \boldsymbol{\mu})(t),$$

(B) a multivariate Hawkes intensity:

$$\sum_{j \in E^c} \sum_{t_k^j < t} \boldsymbol{\varphi}^j(t - t_k^j),$$

(C) a convolution term involving the Hawkes intensity:

$$\sum_{n=1}^{\infty} \varphi_E^{\otimes n} * \sum_{j \in E^c} \sum_{t_k^j < t} \boldsymbol{\varphi}^j(t - t_k^j).$$

We inspect each of these intensities separately.

For the process with intensity  $\xi_E(t)$  to be subcritical, the processes corresponding to each of these three intensities necessarily have to be subcritical.

**Intensity (A).** A Poisson process is independent of the arrival of new events, so the process is subcritical as long as  $\boldsymbol{\mu}(t)$  is a bounded function and  $\sum_{n=1}^{\infty} \varphi_E^{\otimes n}$  is  $\mathcal{L}^1$ -convergent.

**Intensity (B).** The multivariate Hawkes process corresponding to intensity (B) may be viewed as a process with branching matrix

$$\boldsymbol{\alpha}_{E^c} = \left( \begin{array}{c|c} \mathbf{0} & \boldsymbol{\alpha}^{EE^c} \\ \hline \mathbf{0} & \boldsymbol{\alpha}^{E^cE^c} \end{array} \right).$$

By Theorem 5, this process is subcritical if  $\rho(\boldsymbol{\alpha}_{E^c}) < 1$ . The eigenvalues of  $\boldsymbol{\alpha}_{E^c}$  are the solutions  $\lambda$  of

$$\det(\boldsymbol{\alpha}_{E^c} - \lambda \mathbf{I}) = 0. \tag{48}$$

Expanding the left-hand side of Eq. (48),

$$\begin{aligned} \det(\boldsymbol{\alpha}_{E^c} - \lambda \mathbf{I}) &= \left[ \begin{array}{c|c} \mathbf{0} - \lambda \mathbf{I} & \boldsymbol{\alpha}^{EE^c} \\ \hline \mathbf{0} & \boldsymbol{\alpha}^{E^c E^c} - \lambda \mathbf{I} \end{array} \right] = \left[ \begin{array}{c|c} -\lambda \mathbf{I} & \boldsymbol{\alpha}^{EE^c} \\ \hline \mathbf{0} & \boldsymbol{\alpha}^{E^c E^c} - \lambda \mathbf{I} \end{array} \right] \\ &= \det(-\lambda \mathbf{I}) \det(\boldsymbol{\alpha}^{E^c E^c} - \lambda \mathbf{I}) = (-1)^{|E|} \lambda^{|E|} \det(\boldsymbol{\alpha}^{E^c E^c} - \lambda \mathbf{I}), \end{aligned}$$

we see that the eigenvalues of  $\boldsymbol{\alpha}_{E^c}$  are precisely 0 and the eigenvalues of  $\boldsymbol{\alpha}^{E^c E^c}$ . Thus,  $\rho(\boldsymbol{\alpha}_{E^c}) = \rho(\boldsymbol{\alpha}^{E^c E^c})$

By Theorem 5 and given  $\rho(\boldsymbol{\alpha}^{E^c E^c}) < 1$ , the multivariate Hawkes process with intensity (B) is subcritical.

**Intensity (C).** Let  $(i, j) \in D \times D$ . We can see that intensity (C) is intensity (B) (with branching matrix  $\boldsymbol{\alpha}_{E^c}$ ) convolved with the infinite sum  $\sum_{n=1}^{\infty} \boldsymbol{\varphi}_E^{\otimes n}$ .

First, consider the matrix

$$\boldsymbol{\Omega} := \left[ \begin{array}{c|c} (\mathbf{I} - \boldsymbol{\alpha}^{EE})^{-1} - \mathbf{I} & \mathbf{0} \\ \hline \boldsymbol{\alpha}^{E^c E} (\mathbf{I} - \boldsymbol{\alpha}^{EE})^{-1} & \mathbf{0} \end{array} \right]. \quad (49)$$

In Eq. (45) (see: proof of Theorem 13 in Section 4.2), we show that

$$\sum_{n=1}^{\infty} (\|(\boldsymbol{\varphi}_E^{\otimes n})^{ij}\|_1) \leq \boldsymbol{\Omega}. \quad (50)$$

Now, consider the  $(i, j)$  branching factor of the process with intensity (C), which can be expressed as

$$\left\| \sum_k \left( \sum_{n=1}^{\infty} \boldsymbol{\varphi}_E^{\otimes n} \right)^{ik} * \boldsymbol{\varphi}^{kj} \right\|_1. \quad (51)$$

Applying (a) Young's convolution inequality, (b) Minkowski's inequality, and (c) the matrix



upper bound in Eq. (50), we see that Eq. (51) is upper bounded by:

$$\begin{aligned}
& \left\| \sum_k \left( \sum_{n=1}^{\infty} \varphi_E^{\otimes n} \right)^{ik} * \varphi^{kj} \right\|_1 \\
(a) & \leq \sum_k \left\| \left( \sum_{n=1}^{\infty} \varphi_E^{\otimes n} \right)^{ik} \right\|_1 \|\varphi^{kj}\|_1 = \sum_k \left\| \left( \sum_{n=1}^{\infty} \varphi_E^{\otimes n} \right)^{ik} \right\|_1 \alpha^{kj} = \sum_k \left\| \sum_{n=1}^{\infty} (\varphi_E^{\otimes n})^{ik} \right\|_1 \alpha^{kj} \\
(b) & \leq \sum_k \sum_{n=1}^{\infty} \left\| (\varphi_E^{\otimes n})^{ik} \right\|_1 \alpha^{kj} \\
(c) & \leq \sum_k \Omega^{ik} \alpha^{kj} = (\mathbf{\Omega} \boldsymbol{\alpha}_{E^c})^{ij}.
\end{aligned}$$

This tells us that the  $(i, j)$  branching factor of the process with intensity (C) is upper-bounded by the  $(i, j)$  branching factor of a multivariate Hawkes process with branching matrix  $\mathbf{\Omega} \boldsymbol{\alpha}_{E^c}$ . Thus, if we are able to show that the multivariate Hawkes process with branching matrix  $\mathbf{\Omega} \boldsymbol{\alpha}_{E^c}$  is subcritical, *i.e.*,  $\rho(\mathbf{\Omega} \boldsymbol{\alpha}_{E^c}) < 1$ , the process defined by intensity (C) is necessarily subcritical as well.

$\mathbf{\Omega} \boldsymbol{\alpha}_{E^c}$  in block form may be written as:

$$\mathbf{\Omega} \boldsymbol{\alpha}_{E^c} = \left[ \begin{array}{c|c} (\mathbf{I} - \boldsymbol{\alpha}^{EE})^{-1} - \mathbf{I} & \mathbf{0} \\ \hline \boldsymbol{\alpha}^{E^c E} (\mathbf{I} - \boldsymbol{\alpha}^{EE})^{-1} & \mathbf{0} \end{array} \right] \left[ \begin{array}{c|c} \mathbf{0} & \boldsymbol{\alpha}^{EE^c} \\ \hline \mathbf{0} & \boldsymbol{\alpha}^{E^c E^c} \end{array} \right] = \left[ \begin{array}{c|c} \mathbf{0} & [(\mathbf{I} - \boldsymbol{\alpha}^{EE})^{-1} - \mathbf{I}] \boldsymbol{\alpha}^{EE^c} \\ \hline \mathbf{0} & \boldsymbol{\alpha}^{E^c E} (\mathbf{I} - \boldsymbol{\alpha}^{EE})^{-1} \boldsymbol{\alpha}^{E^c E^c} \end{array} \right]$$

The eigenvalues of  $\mathbf{\Omega} \boldsymbol{\alpha}_{E^c}$  are the solutions  $\lambda$  of

$$\det(\mathbf{\Omega} \boldsymbol{\alpha}_{E^c} - \lambda \mathbf{I}) = 0. \tag{52}$$

Expanding the left-hand side of Eq. (52), we see that

$$\begin{aligned}
\det(\mathbf{\Omega}\boldsymbol{\alpha}_{E^c} - \lambda\mathbf{I}) &= \det \left[ \begin{array}{c|c} \mathbf{0} - \lambda\mathbf{I} & [(\mathbf{I} - \boldsymbol{\alpha}^{EE})^{-1} - \mathbf{I}]\boldsymbol{\alpha}^{EE^c} \\ \hline \mathbf{0} & \boldsymbol{\alpha}^{E^cE}(\mathbf{I} - \boldsymbol{\alpha}^{EE})^{-1}\boldsymbol{\alpha}^{E^cE^c} - \lambda\mathbf{I} \end{array} \right] \\
&= \det(-\lambda\mathbf{I}) \det(\boldsymbol{\alpha}^{E^cE}(\mathbf{I} - \boldsymbol{\alpha}^{EE})^{-1}\boldsymbol{\alpha}^{E^cE^c} - \lambda\mathbf{I}) \\
&= (-1)^{|E|} \lambda^{|E|} \det(\boldsymbol{\alpha}^{E^cE}(\mathbf{I} - \boldsymbol{\alpha}^{EE})^{-1}\boldsymbol{\alpha}^{E^cE^c} - \lambda\mathbf{I}).
\end{aligned}$$

Thus we see that the eigenvalues of  $\mathbf{\Omega}\boldsymbol{\alpha}_{E^c}$  are precisely 0 and the eigenvalues of  $\boldsymbol{\alpha}^{E^cE}(\mathbf{I} - \boldsymbol{\alpha}^{EE})^{-1}\boldsymbol{\alpha}^{E^cE^c}$ . This implies that

$$\rho(\mathbf{\Omega}\boldsymbol{\alpha}_{E^c}) = \rho(\boldsymbol{\alpha}^{E^cE}(\mathbf{I} - \boldsymbol{\alpha}^{EE})^{-1}\boldsymbol{\alpha}^{E^cE^c}). \quad (53)$$

By Theorem 5, if  $\rho(\boldsymbol{\alpha}^{E^cE}(\mathbf{I} - \boldsymbol{\alpha}^{EE})^{-1}\boldsymbol{\alpha}^{E^cE^c}) < 1$ , the process with intensity (C) is subcritical.

As the three sub-intensities that consist  $\boldsymbol{\xi}_E(t)$  all correspond to subcritical processes given the assumed conditions,  $\boldsymbol{\xi}_E(t)$  is then subcritical. ■

**Corollary 16** *The regularity conditions for PCMHP( $d, e$ ) in Main Text Theorem 2 cover the Hawkes process and the MBP process as special cases.*

**Proof** If  $e = 0$  (Hawkes), we have  $\boldsymbol{\alpha}^{EE} = \boldsymbol{\alpha}^{EE^c} = \boldsymbol{\alpha}^{E^cE} = \mathbf{0}$  and  $\boldsymbol{\alpha}^{E^cE^c} = \boldsymbol{\alpha}$ . Thus, only the second condition is non-trivially satisfied, yielding  $\rho(\boldsymbol{\alpha}) < 1$ . If  $e = d$  (MBP), we have  $\boldsymbol{\alpha}^{E^cE^c} = \boldsymbol{\alpha}^{EE^c} = \boldsymbol{\alpha}^{E^cE} = \mathbf{0}$  and  $\boldsymbol{\alpha}^{EE} = \boldsymbol{\alpha}$ . Thus, only the first condition is non-trivially satisfied, yielding  $\rho(\boldsymbol{\alpha}) < 1$ . If  $0 < e < d$  (PCMHP), all branching submatrices are possibly nonzero and all three conditions are potentially non-trivially satisfied. ■

## 5 Additional Results and Proofs for Section II.C

**Proof** [of Main Text Theorem 4] Since  $E \supseteq Q$ ,  $\{1, \dots, e\}$  splits as  $\{1, \dots, q\} \cup \{q+1, \dots, e\}$ . Given this observation, the joint probability of the event volumes  $\bigcup_{j \in Q} \{C_k^j\}_{k=1}^{n^j}$  and event times  $\mathcal{H}_{T^-}^{Q^c}$ ,

$$\mathbb{P} \left\{ C_1^1, \dots, C_{n^1}^1, \dots, C_1^q, \dots, C_{n^q}^q, \mathcal{H}_{T^-}^{q+1}, \dots, \mathcal{H}_{T^-}^d \right\},$$

can be written as

$$\mathbb{P} \left\{ C_1^1, \dots, C_{n^1}^1, \dots, C_1^q, \dots, C_{n^q}^q, \mathcal{H}_{T^-}^{q+1}, \dots, \mathcal{H}_{T^-}^e, \mathcal{H}_{T^-}^{e+1}, \dots, \mathcal{H}_{T^-}^d \right\}. \quad (54)$$

Conditioning on the  $E^c$  event times  $\{\mathcal{H}_{T^-}^{e+1}, \dots, \mathcal{H}_{T^-}^d\}$ , Eq. (54) splits as

$$\mathbb{P} \left\{ C_1^1, \dots, C_{n^1}^1, \dots, C_1^q, \dots, C_{n^q}^q, \mathcal{H}_{T^-}^{q+1}, \dots, \mathcal{H}_{T^-}^e \mid \mathcal{H}_{T^-}^{e+1}, \dots, \mathcal{H}_{T^-}^d \right\} \cdot \mathbb{P} \left\{ \mathcal{H}_{T^-}^{e+1}, \dots, \mathcal{H}_{T^-}^d \right\}. \quad (55)$$

In a PCMHP( $d, e$ ) model, events in dimension  $j \in E$  are independent of events in dimension  $k \neq j, k \in E$ , which implies that Eq. (55) splits as a product over dimensions,

$$\prod_{j=1}^q \mathbb{P} \left\{ C_1^j, \dots, C_{n^j}^j \mid \mathcal{H}_{T^-}^{E^c} \right\} \cdot \prod_{j=q+1}^e \mathbb{P} \left\{ \mathcal{H}_{T^-}^j \mid \mathcal{H}_{T^-}^{E^c} \right\} \cdot \mathbb{P} \left\{ \mathcal{H}_{T^-}^{e+1}, \dots, \mathcal{H}_{T^-}^d \right\}. \quad (56)$$

Taking  $-\log(\cdot)$  of both sides of Eq. (56) and converting the product to a sum over logarithms, we get

$$\begin{aligned} \mathcal{L}(\Theta; T) &= - \sum_{j=1}^q \log \mathbb{P} \left\{ C_1^j, \dots, C_{n^j}^j \mid \mathcal{H}_{T^-}^{E^c}; \Theta \right\} - \sum_{j=q+1}^e \log \mathbb{P} \left\{ \mathcal{H}_{T^-}^j \mid \mathcal{H}_{T^-}^{E^c}; \Theta \right\} \\ &\quad - \sum_{j=e+1}^d \log \mathbb{P} \left\{ \mathcal{H}_{T^-}^j; \Theta \right\} \end{aligned} \quad (57)$$

Using Proposition 6 on the first term and Eq. (7) on the second and third terms, we arrive at the desired formula. ■

**Remark 17 Joint fitting.** To jointly fit multiple ( $R > 1$ ) PCMHP( $d, e$ ) realizations, one needs to maximize the sum of log-likelihoods corresponding to each realization. That is,

$$\mathcal{L}(\Theta; T) = \sum_{r=1}^R \mathcal{L}^r(\Theta; T), \quad (58)$$

where  $\mathcal{L}^r(\Theta; T)$  is the negative log-likelihood corresponding to the  $r^{\text{th}}$  realization.

**Additional details on runtime complexity.** Evaluating  $\mathcal{L}(\Theta; T)$  has a runtime complexity of

$$\mathcal{O}((C + n^{E^c}) \cdot (n^Q + n^{Q^c})); \quad (59)$$

which comes from combining the time complexity of calculating the  $\mathcal{L}_{\text{IC-LL}}$  loss  $\mathcal{O}(n^Q(C + n^{E^c}))$  and the  $\mathcal{L}_{\text{PP-LL}}$  loss  $\mathcal{O}(n^{Q^c}(C + n^{E^c}))$ .  $C$  denotes a constant independent of the dimension of the PCMHP and the data. Having closed-form expressions for convolutions on  $\mathbf{h}_E(t)$  simplifies the convolutions in  $\xi_E^j(\cdot)$  (see Main Text Equation 5) and  $\Xi_E^j(\cdot)$  (see Eq. (37)) to function evaluations in  $\mathcal{O}(1)$ . We sketch the proof below.

To calculate  $\mathcal{L}_{\text{IC-LL}}(\Theta; T)$ , we iterate over each dimension  $j \in Q$  and every observation interval  $[o_{k-1}^j, o_k^j)$ , requiring  $n^Q$  loops. For each iteration, we calculate  $\Xi_E^j(o_{k-1}^j, o_k^j)$ , which has time complexity  $\mathcal{O}(n^{E^c})$ , since we need to calculate the influence of each observed event in  $E^c$ . Thus, the total time complexity is  $\mathcal{O}(n^Q \cdot (C + n^{E^c}))$ , where  $C$  accounts for a constant number of calculations independent of the data (ex. calculating the baseline intensity and  $\mathbf{h}_E(t)$ ).

Calculations for  $\mathcal{L}_{\text{PP-LL}}(\Theta; T)$  are similar. Instead of iterating over  $j \in Q$  and  $C_k^j$ , we iterate over  $j \in Q^c$  and  $t_k^j \in \mathcal{H}_{T-}^j$ , requiring  $n^{Q^c}$  loops. Within each loop, we calculate  $\xi_E^j(t_k^j)$ , which has time complexity  $\mathcal{O}(n^{E^c})$ . We note that this dominates the time complexity  $\mathcal{O}(|Q| \cdot n^{E^c})$  of calculating  $\Xi_E^j(T; \Theta)$  in each loop. Thus, the total time complexity is  $\mathcal{O}(n^{Q^c} \cdot (C + n^{E^c}))$ .

In the case  $E = Q = \emptyset$ , the runtime complexity reduces to  $\mathcal{O}((n^{E^c})^2)$ , which is consistent with the multivariate Hawkes process. If  $E = Q = D$ , runtime complexity reduces to  $\mathcal{O}(n^E)$ , which is consistent with the MBP (i.e. Poisson) process.

**Remark 18** *In general, the negative log-likelihood  $\mathcal{L}(\Theta; T)$  is nonconvex in  $\Theta$  due to the presence of nonlinear parameters, e.g.  $\theta^{ij}$  for the exponential kernel (see Section 6 for a special case of PCMHP (2,1) where we have a convex likelihood). Due to this, gradient-based algorithms have no guarantee of attaining the global optimum. Convexity analysis for the general form of  $\mathcal{L}(\Theta; T)$  is difficult due to the complexity of evaluating  $\mathbf{h}_E(t)$  in a high-dimensional setting. In Section 6, we prove convexity for a special case of PCMHP(2,1). For nonconvex cases, global optimization (such as the Lipschitz Global Optimizer LGO (Pintér 1996)) can be leveraged to find the global optimum, for instance using a branch-and-bound or randomized search strategy over the parameter space or iterated local optimization.*

## 6 Convexity Analysis of the PCMHP(2,1) Likelihood

Consider a PCMHP(2,1) process. Suppose the associated kernel can be expressed as  $\varphi^{ij}(t) = \alpha^{ij} f^{ij}(t; \theta^{ij})$ , where  $f^{ij}(t; \theta^{ij})$  is a probability density over  $[0, \infty)$  parametrized by  $\theta^{ij}$ . Given a multiple impulse exogenous input function,

$$\boldsymbol{\mu}(t) = \sum_i \begin{pmatrix} a_i \cdot \delta(t - c_i) \\ b_i \cdot \delta(t - d_i) \end{pmatrix},$$

we show that for a fixed set of  $\{\theta^{ij}\}$  parameters and given observed point data  $\Psi^1 = \{s_k^1\}$  and  $\Psi^2 = \{s_k^2\}$  over  $[0, T)$  for dimensions 1 and 2, the negative point-process log-likelihood (PP-PP NLL) of the PCMHP(2,1) is convex in the  $\{\alpha^{ij}\}$  parameters.

We first consider a single impulse as the exogenous input. Suppose

$$\boldsymbol{\mu}(t) = \begin{pmatrix} a \cdot \delta(t - c) \\ b \cdot \delta(t - d) \end{pmatrix},$$

where  $a, b, c, d \geq 0$ . Given this general impulse exogenous input, we aim to show that the PP-PP NLL is convex in the  $\{\alpha^{ij}\}$  parameters. Given observed data points  $\Psi^1 = \{s_k^1\}$  and  $\Psi^2 = \{s_k^2\}$  over  $[0, T)$  in the two dimensions, the PP-PP NLL is given by

$$\mathcal{L}(\boldsymbol{\alpha}; T) = -\log \sum_{s_k^1} (\xi_1^1(s_k^1; \boldsymbol{\alpha})) - \log \sum_{s_k^2} (\xi_1^2(s_k^2; \boldsymbol{\alpha})) + \Xi_1^1(T; \boldsymbol{\alpha}) + \Xi_1^2(T; \boldsymbol{\alpha}), \quad (60)$$

where

$$\xi_1^1(t; \boldsymbol{\alpha}) = a\delta(t - c) + ah_1^{11}(t - c)\llbracket t > c \rrbracket + \sum_{t_k^2 < t} \varphi_2^{12}(t - t_k^2) + h_1^{11}(t) * \sum_{t_k^2 < t} \varphi_2^{12}(t - t_k^2) \quad (61)$$

$$\xi_1^2(t; \boldsymbol{\alpha}) = b\delta(t - d) + bh_1^{21}(t - d)\llbracket t > d \rrbracket + \sum_{t_k^2 < t} \varphi_2^{22}(t - t_k^2) + h_1^{21}(t) * \sum_{t_k^2 < t} \varphi_2^{12}(t - t_k^2) \quad (62)$$

$$\Xi_1^1(t; \boldsymbol{\alpha}) = a\llbracket t > c \rrbracket + aH_1^{11}(t - c) + \sum_{t_k^2 < t} \Phi_2^{12}(t - t_k^2) + h_1^{11}(t) * \sum_{t_k^2 < t} \Phi_2^{12}(t - t_k^2) \quad (63)$$

$$\Xi_1^2(t; \boldsymbol{\alpha}) = b\llbracket t > d \rrbracket + bH_1^{21}(t - d) + \sum_{t_k^2 < t} \Phi_2^{22}(t - t_k^2) + h_1^{21}(t) * \sum_{t_k^2 < t} \Phi_2^{12}(t - t_k^2), \quad (64)$$

and

$$\mathbf{h}_1(t) = \sum_{n=1}^{\infty} \begin{pmatrix} \alpha^{11} f^{11}(t; \theta^{11}) & 0 \\ \alpha^{21} f^{21}(t; \theta^{21}) & 0 \end{pmatrix}^{\otimes n} \quad (65)$$

$$H_1^{ij}(t - u) = \int_0^t h_1^{ij}(\tau - u)\llbracket \tau > u \rrbracket d\tau = \int_u^t h_1^{ij}(\tau - u) d\tau \quad (66)$$

$$\Phi_2^{ij}(t) = \alpha^{ij} \int_0^t f_2^{ij}(\tau; \{\theta^{ij}\}) d\tau = \alpha^{ij} F_2^{ij}(t; \{\theta^{ij}\}) \quad (67)$$

Our goal is to show that Eq. (60) is convex in the  $\{\alpha^{ij}\}$  parameters for fixed  $\{\theta^{ij}\}$ . Our strategy is to show that each of the four terms in Eq. (60) is a convex function of  $\{\alpha^{ij}\}$ .

First, note that the map  $l : x \mapsto -\sum \log x$  is convex and non-decreasing. As such, for  $-\log \sum_{s_k^1} (\xi_1^1(s_k^1; \{\alpha^{ij}\})) = l \circ \xi_1^1(\cdot; \{\alpha^{ij}\})$  to be convex in  $\{\alpha^{ij}\}$  (where  $\xi_1^1(\cdot; \{\alpha^{ij}\})$  is inter-

preted as a map from  $\alpha$  parameters to the conditional intensity, *i.e.*,  $(0, 1)^4 \mapsto \mathbb{R}^+$ ), it is sufficient to show that  $\xi_1^1(\cdot; \{\alpha^{ij}\})$  is a convex function. Similarly, for  $-\log \sum_{s_k^2} (\xi_1^2(s_k^2; \{\alpha^{ij}\}))$  to be convex,  $\xi_1^2(\cdot; \{\alpha^{ij}\})$  has to be convex. For the last two terms of Eq. (60) to be convex,  $\Xi_1^1(T; \{\alpha^{ij}\})$  and  $\Xi_1^2(T; \{\alpha^{ij}\})$  have to be convex.

**I. Convexity of  $\xi_1^1(\cdot; \{\alpha^{ij}\})$ .** Let us split Eq. (61) as follows:

$$\xi_1^1(t) = \overbrace{a\delta(t-c) + ah_1^{11}(t-c)}^{I.A} + \overbrace{\sum_{t_k^2 < t} \varphi_2^{12}(t-t_k^2)}^{I.B} + \overbrace{h_1^{11}(t) * \sum_{t_k^2 < t} \varphi_2^{12}(t-t_k^2)}^{I.C} \quad (68)$$

To show convexity of  $\xi_1^1$ , we need to show convexity of each of the indicated terms.

For the I.A term, we compute the Hessian matrix with respect to  $\{\alpha^{ij}\}$  as

$$\mathbf{Hess}_{I.A} = \left[ \frac{\partial^2(I.A)}{(\partial\alpha^{ij})^2} \right] = \begin{pmatrix} \frac{\partial^2 h_1^{11}}{(\partial\alpha^{11})^2} & \frac{\partial^2 h_1^{11}}{(\partial\alpha^{12})^2} \\ \frac{\partial^2 h_1^{11}}{(\partial\alpha^{21})^2} & \frac{\partial^2 h_1^{11}}{(\partial\alpha^{22})^2} \end{pmatrix}. \quad (69)$$

Let us compute each of these terms. First, observe that from Eq. (65) we can write

$$\mathbf{h}_1(t) = \begin{pmatrix} \sum_{n=1}^{\infty} (\alpha^{11})^n (f^{11})^{\otimes n} & 0 \\ \alpha^{21} \sum_{n=1}^{\infty} (\alpha^{11})^{n-1} f^{21} * (f^{11})^{\otimes(n-1)} & 0 \end{pmatrix}. \quad (70)$$

Immediately, we see that

$$\begin{aligned} \frac{\partial^2 h_1^{11}}{(\partial\alpha^{11})^2} &= \sum_{n=2}^{\infty} n(n-1) (\alpha^{11})^{n-2} (f^{11})^{\otimes n} = \frac{1}{(\alpha^{11})^2} \sum_{n=2}^{\infty} n(n-1) (\alpha^{11})^n (f^{11})^{\otimes n} \geq 0 \quad (71) \\ \frac{\partial^2 h_1^{11}}{(\partial\alpha^{12})^2} &= \frac{\partial^2 h_1^{11}}{(\partial\alpha^{21})^2} = \frac{\partial^2 h_1^{11}}{(\partial\alpha^{22})^2} = 0 \end{aligned}$$

Since  $\|f^{ij}\| = 1$ ,  $\sum_{n=2}^{\infty} n(n-1) (\alpha^{11})^n (f^{11})^{\otimes n}$  is upper bounded by  $\sum_{n=2}^{\infty} n(n-1) (\alpha^{11})^n$ , which can be shown to be convergent by the Integral Test.

It follows that the set of eigenvalues of  $\mathbf{Hess}_{I.A}$  is  $\{0, \frac{a}{(\alpha^{11})^2} \sum_{n=2}^{\infty} n(n-1)(\alpha^{11})^n (f^{11})^{\otimes n} (t-a)\}$ . Since all of the eigenvalues of  $\mathbf{Hess}_{I.A}$  are non-negative,  $\mathbf{Hess}_{I.A}$  is positive-semidefinite and the term I.A is convex.

For the I.B term, since  $\varphi^{ij} = \alpha^{ij} f^{ij}(\cdot; \theta^{ij})$  is linear in  $\alpha^{ij}$ , it follows that the Hessian matrix of  $\varphi_2^{12}(t - t_k^2)$  is identically zero, and thus I.B is trivially convex.

For the I.C term, since  $h^{11}$  and  $\varphi^{12}$  are differentiable functions of  $\alpha^{ij}$ , it follows that

$$\begin{aligned} \frac{\partial^2}{(\partial \alpha^{ij})^2} \left( h_1^{11}(t) * \sum_{t_k^2 < t} \varphi_2^{12}(t - t_k^2) \right) &= h_1^{11}(t) * \sum_{t_k^2 < t} \frac{\partial^2}{(\partial \alpha^{ij})^2} \varphi_2^{12}(t - t_k^2) + \\ &\quad \frac{\partial^2}{(\partial \alpha^{ij})^2} h_1^{11}(t) * \sum_{t_k^2 < t} \varphi_2^{12}(t - t_k^2) \end{aligned}$$

Since the Hessian for  $\varphi_2^{12}(t - t_k^2)$  is trivially 0, the first term of I.C is trivially zero. For the second term, since  $\frac{\partial^2 h_1^{11}}{(\partial \alpha^{ij})^2} = 0$  unless  $i = j = 1$ , we only need to consider the  $i = j = 1$  case. Using Eq. (71), we have

$$\begin{aligned} \frac{\partial^2}{(\partial \alpha^{11})^2} h_1^{11}(t) * \sum_{t_k^2 < t} \varphi_2^{12}(t - t_k^2) &= \frac{1}{(\alpha^{11})^2} \sum_{n=2}^{\infty} n(n-1)(\alpha^{11})^n (f^{11})^{\otimes n}(t) * \sum_{t_k^2 < t} \varphi_2^{12}(t - t_k^2) \\ &= \frac{1}{(\alpha^{11})^2} \sum_{t_k^2 < t} \sum_{n=2}^{\infty} n(n-1)(\alpha^{11})^n (f^{11})^{\otimes n}(t) * \varphi_2^{12}(t - t_k^2) \\ &= \frac{\alpha^{12}}{(\alpha^{11})^2} \sum_{t_k^2 < t} \sum_{n=2}^{\infty} n(n-1)(\alpha^{11})^n (f^{11})^{\otimes n}(t) * f_2^{12}(t - t_k^2), \end{aligned}$$

which is upper-bounded by  $\frac{\alpha^{12}}{(\alpha^{11})^2} |\mathcal{H}_t^2| \sum_{n=2}^{\infty} n(n-1)(\alpha^{11})^n$ , which is convergent and positive.

Thus, I.C is convex.

Since I.A, I.B, I.C are all convex,  $\xi_1^1$  is convex in  $\{\alpha^{ij}\}$ .

**II. Convexity of  $\xi_1^2(\cdot; \{\alpha^{ij}\})$ .** Let us split Eq. (62) as follows:

$$\xi_1^2(t) = \overbrace{b\delta(t-d) + bh_1^{21}(t-d)}^{II.A} + \overbrace{\sum_{t_k^2 < t} \varphi_2^{22}(t - t_k^2)}^{II.B} + \overbrace{h_1^{21}(t) * \sum_{t_k^2 < t} \varphi_2^{12}(t - t_k^2)}^{II.C} \quad (72)$$

II.B and II.C are trivially convex, similar to I.B and I.C.



For II.A, observe that

$$\mathbf{Hess}_{II.A} = \left[ \frac{\partial^2(II.A)}{(\partial\alpha^{ij})^2} \right] = b \begin{pmatrix} \frac{\partial^2 h_1^{21}}{(\partial\alpha^{11})^2} & \frac{\partial^2 h_1^{21}}{(\partial\alpha^{12})^2} \\ \frac{\partial^2 h_1^{21}}{(\partial\alpha^{21})^2} & \frac{\partial^2 h_1^{21}}{(\partial\alpha^{22})^2} \end{pmatrix}. \quad (73)$$

From Eq. (70), we see that

$$\begin{aligned} \frac{\partial^2 h_1^{21}}{(\partial\alpha^{11})^2} &= \alpha^{21} \sum_{n=3}^{\infty} (n-1)(n-2)(\alpha^{11})^{n-3} f^{21} * (f^{11})^{\otimes(n-1)} \\ &= \frac{\alpha^{21}}{(\alpha^{11})^3} \sum_{n=3}^{\infty} (n-1)(n-2)(\alpha^{11})^n f^{21} * (f^{11})^{\otimes(n-1)} \geq 0 \\ \frac{\partial^2 h_1^{21}}{(\partial\alpha^{12})^2} &= \frac{\partial^2 h_1^{21}}{(\partial\alpha^{21})^2} = \frac{\partial^2 h_1^{21}}{(\partial\alpha^{22})^2} = 0 \end{aligned}$$

Since  $\|f^{ij}\| = 1$ , it can be shown that  $\frac{\alpha^{21}}{(\alpha^{11})^3} \sum_{n=3}^{\infty} (n-1)(n-2)(\alpha^{11})^n f^{21} * (f^{11})^{\otimes(n-1)} < \infty$

by the Integral Test.

The set of eigenvalues of  $\mathbf{Hess}_{II.A}$  is  $\{0, b \frac{\alpha^{21}}{(\alpha^{11})^3} \sum_{n=3}^{\infty} (n-1)(n-2)(\alpha^{11})^n f^{21} * (f^{11})^{\otimes(n-1)}(t-d)\}$ . Since all of the eigenvalues of  $\mathbf{Hess}_{II.A}$  are non-negative,  $\mathbf{Hess}_{II.A}$  is positive-semidefinite and the term II.A is convex.

It follows that  $\xi_1^2$  is convex.

### III. Convexity of $\Xi_1^1(T; \{\alpha^{ij}\})$ .

$$\Xi_1^1(t) = \overbrace{a\llbracket t > c \rrbracket + aH_1^{11}(t-c)}^{III.A} + \overbrace{\sum_{t_k^2 < t} \Phi_2^{12}(t-t_k^2)}^{III.B} + \overbrace{h_1^{11}(t) * \sum_{t_k^2 < t} \Phi_2^{12}(t-t_k^2)}^{III.C}$$

Similar to I and II, III.B and III.C have zero Hessians as  $\Phi_2^{ij}$  is linear in  $\alpha^{ij}$ .

For III.A, see that

$$\mathbf{Hess}_{III.A} = \left[ \frac{\partial^2(III.A)}{(\partial\alpha^{ij})^2} \right] = a \begin{pmatrix} \frac{\partial^2 H_1^{11}}{(\partial\alpha^{11})^2} & \frac{\partial^2 H_1^{11}}{(\partial\alpha^{12})^2} \\ \frac{\partial^2 H_1^{11}}{(\partial\alpha^{21})^2} & \frac{\partial^2 H_1^{11}}{(\partial\alpha^{22})^2} \end{pmatrix}. \quad (74)$$

Integrating Eq. (70), we see that

$$\mathbf{H}_1(t-c) = \begin{pmatrix} \sum_{n=1}^{\infty} (\alpha^{11})^n \int_c^t (f^{11})^{\otimes n}(\tau-c) d\tau & 0 \\ \alpha^{21} \sum_{n=1}^{\infty} (\alpha^{11})^{n-1} \int_c^t f^{21} * (f^{11})^{\otimes(n-1)}(\tau-c) d\tau & 0 \end{pmatrix}. \quad (75)$$

We then have

$$\begin{aligned} \frac{\partial^2 H_1^{11}}{(\partial \alpha^{11})^2} &= \sum_{n=2}^{\infty} n(n-1) (\alpha^{11})^{n-2} \int_c^t (f^{11})^{\otimes n}(\tau-c) d\tau \\ &= \frac{1}{(\alpha^{11})^2} \sum_{n=2}^{\infty} n(n-1) (\alpha^{11})^n \int_c^t (f^{11})^{\otimes n}(\tau-c) d\tau \geq 0 \\ \frac{\partial^2 H_1^{11}}{(\partial \alpha^{12})^2} &= \frac{\partial^2 H_1^{11}}{(\partial \alpha^{21})^2} = \frac{\partial^2 H_1^{11}}{(\partial \alpha^{22})^2} = 0 \end{aligned}$$

Note that  $\frac{1}{(\alpha^{11})^2} \sum_{n=2}^{\infty} n(n-1) (\alpha^{11})^n \int_c^t (f^{11})^{\otimes n}(\tau-c) d\tau$  is upper-bounded (term-by-term) by  $\frac{1}{(\alpha^{11})^2} \sum_{n=2}^{\infty} n(n-1) (\alpha^{11})^n$ , which can be shown to be convergent by the Integral Test.

Since the eigenvalues of  $\mathbf{Hess}_{III.A}$ ,  $\{0, \frac{a}{(\alpha^{11})^2} \sum_{n=2}^{\infty} n(n-1) (\alpha^{11})^n \int_c^t (f^{11})^{\otimes n}(\tau-c) d\tau\}$ , are nonnegative, III.A is convex, and consequently  $\Xi_1^1$  is convex.

#### IV. Convexity of $\Xi_1^2(T; \{\alpha^{ij}\})$ .

$$\Xi_1^2(t) = \overbrace{b \llbracket t > d \rrbracket + b H_1^{21}(t-d)}^{IV.A} + \overbrace{\sum_{t_k^2 < t} \Phi_2^{22}(t-t_k^2)}^{IV.B} + \overbrace{h_1^{21}(t) * \sum_{t_k^2 < t} \Phi_2^{12}(t-t_k^2)}^{IV.C}$$

Similar to III, IV.B and IV.C have zero Hessians as  $\alpha^{ij}$  is linear in  $\Phi_2^{ij}$ .

For IV.A, see that

$$\mathbf{Hess}_{IV.A} = \left[ \frac{\partial^2(IV.A)}{(\partial \alpha^{ij})^2} \right] = a \begin{pmatrix} \frac{\partial^2 H_1^{21}}{(\partial \alpha^{11})^2} & \frac{\partial^2 H_1^{21}}{(\partial \alpha^{12})^2} \\ \frac{\partial^2 H_1^{21}}{(\partial \alpha^{21})^2} & \frac{\partial^2 H_1^{21}}{(\partial \alpha^{22})^2} \end{pmatrix}. \quad (76)$$

From Eq. (75), we get

$$\begin{aligned}
\frac{\partial^2 H_1^{21}}{(\partial \alpha^{11})^2} &= \alpha^{21} \sum_{n=3}^{\infty} (n-1)(n-2)(\alpha^{11})^{n-3} \int_d^t f^{21} * (f^{11})^{\otimes(n-1)}(\tau-d) d\tau \\
&= \frac{\alpha^{21}}{(\alpha^{11})^3} \sum_{n=3}^{\infty} (n-1)(n-2)(\alpha^{11})^n \int_d^t f^{21} * (f^{11})^{\otimes(n-1)}(\tau-d) d\tau \geq 0 \\
\frac{\partial^2 H_1^{21}}{(\partial \alpha^{12})^2} &= \frac{\partial^2 H_1^{21}}{(\partial \alpha^{21})^2} = \frac{\partial^2 H_1^{21}}{(\partial \alpha^{22})^2} = 0
\end{aligned}$$

Note that  $\frac{\alpha^{21}}{(\alpha^{11})^3} \sum_{n=3}^{\infty} (n-1)(n-2)(\alpha^{11})^n \int_d^t f^{21} * (f^{11})^{\otimes(n-1)}(\tau-d) d\tau$  is upper-bounded by  $\frac{\alpha^{21}}{(\alpha^{11})^3} \sum_{n=3}^{\infty} (n-1)(n-2)(\alpha^{11})^n$ , which is convergent by the Integral Test.

From this we see that the eigenvalues of  $\mathbf{Hess}_{IV.A}$  are  $\{0, b \frac{\alpha^{21}}{(\alpha^{11})^3} \sum_{n=3}^{\infty} (n-1)(n-2)(\alpha^{11})^n \int_d^t f^{21} * (f^{11})^{\otimes(n-1)}(\tau-d) d\tau\}$ . As these are nonnegative, we have that  $\mathbf{Hess}_{IV.A}$  is positive-semidefinite, and so IV.A is convex. Consequently,  $\Xi_1^2$  is convex.

As  $\xi_1^1, \xi_1^2, \Xi_1^1, \Xi_1^2$  are all convex in  $\{\alpha^{ij}\}$ , it follows that the PP-PP NLL for the given exogenous function  $\boldsymbol{\mu}(t)$  is convex in  $\{\alpha^{ij}\}$ .

Now, suppose that we have a multi-impulse exogenous input, given by

$$\boldsymbol{\mu}(t) = \sum_i \begin{pmatrix} a_i \cdot \delta(t - c_i) \\ b_i \cdot \delta(t - d_i) \end{pmatrix}.$$

Since the multi-impulse exogenous input is a sum of single exogenous input functions, the effect of each impulse is simply additive on the conditional intensity  $\xi_1^1, \xi_1^2$  and the compensators  $\Xi_1^1, \Xi_1^2$ . Since a nonnegative-weighted sum of convex functions is still convex, it follows that the PP-PP NLL for the multi-impulse exogenous input is also convex in  $\{\alpha^{ij}\}$  for fixed  $\{\theta^{ij}\}$ .

## 7 Approximating the Conditional Intensity $\xi_E(t)$

As discussed in Main Text Section II.B, in general, a closed-form solution for the conditional intensity  $\xi_E(t)$  in Main Text Equation 5 is not guaranteed to exist since the infinite sum of convolutions  $\mathbf{h}_E(t) = \sum_{n=1}^{\infty} \varphi_E^{\otimes n}(t)$  cannot be expressed in closed form. In order to calculate  $\xi_E(t)$  given a sequence of observations and sample the PCMHP( $d, e$ ) process, we require the development of numerical techniques to approximate  $\xi_E(t)$ . In this section, we describe two approximations that enable calculation of  $\xi_E(t)$ .

Given the set of observed histories  $\mathcal{H}_t^{E^c}$  on  $[0, t)$ , suppose that we are interested in approximating the intensity  $\xi_E(t)$ . Main Text Equation 5 can be used for this task, however, there are two issues that we first need to address. First, the formula involves taking the convolution of functions. If the functions involved are not too complex, the convolution can be calculated in closed form. In general, however, this is not the case and we need to approximate it numerically. Second, Main Text Equation 5 contains the infinite sum of convolutions  $\mathbf{h}_E(t)$ , which in most cases cannot be written in closed form and has to be approximated as well.

To address these two issues, we introduce two approximations:

- Approximating continuous convolution with numerical convolution;
- And, approximating the infinite series  $\mathbf{h}_E(t)$  with the sum of the first  $k$  terms  $\mathbf{h}_E^k(t)$ .

### 7.1 Numerical Convolution

Let  $\mathbf{f}$  and  $\mathbf{g}$  be matrix functions defined over  $[0, t]$  such that the number of columns of  $\mathbf{f}(s)$  and the number of rows  $\mathbf{g}(s)$  are equal, *i.e.*, the matrix product  $\mathbf{f}(s) \cdot \mathbf{g}(s)$  can be calculated. Assume that we are given a partition  $\mathcal{P}[0, t]$  of  $[0, t]$  with constant increment  $\Delta^{\mathcal{P}}$ , such that

$\mathcal{P}[0, t] = \{t_0 = 0 < t_1 = \Delta^{\mathcal{P}} < t_2 = 2\Delta^{\mathcal{P}} < \dots < (P - 1)\Delta^{\mathcal{P}} = t_{P-1} < t = t_P\}$ , where  $P = \lceil t/\Delta^{\mathcal{P}} \rceil$ . Let  $\mathbf{f}[0 : t]$  be the numerical array obtained by sampling the function  $\mathbf{f}(t)$  on each point of  $\mathcal{P}[0, t]$ , *i.e.*,  $[\mathbf{f}(0), \mathbf{f}(1), \dots, \mathbf{f}(t)]$ . The array  $\mathbf{g}[0 : t]$  is defined similarly.

We introduce the conv operator, a discrete approximation to continuous function convolution, where the convolution  $\mathbf{f} * \mathbf{g}$  on  $[0, t]$  is approximated as a sum of convolution terms over the partition  $\mathcal{P}[0, t]$ . Within each subinterval, we fix  $\mathbf{g}$  at the left endpoint and perform the integration on  $\mathbf{f}$ . The univariate version of this convolution approximation scheme was considered by Rizoiu et al. (2022).

**Proposition 19** *Given a partition  $\mathcal{P}[0, t]$  of  $[0, t]$  and functions  $\mathbf{f}$  and  $\mathbf{g}$ ,  $(\mathbf{f} * \mathbf{g})(t)$  is approximated by*

$$\text{conv}(\mathbf{f}, \mathbf{g}, \mathcal{P}[0, t]) = \sum_{t_i \in \mathcal{P}[0, t]} [\mathbf{F}(t_i) - \mathbf{F}(t - \min(t_{i+1}, t))] \cdot \mathbf{g}(t_i), \quad (77)$$

where  $\cdot$  is matrix multiplication and

$$\mathbf{F}(t) = \int_0^t \mathbf{f}(\tau) d\tau.$$

**Proof**

$$\begin{aligned} \int_0^t \mathbf{f}(t - \tau) \cdot \mathbf{g}(\tau) d\tau &= \sum_{t_i \in \mathcal{P}[0, t]} \int_{t_i}^{\min(t_{i+1}, t)} \mathbf{f}(t - \tau) \cdot \mathbf{g}(\tau) d\tau \\ &\approx \sum_{t_i \in \mathcal{P}[0, t]} \left[ \int_{t_i}^{\min(t_{i+1}, t)} \mathbf{f}(t - \tau) d\tau \right] \cdot \mathbf{g}(t_i) \\ &= \sum_{t_i \in \mathcal{P}[0, t]} [\mathbf{F}(t_i) - \mathbf{F}(t - \min(t_{i+1}, t))] \cdot \mathbf{g}(t_i). \end{aligned}$$

■

To obtain an approximation for  $\varphi_E^{\otimes n}(t)$  over  $\mathcal{P}[0, t]$  for  $n \geq 2$ , Proposition 19 can be applied  $n$  times to  $\varphi_E(t)$ . Summing the resulting expressions and applying the infinite series truncation in Section 7.2 allow us to obtain the approximation  $\mathbf{h}_E[0 : t]$ .

Given  $\mathbf{h}_E[0 : t]$ , we see in Main Text Equation 5 that calculating  $\boldsymbol{\xi}_E[0 : t]$  involves a second set of convolutions, where we pair  $\mathbf{h}_E[0 : t]$  with the background intensity  $\boldsymbol{\mu}[0 : t]$  and the influence contributions of the events in the  $E^c$  dimensions. Applying Proposition 19 to these convolutions requires the integrated  $\mathbf{h}_E(t)$ , denoted as  $\mathbf{H}_E(t)$ . Proposition 20 writes this as a function of the integrated Hawkes kernel  $\Phi_E(t)$  and  $\mathbf{h}_E(t)$ .

**Proposition 20**

$$\mathbf{H}_E(t) = \Phi_E(t) + \mathbf{h}_E(t) * \Phi_E(t) \tag{78}$$

**Proof**

$$\begin{aligned} \mathbf{H}_E(t) &= \int_0^t \mathbf{h}_E(s) ds \\ &= \int_0^t \sum_{n=1}^{\infty} \varphi_E^{\otimes n}(s) ds \\ &= \sum_{n=1}^{\infty} \int_0^t \varphi_E^{\otimes n}(s) ds \\ &= \int_0^t \varphi_E(s) ds + \sum_{n=2}^{\infty} \int_0^t \varphi_E^{\otimes n}(s) ds \\ &= \Phi_E(t) + \sum_{n=2}^{\infty} \int_0^t (\varphi_E * \varphi_E^{\otimes n-1})(s) ds \\ &= \Phi_E(t) + \int_0^t \sum_{n=2}^{\infty} (\varphi_E^{\otimes n-1} * \varphi_E)(s) ds \\ &= \Phi_E(t) + \int_0^t \sum_{n=1}^{\infty} (\varphi_E^{\otimes n} * \varphi_E)(s) ds \\ &= \Phi_E(t) + \int_0^t (\mathbf{h}_E * \varphi_E)(s) ds \\ &= \Phi_E(t) + \mathbf{H}_E(t) * \Phi_E(t), \end{aligned}$$

where the last line follows from the Fubini-Tonelli Theorem and that  $\mathbf{h}_E$  and  $\varphi_E$  are  $\mathcal{L}^1$ -integrable. ■

## 7.2 Infinite Series Truncation

The infinite series  $\mathbf{h}_E(t) = \sum_{n=1}^{\infty} \varphi_E^{\otimes n}(t)$  is approximated by truncating the series up to the  $k^{\text{th}}$  term, where  $k^*$  is selected based on a convergence threshold we discuss below, and replacing the continuous convolution  $*$  with the numerical convolution operator  $\text{conv}$ . If we set

$$\text{conv}^n(\varphi_E, \mathcal{P}[0, t]) = \begin{cases} \varphi_E[0 : t] & n = 1, \\ \text{conv}(\text{conv}^{n-1}(\varphi_E, \mathcal{P}[0, t]), \varphi_E, \mathcal{P}[0, t]) & n > 1, \end{cases}$$

then our approximation to  $\mathbf{h}_E(t)$  is given by

$$\mathbf{h}_E(t) \approx \sum_{n=1}^{k^*} \text{conv}^n(\varphi_E, \mathcal{P}[0, t]). \quad (79)$$

The accuracy of this approximation can be specified by a threshold on the max norm.

**Definition 21** *Given a real matrix  $\mathbf{M} = (m^{ij})$ , we define its max norm  $\|\mathbf{M}\|_{\max}$  as*

$$\|\mathbf{M}\|_{\max} = \max_{i,j} |m^{ij}|. \quad (80)$$

Our approximation of the function  $\mathbf{h}_E$  over  $\mathcal{P}[0, t]$  is the set of points  $\mathbf{h}_E^{k^*}[0 : t]$ , where  $k^*$  is chosen to be the smallest  $k \geq 1$  such that

$$\max_{s \in \mathcal{P}[0, t]} \|\text{conv}^k(\varphi_E, \mathcal{P}[0, s])\|_{\max} < \gamma^h, \quad (81)$$

where  $\gamma^h > 0$  is a predetermined convergence threshold.

## 7.3 Algorithm to Approximate $\xi_E(t)$

Algorithm 2 combines the approximation techniques in Sections 7.1 and 7.2 to compute  $\xi_E[0 : T]$  for a pretermined maximum time  $T > 0$  and observed data  $\mathcal{H}_T^{E_c}$ . This algorithm involves three steps: (1) calculating the infinite sum approximation  $\mathbf{h}_E^{k^*}[0 : T]$ ; (2) iterating

over the events in  $E^c$  and getting the running total intensity contributed by these events; and (3) calculating  $\xi_E[0 : T]$  using Main Text Equation 5.

The two hyperparameters  $\Delta^{\mathcal{P}}$  and  $\gamma^h$  control the approximation error involved in calculating  $\xi_E(t)$ . The higher  $\Delta^{\mathcal{P}}$  and the lower  $\gamma^h$ , the better the approximation. This, of course, comes with the tradeoff of a longer computation time. Note that  $\Delta^{\mathcal{P}}$  depends on the timescale of the process considered. A simple heuristic for  $\Delta^{\mathcal{P}}$  is setting it with consideration of the interevent distribution of the point process history  $\mathcal{H}_T^{E^c}$ , i.e.  $\{t_k - t_{k-1}\}$ . One can start by setting  $\Delta^{\mathcal{P}}$  as  $M = \text{median}(\{t_k - t_{k-1}\})$ , then setting it as  $\frac{1}{2}M$ ,  $\frac{1}{3}M$ , and so on, and calculating the relative difference of  $\xi_E(t)$  for progressively smaller  $\Delta^{\mathcal{P}}$ . One then chooses  $\Delta^{\mathcal{P}}$  with a relative error lower than a predefined error threshold.

An alternative way to calculate  $\xi_E(t)$  is to interpret the PCMHP( $d, e$ ) intensity in Main Text Definition 1 as an expectation of the multivariate Hawkes intensity, with respect to the events in the  $E$  dimensions conditioned on the events in the  $E^c$  dimensions. To compute this expectation, we simply sample Hawkes event histories over the  $E$  dimensions using the Hawkes thinning algorithm, calculating the Hawkes intensity given each sample, and then average the resulting intensities. The method is presented in Section 8.

We have presented three approaches to compute  $\xi_E(t)$ : (1) a closed-form solution for the PCMHP(2, 1) process with exponential kernel derived in Section 3; (2) the approach developed in this section based on numerical convolution and infinite series truncation; and (3) a sample-based approach developed in Section 8. A comparison of  $\xi_E(t)$  obtained from these three approaches for the PCMHP(2, 1) process is presented in Section 9.



## 8 $\xi_E(t)$ as a Conditional Expectation over MHP Samples

With our definition of the PCMHP( $d, e$ ) conditional intensity  $\xi_E(t)$  as the expectation of the conditional intensity of a  $d$ -dimensional Hawkes process given observed event sequences  $\mathcal{H}_{T-}^{Ec}$ , a straightforward way to calculate  $\xi_E(t)$  is as follows:

1. Use Algorithm 3 to obtain  $n_{samples}$  samples of  $\mathcal{H}_{T-}^E$ .
2. Given the  $n^{th}$  sample  $\{\mathcal{H}_{T,n}^j = \{t_{k,n}^j\} | j \in E\}$ , calculate the Hawkes conditional intensity:

$$\lambda_n(t) = \boldsymbol{\mu} + \sum_{j \in E^c} \sum_{t_{k,n}^j < t} \boldsymbol{\varphi}^j(t - t_{k,n}^j) + \sum_{j \in E} \sum_{t_{k,n}^j < t} \boldsymbol{\varphi}^j(t - t_{k,n}^j) \quad (82)$$

3. Calculate the average to get the MBP conditional intensity:

$$\xi_E(t) = \frac{1}{n_{samples}} \sum_{n=1}^{n_{samples}} \lambda_n(t) \quad (83)$$

The approximation error of this method depends on the number of samples we take  $n_{samples}$ . The higher  $n_{samples}$  we take, the lower the standard error of our average Eq. (83).

Algorithm 3 is a modification of Ogata's thinning algorithm in Algorithm 1, where we consider the intensity contributed by the event sequences in  $\mathcal{H}_{T-}^{Ec}$  as part of the exogenous intensity, which in the usual case is just the constant  $\boldsymbol{\mu}$ .

Since the exogenous intensity is nonconstant due to this modification, Algorithm 1 has to be adjusted since it assumes a constant exogenous excitation. Specifically, we need to adjust the upper bound

$$\bar{\lambda}(t) = \sum_{i=1}^d \lambda^i(t^+) \quad (84)$$

so that its dominance holds until the next event after  $t$ .

The  $i^{th}$  component of the conditional intensity  $\lambda(t)$  given event sequences  $\mathcal{H}_{T-}^{E^c}$  can be written as

$$\lambda^i(t) = \mu^i + \sum_{j \in E^c} \sum_{t_k^j < t} \varphi^{ij}(t - t_k^j) + \sum_{j \in E} \sum_{t_k^j < t} \varphi^{ij}(t - t_k^j). \quad (85)$$

Given that every component in  $\varphi$  is non-decreasing, a natural upper bound on  $\varphi^{ij}(t - t_k^j)$  is  $\varphi^{ij}(0)$ . Thus we can write

$$\begin{aligned} \lambda^i(t) &\leq \mu^i + \sum_{j \in E^c} \varphi^{ij}(0) \sum_{t_k^j < t} 1 + \sum_{j \in E} \sum_{t_k^j < t} \varphi^{ij}(t - t_k^j) \\ &= \mu^i + \sum_{j \in E^c} \varphi^{ij}(0) |\mathcal{H}_t^j| + \sum_{j \in E} \sum_{t_k^j < t} \varphi^{ij}(t - t_k^j) \end{aligned}$$

The upper bound  $\bar{\lambda}(t)$  has to hold until the stochastic time of next event. The only non-stochastic upper bound for  $|\mathcal{H}_t^j|$  until the next event is  $|\mathcal{H}_T^j|$ . Setting this upper bound we get

$$\bar{\lambda}(t) = \sum_{i=1}^d \left[ \mu^i + \sum_{j \in E^c} |\mathcal{H}_T^j| \varphi^{ij}(0) + \sum_{j \in E} \sum_{t_k^j < t} \varphi^{ij}(t - t_k^j) \right], \quad (86)$$

which is now a correct upper bound for this setup.

---

**Algorithm 3:** Simulating an  $e$ -dimensional Hawkes Process on  $[0, T)$  Given Observed Event Sequences  $\bigcup_{j \in E^c} \mathcal{H}_T^j$  by Thinning

---

**Input:** kernel matrix  $\varphi(t)$ , exogenous excitation  $\boldsymbol{\mu}$ ; observed event sequences

$$\mathcal{H}_T^j = \{t_k^j\} \text{ for } j \in E^c; \text{ time horizon } T > 0$$

**Output:**  $\mathcal{H}_T^j = \{t_k^j\}$  for  $j \in E$

**initialize**  $t = 0$ ;  $\mathcal{H}_T^j = \emptyset$  for  $j \in E$ ;

**while**  $t < T$  **do**

$$\bar{\lambda} = \sum_{i \in E} \left[ \mu^i + \sum_{j \in E^c} |\mathcal{H}_T^j| \varphi^{ij}(0) + \sum_{j \in E} \sum_{t_k^j \leq t} \varphi^{ij}(t - t_k^j) \right];$$

$u \sim \text{uniform}(0, 1)$ ;

$$w = -\log \frac{u}{\bar{\lambda}};$$

$$t = t + w;$$

$U \sim \text{uniform}(0, 1)$ ;

**if**  $U\bar{\lambda} \leq \sum_{i \in E} \lambda^m(t)$  **then**

$$j = 1;$$

**while**  $U\bar{\lambda} \leq \sum_{i=1}^j \lambda^m(t)$  **do**

$$j = j + 1;$$

**end**

$$t_k^j = t;$$

$$\mathcal{H}_T^j = \mathcal{H}_T^j \cup \{t_k^j\};$$

**end**

**end**

**if**  $t_k^j < T$  **then**

**return**  $\mathcal{H}_T^j$  for  $j \in E$ ;

**else**

**return**  $\mathcal{H}_T^1, \dots, \mathcal{H}_T^j \setminus \{t_k^j\}, \dots, \mathcal{H}_T^e$ ;

**end**

## 9 Comparison of $\xi_E(t)$ Evaluation Methods

As noted in the main text, a closed form solution for  $\xi_E(t)$  of a generic PCMHP( $d, e$ ) process cannot be written down except in special cases. One of these special cases as we have shown in Section 3 is the PCMHP(2, 1) process with the exponential kernel. Here we present a comparison of the two approximation schemes, developed in Section 7 and Section 8, with the closed form solution for the exponential PCMHP(2, 1) process.

Fig. 2 shows a comparison of  $\xi_1^1(t)$  and  $\xi_1^2(t)$  computed through the numerical convolution approximation, as an expectation over Hawkes processes, and the closed form solution in the Appendix. We see that there is agreement in all cases, showing the viability of our two approximation methods.

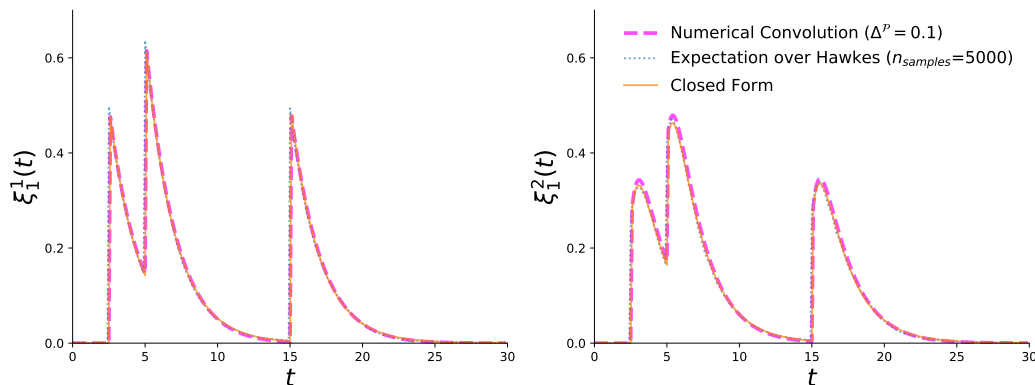


Figure 2: Comparison of the exponential PCMHP(2, 1) conditional intensity obtained three ways: (1) the method based on numerical convolution in Section 7, (2) the expectation-over-Hawkes method presented in this section, and (3) the closed-form solution in Section 3. Parameter set:  $\theta = [1, 1, 0.2, 0.5]$ ,  $\alpha = [0.5, 0.5, 0.5, 0.5]$ . Event sequence in dimension 2:  $\mathcal{H}_{30}^2 = \{2.5, 5, 15\}$ .

## 10 Numerical Scheme to Calculate PCMHP Likelihood

For this section, we assume that  $Q = E$  (see Main Text Section II.C). Algorithm 2 can be used to calculate the negative log-likelihood of a PCMHP( $d, e$ ) process given interval-censored counts in the  $E$  dimensions and event sequences in the  $E^c$  dimensions. However, it only returns the conditional intensity  $\xi_E(t)$  on the points on the partition  $\mathcal{P}[0, T]$  and does not return the compensator  $\Xi_E(t)$ . These two observations are problematic if we want to compute the negative log-likelihood  $\mathcal{L}(\Theta; T)$  because (1) we need the compensator  $\Xi_E(t)$  to compute  $\mathcal{L}(\Theta; T)$ , and (2) we would have to evaluate  $\xi_E(t)$  for every timestamp in  $\bigcup_{j \in E^c} \mathcal{H}_t^j$  and the compensator on the left and right endpoints of the observation intervals. Points where we need to evaluate these functions may not coincide with the points on  $\mathcal{P}[0, T]$ . Though we can interpolate our points of interest (*i.e.*, the event timestamps and the censor points) on the partition, it is prone to error. A more accurate approach would be to calculate the  $\xi_E(t)$  and  $\Xi_E(t)$  directly at the points of interest.

In this section, we introduce Algorithm 4, which allows us to compute  $\mathcal{L}(\Theta; T)$  given a set of event sequences and observed counts.

Let  $\mathcal{T} = \bigcup_{j \in E^c} \{T_p^j\}$  be the collection of all observed event timestamps in the  $E^c$  dimensions. Let  $\mathcal{O} = \bigcup_{j \in E} \{o_p^j\} = \bigcup_{j \in E} \mathcal{O}^j$  be the collection of all censor points in the  $E$  dimensions. Let  $\mathcal{P} = \{0 = t_0 < \dots < t_P = T\}$  be a partition of the time interval  $[0, T]$  with step size  $\frac{P}{T}$ . Define the points-of-interest set  $\tilde{\mathcal{T}}$  as the union of these three sets supplied with labels  $\mathcal{C}_i$ . Let

$$\tilde{\mathcal{T}} = \{(t_i, \mathcal{C}_i)\} = \mathcal{T} \cup \mathcal{O} \cup \mathcal{P}, \quad (87)$$

where  $t_i$  is the  $i^{\text{th}}$  point-of-interest,  $\mathcal{C}_i = \{(r_j, d_j)\}$  is a set of ordered pairs containing

point  $t_i$ 's roles  $\{r_j\}$  and corresponding dimensions of interest  $\{d_j\}$ . Here,  $r_j \in \{ts, o, p\}$ , where  $ts$ ,  $o$  and  $p$  represent event timestamp, observation censor point and partition point, respectively. In the case that  $r_j = p$ ,  $d_j$  is unspecified. Otherwise,  $d_j \in D$ .

We iterate over  $\tilde{\mathcal{T}}$  in Algorithm 4, storing the contribution of each point-of-interest to the interval-censored log-likelihood and point-process log-likelihood defined in Main Text Equations 7 and 8, respectively. The overall log-likelihood  $\mathcal{L}(\Theta; T)$  is then the sum of these two.

**Runtime Complexity.** To get an estimate of the runtime complexity, observe that Algorithm 4 can be decomposed into three major steps.

1. pre-compute  $\mathbf{h}_E[t_0 : t_P]$  and  $\mathbf{H}_E[t_0 : t_P]$ ,
2. iterate over  $k \in \tilde{\mathcal{T}}$ , computing  $\mathbf{a}[t_k]$  and  $\mathbf{A}[t_k]$ ,  $\boldsymbol{\xi}_E$  if  $t_k$  is an  $E^c$ -timestamp (to calculate the PP-LL contribution), and  $\boldsymbol{\Xi}_E$  if  $t_k$  is an  $E$ -censor point, and
3. iterate over  $E$  to calculate the total IC-LL.

To get the runtime complexity of the first step, we first observe that  $\mathbf{h}_E[t_0 : t_P]$  is composed of an infinite sum of self-convolutions of  $\boldsymbol{\varphi}_E$  over the partition  $\mathcal{P}$  (see Eq. (79)). Given the partition length  $\Delta^P$ , there are  $\lceil \frac{T}{\Delta^P} \rceil$  partition points. For each partition point, we perform a matrix multiplication of  $\mathcal{O}(d \cdot e)$  entries, since  $\boldsymbol{\varphi}_E$  is a  $d \times d$  matrix with  $e$  nonzero columns. Thus a single convolution scales as  $\mathcal{O}(\lceil \frac{T}{\Delta^P} \rceil \cdot d \cdot e)$ . Consequently,  $\mathbf{h}_E[t_0 : t_P]$  is obtained by recursively applying the convolution operation and summing up the  $k^*$  terms (see Eq. (81)), yielding  $\mathcal{O}(k^* \cdot \lceil \frac{T}{\Delta^P} \rceil \cdot d \cdot e)$  operations.

For the second step, we assume that  $\tilde{\mathcal{T}} = \{\mathcal{T}, \mathcal{O}, \mathcal{P}\}$  are pairwise disjoint, so that we can write  $|\tilde{\mathcal{T}}| = |\mathcal{T}| + |\mathcal{O}| + |\mathcal{P}| = n^E + n^{E^c} + \lceil \frac{T}{\Delta^P} \rceil$ . For each point  $t_k$  in  $\tilde{\mathcal{T}}$ , we pre-compute  $\mathbf{a}[t_k]$  and  $\mathbf{A}[t_k]$ , which takes  $\mathcal{O}(n^{E^c} \cdot d)$  operations (since we loop over all Hawkes datapoints

in  $E^c$  and we have to compute  $\mathbf{a}$  and  $\mathbf{A}$  values in each dimension. Next, we compute  $\xi_E$  only for points  $t_k \in \mathcal{T}$  (since we need them for PP-LL calculations). Each point  $t_k \in \mathcal{T}$  (of which there are  $\frac{n^{E^c}}{n^E + n^{E^c} + \lceil \frac{T}{\Delta^P} \rceil}$ ) requires  $\mathcal{O}(d + \lceil \frac{T}{\Delta^P} \rceil \cdot d \cdot e)$  operations (evaluation of exogenous intensity and the convolution operation). Similarly, each point  $t_k \in \mathcal{O}$  (of which there are  $\frac{n^E}{n^E + n^{E^c} + \lceil \frac{T}{\Delta^P} \rceil}$ ) requires  $\mathcal{O}(d + \lceil \frac{T}{\Delta^P} \rceil \cdot d \cdot e)$  operations. Thus, the second step has runtime complexity  $\mathcal{O}\left(|\tilde{\mathcal{T}}| \cdot \left[ n^{E^c} \cdot d + \frac{n^E + n^{E^c}}{|\tilde{\mathcal{T}}|} \cdot \lceil \frac{T}{\Delta^P} \rceil \cdot d \cdot e \right]\right)$ . The first term, being quadratic in the number of events, dominates over the second, being linear, hence we can simplify the complexity as  $\mathcal{O}\left(|\tilde{\mathcal{T}}| \cdot n^{E^c} \cdot d\right)$ .

The third step has complexity  $\mathcal{O}(n^E)$ .

Consider two cases.

(a) If  $E^c = \emptyset$ , then  $n^{E^c} = 0$ , simplifying the second step's complexity to  $\mathcal{O}\left(n^E \cdot \lceil \frac{T}{\Delta^P} \rceil \cdot d \cdot e\right)$ . The total runtime complexity is then linear in  $n^E$ , similar to that of the MBP (Poisson) process.

(b) If  $E^c \neq \emptyset$ , we observe that the first term of the second step's complexity is quadratic in  $n^{E^c}$ , similar to the MHP. In practice (particularly for high-frequency data), the number of observed Hawkes events  $n^{E^c}$  dominates in magnitude over the other parameters, which leads to the second step dominating the time complexity. Thus, the runtime complexity of Algorithm 4 scales as  $\mathcal{O}\left(|n^E + n^{E^c} + \lceil \frac{T}{\Delta^P} \rceil| \cdot n^{E^c} \cdot d\right)$ .

Thus the runtime complexity of evaluating the PCMHP likelihood intuitively lies in between the complexity of the MBP (Poisson) process and MHP.

## 11 Gradient $\mathcal{L}_{\Theta}(\Theta; T)$ Calculations

In this section we calculate the gradient of the negative log-likelihood  $\mathcal{L}(\Theta; T)$ . Our starting point is Main Text Equation 6. Taking the gradient with respect to the parameter

vector  $\Theta$  of both sides and using linearity of the gradient operator, we have

$$\mathcal{L}_\Theta(\Theta; T) = \sum_{j \in E} \partial_\Theta \mathcal{L}_{\text{IC-LL}}^j(\Theta; T) + \sum_{j \in E^c} \partial_\Theta \mathcal{L}_{\text{PP-LL}}^j(\Theta; T). \quad (88)$$

Taking the gradient of Main Text Equation 7 and Main Text Equation 8, we obtain:

$$\partial_\Theta \mathcal{L}_{\text{IC-LL}}^j(\Theta; T) = \sum_{k=1}^{n^j} [\partial_\Theta \Xi^j(\sigma_k^j) - \partial_\Theta \Xi^j(\sigma_{k-1}^j)] \left[ 1 - \frac{C_k^j}{\Xi^j(\sigma_k^j) - \Xi^j(\sigma_{k-1}^j)} \right] \quad (89)$$

$$\partial_\Theta \mathcal{L}_{\text{PP-LL}}^j(\Theta; T) = \sum_{t_k^j \in \mathcal{H}_T^j} \frac{-\partial_\Theta \xi^j(t_k^j)}{\xi^j(t_k^j)} + \partial_\Theta \Xi^j(T). \quad (90)$$

Now we would need to calculate the gradients of the conditional intensity  $\xi_E$  and the compensator  $\Xi_E$ . Recall that our parameter vector  $\Theta$  consists of the Hawkes kernel parameters contained in  $\varphi$  and the exogenous parameters  $\gamma$  and  $\nu$ , in view of Eq. (93).

Let  $\theta \in \{\gamma^i, \nu^i\}$ . Taking derivatives of Main Text Equation 5 and Eq. (37), we see that

$$\partial_{\gamma^k} \xi^i(t) = \delta_{ik} \cdot \delta^k(t) + h_E^{ik}(t)$$

$$\partial_{\nu^k} \xi^i(t) = \delta_{ik} + H_E^{ik}(t)$$

$$\partial_{\gamma^k} \Xi^i(t) = \delta_{ik} + H_E^{ik}(t)$$

$$\partial_{\nu^k} \Xi^i(t) = t \cdot \delta_{ik} + h_E^{ik}(t) * t.$$

Let  $\theta$  be a parameter of the Hawkes kernel  $\varphi$ . For example, if we use the exponential kernel, then  $\theta \in \{\theta^{ij}, \alpha^{ij}\}$ . Again, taking derivatives of Main Text Equation 5 and Eq. (37), we get

$$\begin{aligned} \partial_\theta \xi(t) &= \sum_{i \in E^c} \sum_{t_k^i < t} \partial_\theta \varphi_{E^c}^i(t - t_k^i) + \mathbf{h}_E(t) * \sum_{i \in E^c} \sum_{t_k^i < t} \partial_\theta \varphi_{E^c}^i(t - t_k^i) \\ &\quad + \partial_\theta \mathbf{h}_E(t) \cdot \gamma + \partial_\theta \mathbf{h}_E(t) * \left( \nu + \sum_{i \in E^c} \sum_{t_k^i < t} \partial_\theta \varphi_{E^c}^i(t - t_k^i) \right), \end{aligned} \quad (91)$$

$$\begin{aligned} \partial_\theta \Xi(t) &= \sum_{i \in E^c} \sum_{t_k^i < t} \partial_\theta \Phi_{E^c}^i(t - t_k^i) + \mathbf{h}_E(t) * \sum_{i \in E^c} \sum_{t_k^i < t} \partial_\theta \Phi_{E^c}^i(t - t_k^i) \\ &\quad + \partial_\theta \mathbf{h}_E(t) * \left( \gamma + \nu \cdot t + \sum_{i \in E^c} \sum_{t_k^i < t} \partial_\theta \Phi_{E^c}^i(t - t_k^i) \right). \end{aligned} \quad (92)$$



The derivatives involving  $\varphi_{E^c}$  and  $\Phi_{E^c}$  are straightforward to calculate given the form of the Hawkes kernel. The derivative involving  $\partial_\theta \mathbf{h}_E(t)$  can be calculated from  $\varphi_E(t)$  and its self-convolutions using the following observation:

$$\begin{aligned}
\partial_\theta \mathbf{h}_E &= \partial_\theta \sum_{n=1}^{\infty} \varphi_E^{\otimes n} \\
&= \sum_{n=1}^{\infty} \partial_\theta \varphi_E^{\otimes n} \\
&= \partial_\theta \varphi_E + \sum_{n=2}^{\infty} \partial_\theta \varphi_E^{\otimes n} \\
&= \partial_\theta \varphi_E + \sum_{n=2}^{\infty} \partial_\theta (\varphi_E^{\otimes n-1} * \varphi_E) \\
&= \partial_\theta \varphi_E + \sum_{n=2}^{\infty} (\varphi_E^{\otimes n-1} * \partial_\theta \varphi_E + \partial_\theta \varphi_E^{\otimes n-1} * \varphi_E) \\
&= \partial_\theta \varphi_E + \sum_{n=2}^{\infty} \left( \varphi_E^{\otimes n-1} * \partial_\theta \varphi_E + \partial_\theta \varphi_E * \varphi_E^{\otimes n-1} + \sum_{k=1}^{n-2} \varphi_E^{\otimes k} * \partial_\theta \varphi_E * \varphi_E^{\otimes n-k-1} \right).
\end{aligned}$$

We can leverage this recursive calculation to compute  $\partial_\theta \mathbf{h}_E(t)$  efficiently. The method is presented in Algorithm 5.

---

**Algorithm 5:** Computing  $\partial_\theta \mathbf{h}_E$  recursively over a partition of  $[0, T]$

---

**Input:** partition, convergence threshold  $\gamma$

**Output:**  $\partial_\theta \mathbf{h}_E$

$B = \partial_\theta \varphi_E;$

$S, A = B$

**do**

$B = \varphi_E * B;$

$A = B + A * \varphi_E;$

$S = S + A;$

**while**  $\|A\| \geq \gamma;$

**return**  $S$

---

Lastly, observe that Eq. (91) and Eq. (92) both contain a term involving convolution with  $\partial_\theta \mathbf{h}_E(t)$ . From Proposition 19, computing this convolution requires us to have an

expression for  $\partial_\theta \mathbf{H}_E(t)$ , the integral of  $\partial_\theta \mathbf{h}_E(t)$ . We can obtain this expression from  $\partial_\theta \mathbf{h}_E(t)$  as follows:

$$\begin{aligned}
\mathbf{h}_E(t) &= \sum_{n=1}^{\infty} \varphi_E^{\otimes n}(t) \\
&= \varphi_E(t) + \sum_{n=2}^{\infty} \varphi_E^{\otimes n}(t) \\
&= \varphi_E(t) + \sum_{n=1}^{\infty} (\varphi_E^{\otimes n} * \varphi_E)(t) \\
&= \varphi_E(t) + (\mathbf{h}_E * \varphi_E)(t).
\end{aligned}$$

Integrating both sides, we get

$$\mathbf{H}_E(t) = \Phi_E(t) + (\mathbf{h}_E * \Phi_E)(t)$$

Taking the derivative of both sides with respect to  $\theta$  and then applying the convolution product rule, we get

$$\begin{aligned}
\partial_\theta \mathbf{H}_E(t) &= \partial_\theta \Phi_E(t) + \partial_\theta (\mathbf{h}_E(t) * \Phi_E(t)) \\
&= \partial_\theta \Phi_E(t) + \partial_\theta \mathbf{h}_E(t) * \Phi_E(t) + \mathbf{h}_E(t) * \partial_\theta \Phi_E(t).
\end{aligned}$$

In every iteration of Algorithm 4, the gradients  $\partial_\theta \boldsymbol{\xi}(t)$  and  $\partial_\theta \boldsymbol{\Xi}(t)$  can be computed alongside  $\boldsymbol{\xi}(t)$  and  $\boldsymbol{\Xi}(t)$  for every  $\theta \in \Theta$ . These values are then passed one layer above to Eq. (89) and Eq. (90) to get the ICLL and PPLL gradients, respectively. Finally, the return values are passed to Eq. (88) to compute the overall gradient  $\mathcal{L}_\Theta(\Theta; T)$ . Computing the gradients does not affect the runtime complexity of Algorithm 4.

## 12 Sampling from PCMHP

Given  $\bigcup_{j \in E^c} \mathcal{H}_{t^-}^j$ , Algorithm 2 allows us to calculate the PCMHP( $d, e$ ) conditional intensity  $\boldsymbol{\xi}_E(t)$ . However, to ‘continue’ the process, we need to be able to sample events that

occur beyond  $t$ . We can obtain samples from a  $\text{PCMHP}(d, e)$  process using the thinning algorithm presented in Algorithm 6. Here, we consider a specific form of the exogenous rate  $\boldsymbol{\mu}(t)$ , given by

$$\boldsymbol{\mu}(t) = \boldsymbol{\gamma} \cdot \boldsymbol{\delta}(t) + \boldsymbol{\nu}, \quad (93)$$

where  $\boldsymbol{\gamma}, \boldsymbol{\nu} \in (\mathbb{R}^+)^d$  are learnable parameters.

Intuitively, this corresponds to a spike of magnitude  $\boldsymbol{\gamma}$  at  $t = 0$  and a constant rate  $\boldsymbol{\nu}$  over time. This form of  $\boldsymbol{\mu}(t)$  follows Rizoiu et al. (2017, 2022).

## 12.1 Thinning Algorithm

Algorithm 6 is a modified version of Ogata’s thinning algorithm (Ogata 1988) for the multivariate Hawkes process, with two modifications. First, this version of the thinning algorithm uses the appropriate upper bound  $\xi_E^{ub}$  for  $\text{PCMHP}(d, e)$ , considering that the  $\text{PCMHP}(d, e)$  has a different conditional intensity from Hawkes, and the latter’s upper bound will not be valid for  $\text{PCMHP}(d, e)$  except in the special case  $E = \emptyset$ . We derive this upper bound in Section 12.2. Second, given that the conditional intensity  $\boldsymbol{\xi}_E(t)$  in general cannot be written in closed form, we would need to apply the approximations detailed in Section 7. In addition, sampling forward in time requires us to be able to compute  $\boldsymbol{\xi}_E(t)$  at every candidate event time, and due to the convolution term, we have to keep track of the Hawkes intensity contributed by every previous event accepted by the thinning algorithm. We introduce a stepsize parameter  $\Delta^t > 0$  that controls the discretization in time when we approximate the Hawkes intensity.

---

**Algorithm 6:** Simulating a Partial MBP Process on  $[0, T]$  with Thinning
 

---

**Input:** kernel matrix  $\varphi(t)$ , kernel integral matrix  $\Phi(t)$ , exogenous parameters  $\gamma, \nu$ ; dimension labels  $E, E^c$ ; time horizon  $T > 0$ ;  
 partition  $\mathcal{P}[0, T] = [0 : T]$  with increment  $\Delta^{\mathcal{P}}$ ; threshold  $\gamma^h > 0$ ; stepsize  $\Delta^t > 0$

**Output:**  $\mathcal{H}_T^j = \{t_k^j\}$  for  $j = 1 : d$

**initialize**  $t = 0$ ;  $\mathcal{H}_T^j = \emptyset$  for  $j = 1 : d$ ;  $\mathcal{T}_U = \mathbf{a}_U = []$ ;

**do**

- $\Delta[0 : T] = \text{conv}(\Delta, \varphi_E, [0 : T])$ ;
- $\mathbf{h}_E[0 : T] = \mathbf{h}_E[0 : T] + \Delta[0 : T]$ ;

**while**  $\max_{p=0:P} (\|\Delta[t_p]\|_{\max}) \geq \gamma^h$ ;

$\mathbf{H}_E[0 : T] = \Phi[0 : T] + \text{conv}(\mathbf{h}_E, \Phi, [0 : T])$ ;

$\mathbf{h}_E^{ub} = \max \mathbf{h}_E[0 : T]$ , entrywise;

**while**  $t < T$  **do**

- $\xi_E^{ub} = \nu + \mathbf{h}_E^{ub} \cdot (\gamma + T\nu + \sum_{j \in E^c} |\mathcal{H}_T^j| \Phi_{E^c}^j(T)) + \sum_{j \in E^c} \sum_{t_k^j \leq t} \varphi_{E^c}^j(t - t_k^j)$ ;
- $\xi_E^{ub} = \sum_{i=1}^d (\xi_E^{ub})^i$ ;
- $u \sim \text{uniform}(0, 1)$ ;
- $w = -\log \frac{u}{\xi_E^{ub}}$ ;
- $\mathcal{T} = \text{discretize}([t, t + w], \Delta^t)$ ;
- $\mathbf{a}[0 : |\mathcal{T}|] = \mathbf{0}$ ;
- for**  $i = 0 : |\mathcal{T}|$  **do**

  - $\mathbf{a}[i] = \sum_{j \in E^c} \sum_{s \in \mathcal{H}_T^j} \varphi_{E^c}^j(\mathcal{T}[i] - s)$ ;

- end**
- $t = t + w$ ;
- $\mathcal{T}_U = \mathcal{T}_U \cup \mathcal{T}$ ;
- $\mathbf{a}_U[0 : |\mathcal{T}_U|] = [\mathbf{a}_U, \mathbf{a}]$ ;
- $\xi_E = \nu + \mathbf{h}_E(t) \cdot \gamma + \text{conv}(\mathbf{h}_E, \nu + \mathbf{a}_U, \mathcal{T}_U \cup \{t\}) + \sum_{j \in E^c} \sum_{t_k^j < t} \varphi_{E^c}^j(t - t_k^j)$ ;
- $U \sim \text{uniform}(0, 1)$ ;
- if**  $U \xi_E^{ub} \leq \sum_{i=1}^d \xi_E^m(t)$  **then**

  - $j = 1$ ;
  - while**  $U \xi_E^{ub} \leq \sum_{i=1}^j \xi_E^m(t)$  **do**

    - $j = j + 1$ ;

  - end**
  - $t_k^j = t$ ;
  - $\mathcal{H}_T^j = \mathcal{H}_T^j \cup \{t_k^j\}$ ;

- end**

**end**

**if**  $t_{kj}^j < T$  **then**

- return**  $\mathcal{H}_T^j$  for  $j = 1 : d$ ;

**else**

- return**  $\mathcal{H}_T^1, \dots, \mathcal{H}_T^d \setminus \{t_k^j\}, \dots, \mathcal{H}_T^d$ ;

**end**

---

**Remark 22** Algorithm 6 has two discretization parameters  $\Delta^{\mathcal{P}}$  and  $\Delta^t$ . The first increment  $\Delta^{\mathcal{P}}$  controls the discretization for  $\mathbf{h}_E$ , while the second increment  $\Delta^t$  controls the discretization for the Hawkes intensity term  $\sum_{j \in E^c} \sum_{s \in \mathcal{H}_T^j} \varphi_{E^c}^j(t - s)$ . In general, we would like to keep both increments as small as possible, but this comes at a tradeoff of computation

time. However, there is a higher priority to keep  $\Delta^{\mathcal{P}}$  small as  $\mathbf{h}_E$ , being an infinite sum, could hit convergence issues if  $\Delta^{\mathcal{P}}$  is not small enough.

## 12.2 Derivation of Thinning Upper Bounds for PCMHP( $d, e$ )

In this section we derive the appropriate upper bounds for the PCMHP( $d, e$ ) process used in the thinning algorithm.

We were able to derive two different upper bounds. The first one can be calculated in a simple manner, and we use this in our implementation of Algorithm 3 to generate samples from PCMHP( $d, e$ ). However, this upper bound has the potential to be large if for some  $(i, j) \in D \times D$ ,  $\max_{t \leq T} \mathbf{h}_E^{ij}(t)$  is high, causing the thinning algorithm to propose and subsequently reject many trial points. We therefore introduce a second upper bound that bounds the intensity more closely, leading to faster sampling. We use this in our popularity prediction use case in Main Text Section IV.

**Upper Bound 1.** We need to find an upper bound at arbitrary time  $t > 0$  (that holds up until the next stochastic event) for each of the terms in the conditional intensity below.

$$\boldsymbol{\xi}_E(t) = \boldsymbol{\mu}(t) + (\mathbf{h}_E * \boldsymbol{\mu})(t) + \sum_{j \in E^c} \sum_{t_k^j < t} \boldsymbol{\varphi}_{E^c}^j(t - t_k^j) + \left( \mathbf{h}_E(t) * \left[ \sum_{j \in E^c} \sum_{t_k^j < t} \boldsymbol{\varphi}_{E^c}^j(t - t_k^j) \right] \right), \quad (94)$$

where

$$\boldsymbol{\mu}(t) = \boldsymbol{\gamma} \cdot \boldsymbol{\delta}(t) + \boldsymbol{\nu}(t).$$

Let  $\bar{\mathbf{h}}_E$  be the matrix whose  $(i, j)$  entry is  $\max_{t \leq T} \mathbf{h}_E^{ij}(t)$ .

Let  $\bar{\boldsymbol{\nu}} = \max \boldsymbol{\nu}_{s \leq T}(t)$ . Then the first term is bounded above by  $\bar{\boldsymbol{\nu}}$ .

For the second term, we have the following upper bound that holds for all  $t$ :

$$\begin{aligned}
(\mathbf{h}_E * \boldsymbol{\mu})(t) &= \mathbf{h}_E(t) * (\boldsymbol{\gamma} \cdot \boldsymbol{\delta}(t) + \boldsymbol{\nu}(t)) \\
&= \mathbf{h}_E(t) \cdot \boldsymbol{\gamma} + \int_0^t \mathbf{h}_E(t-s) \cdot \boldsymbol{\nu}(s) ds \\
&\leq \bar{\mathbf{h}}_E \cdot \boldsymbol{\gamma} + \int_0^T \bar{\mathbf{h}}_E \cdot \bar{\boldsymbol{\nu}} ds \\
&= \bar{\mathbf{h}}_E \cdot (\boldsymbol{\gamma} + T\bar{\boldsymbol{\nu}}).
\end{aligned}$$

For the third term, as in the usual Thinning algorithm for Hawkes, an upper bound that holds until the next event is  $\sum_{j \in E^c} \sum_{t_k^j \leq t} \boldsymbol{\varphi}_{E^c}^j(t - t_k^j)$ .

Lastly, for the fourth term, an upper bound that holds until the next event is given by:

$$\begin{aligned}
\mathbf{h}_E(t) * \sum_{j \in E^c} \sum_{t_k^j < t} \varphi_{E^c}^j(t - t_k^j) &\leq \mathbf{h}_E(t) * \sum_{j \in E^c} \sum_{t_k^j \leq t} \varphi_{E^c}^j(t - t_k^j) \\
&= \int_0^t \mathbf{h}_E(t - s) \cdot \sum_{j \in E^c} \sum_{t_k^j \leq t} \varphi_{E^c}^j(s - t_k^j) ds \\
&= \bar{\mathbf{h}}_E \cdot \int_0^t \sum_{j \in E^c} \sum_{t_k^j \leq t} \varphi_{E^c}^j(s - t_k^j) ds \\
&= \bar{\mathbf{h}}_E \cdot \sum_{j \in E^c} \sum_{t_k^j \leq t} \int_0^t \varphi_{E^c}^j(s - t_k^j) ds \\
\text{(a)} &= \bar{\mathbf{h}}_E \cdot \sum_{j \in E^c} \sum_{t_k^j \leq t} \int_{-t_k^j}^{t-t_k^j} \varphi_{E^c}^j(u) du \\
\text{(b)} &= \bar{\mathbf{h}}_E \cdot \sum_{j \in E^c} \sum_{t_k^j \leq t} \int_0^{t-t_k^j} \varphi_{E^c}^j(u) du \\
&= \bar{\mathbf{h}}_E \cdot \sum_{j \in E^c} \sum_{t_k^j \leq t} \Phi_{E^c}^j(t - t_k^j) \\
\text{(c)} &\leq \bar{\mathbf{h}}_E \cdot \sum_{j \in E^c} \sum_{t_k^j \leq t} \Phi_{E^c}^j(t) \\
&= \bar{\mathbf{h}}_E \cdot \sum_{j \in E^c} |\mathcal{H}_t^j| \Phi_{E^c}^j(t) \\
\text{(d)} &\leq \bar{\mathbf{h}}_E \cdot \sum_{j \in E^c} |\mathcal{H}_t^j| \Phi_{E^c}^j(T).
\end{aligned}$$

where in (a) we made a change of variable  $u = s - t_k^j$ , in (b) we used the fact that  $\varphi^{ij}(t) = 0$  for  $t < 0$ , in (c) we used the fact that since  $\varphi^{ij}(t)$  is non-increasing,  $\Phi^{ij}(t)$  is non-decreasing and thus  $\Phi^{ij}(t) \geq \Phi^{ij}(t - s)$  for  $s \geq 0$ , and finally in (d) we bound  $\Phi_{E^c}^j$  by its maximum value on  $[0, T]$ .

Thus an upper bound at  $t$  until the next event is given by

$$\text{u.b.}(t) = \bar{\nu} + \bar{\mathbf{h}}_E \cdot \left( \gamma + T\bar{\nu} + \sum_{j \in E^c} |\mathcal{H}_t^j| \Phi_{E^c}^j(T) \right) + \sum_{j \in E^c} \sum_{t_k^j \leq t} \varphi_{E^c}^j(t - t_k^j). \quad (95)$$

Suppose we are given an exponential kernel  $\varphi^{ij}(t) = \kappa^{ij} \theta^{ij} \exp^{-\theta^{ij}t}$ , with corresponding

$\Phi^{ij}(t) = \kappa^{ij} \left(1 - \exp^{-\theta^{ij}t}\right)$ . We can simplify the upper bound by using  $\Phi_{E^c}^j(\infty) = \kappa^j$  instead of  $\Phi_{E^c}^j(T)$ , since  $\Phi_{E^c}^j(\infty) \geq \Phi_{E^c}^j(t)$  for any time  $t$ . Then we would have

$$\text{u.b.}(t) = \bar{\nu} + \bar{\mathbf{h}}_E \cdot \left( \gamma + T\bar{\nu} + \sum_{j \in E^c} |\mathcal{H}_t^j| \kappa^j \right) + \sum_{j \in E^c} \sum_{t_k^j \leq t} \varphi_{E^c}^j(t - t_k^j).$$

**Upper Bound 2.** Suppose the exogenous intensity is given by

$$\boldsymbol{\mu}(t) = \boldsymbol{\gamma} \cdot \boldsymbol{\delta}(t) + \boldsymbol{\nu}.$$

An upper bound for the conditional intensity at  $t$  until the next stochastic event is

$$\begin{aligned} & \boldsymbol{\nu} + \sum_{j \in E^c} \sum_{t_k^j \leq t} \varphi^j(t - t_k^j) + \max_{s \geq t} \mathbf{h}_E(s) \cdot \boldsymbol{\gamma} \\ & + \mathbf{H}_E(\infty) \cdot \boldsymbol{\nu} + \left[ \text{upper bound of } \mathbf{h}_E(t) * \sum_{j \in E^c} \sum_{t_k^j < t} \varphi^j(t - t_k^j) \right], \end{aligned} \quad (96)$$

which we get by upper bounding each term in Eq. (94). The fourth term  $\mathbf{H}_E(\infty) \cdot \boldsymbol{\nu}$  is obtained by noting that  $\mathbf{H}_E(t)$  is a non-decreasing function and hence upper-bounded by  $\mathbf{H}_E(\infty)$ .

The tricky part here is obtaining an expression for the rightmost term. Let  $t' \geq t$ . Our goal is to find a function  $\mathbf{f}(t)$  that satisfies

$$\mathbf{f}(t') \geq \mathbf{h}_E(t') * \sum_{j \in E^c} \sum_{t_k^j < t'} \varphi^j(t' - t_k^j) = \int_0^{t'} \mathbf{h}_E(t' - s) \cdot \sum_{j \in E^c} \sum_{t_k^j < s} \varphi^j(s - t_k^j) ds \quad (97)$$

We split the rightmost integral as

$$\int_0^t \mathbf{h}_E(t' - s) \cdot \sum_{j \in E^c} \sum_{t_k^j < s} \varphi^j(s - t_k^j) ds + \int_t^{t'} \mathbf{h}_E(t' - s) \cdot \sum_{j \in E^c} \sum_{t_k^j < s} \varphi^j(s - t_k^j) ds \quad (98)$$

and aim to bound these two terms separately.

To proceed, introduce

$$\hat{h}_E^{ij}(t) = \begin{cases} \max_s h_E^{ij}(s) & t < \operatorname{argmax}_s h_E^{ij}(s) \\ h_E^{ij}(t) & \text{otherwise} \end{cases}$$



Let  $\hat{\mathbf{h}}_E(t) = [\hat{h}_E^{ij}(t)]$ . Observe that

$$\hat{\mathbf{h}}_E(t) \geq \mathbf{h}_E(t) \quad (99)$$

for all  $t \geq 0$ .

Let  $t' \geq s \geq t \geq 0$ . We have  $\hat{\mathbf{h}}_E(t' - s) \geq \mathbf{h}_E(t' - s)$ . Multiplying both sides by  $\sum_{j \in E^c} \sum_{t_k^j < s} \varphi^j(s - t_k^j)$  and integrating over  $s \in [0, t)$ , we get

$$\int_0^t \hat{\mathbf{h}}_E(t' - s) \cdot \sum_{j \in E^c} \sum_{t_k^j < s} \varphi^j(s - t_k^j) ds \geq \int_0^t \mathbf{h}_E(t' - s) \cdot \sum_{j \in E^c} \sum_{t_k^j < s} \varphi^j(s - t_k^j) ds \quad (100)$$

Next, note that  $\hat{\mathbf{h}}_E(t)$  is non-increasing. That is, given  $t' \geq t \geq s$ ,

$$\hat{\mathbf{h}}_E(t - s) \geq \hat{\mathbf{h}}_E(t' - s) \quad (101)$$

So we have

$$\int_0^t \hat{\mathbf{h}}_E(t - s) \cdot \sum_{j \in E^c} \sum_{t_k^j < s} \varphi^j(s - t_k^j) ds \geq \int_0^t \mathbf{h}_E(t' - s) \cdot \sum_{j \in E^c} \sum_{t_k^j < s} \varphi^j(s - t_k^j) ds \quad (102)$$

Thus we have an upper bound for the first term.

For the second term, observe that since we are working under the assumption of no events between  $t$  and  $t'$ ,

$$\begin{aligned} \int_t^{t'} \hat{\mathbf{h}}_E(t' - s) \cdot \sum_{j \in E^c} \sum_{t_k^j < s} \varphi^j(s - t_k^j) ds &= \int_t^{t'} \hat{\mathbf{h}}_E(t' - s) \cdot \sum_{j \in E^c} \sum_{t_k^j \leq t} \varphi^j(s - t_k^j) ds \\ &\leq \int_t^{t'} \hat{\mathbf{h}}_E(t' - s) \cdot \sum_{j \in E^c} \sum_{t_k^j \leq t} \varphi^j(t - t_k^j) ds \\ &= \int_t^{t'} \hat{\mathbf{h}}_E(t' - s) ds \cdot \sum_{j \in E^c} \sum_{t_k^j \leq t} \varphi^j(t - t_k^j) \\ &= [\hat{\mathbf{H}}_E(t' - t) - \hat{\mathbf{H}}_E(0)] \cdot \sum_{j \in E^c} \sum_{t_k^j \leq t} \varphi^j(t - t_k^j) \\ &= \hat{\mathbf{H}}_E(t' - t) \cdot \sum_{j \in E^c} \sum_{t_k^j \leq t} \varphi^j(t - t_k^j) \\ &\leq \hat{\mathbf{H}}_E(T - t) \cdot \sum_{j \in E^c} \sum_{t_k^j \leq t} \varphi^j(t - t_k^j) \end{aligned}$$

This is the upper bound for the second term. Here,  $\hat{\mathbf{H}}_E(t)$  is given by

$$\hat{H}_E^{ij}(t) = \begin{cases} \max_s h_E^{ij}(s) \cdot t & t < u = \operatorname{argmax}_s h_E^{ij}(s) \\ H_E^{ij}(t) + [\max_s h_E^{ij}(s) \cdot u - H_E^{ij}(u)] & \text{otherwise} \end{cases}$$

### 13 Prediction of Expected Counts with PCMHP( $d, e$ )

Once a PCMHP( $d, e$ ) model is fitted to a set of event sequences  $\bigcup_{j \in E^c} \mathcal{H}_{T^-}^j$  and interval-censored counts  $\bigcup_{j \in E} \{\mathbf{C}_k^j\}_{k=1}^{n^j}$ , this can be used to predict the expected count of events in any interval of time past  $t = T$ .

Suppose that we observe events and counts on  $[0, T^{\text{train}})$  and we wish to predict the expected count of events in every dimension on every subinterval of the partition  $\mathcal{P}[T^{\text{train}}, T^{\text{test}})$ , where  $T^{\text{test}} > T^{\text{train}}$ . The most straightforward way to do this is to continue the PCMHP( $d, e$ ) process on  $[T^{\text{train}}, T^{\text{test}})$  by using Algorithm 6 to draw sample histories. For each sample, we count the number of events in each dimension on each subinterval of  $\mathcal{P}[T^{\text{train}}, T^{\text{test}})$ . The expected count on a subinterval would then be the average of the counts on the selected subinterval over the set of sample histories.

The problem with the previous approach is that it is not computationally efficient to perform the sampling, as we have to sample all dimensions simultaneously in Algorithm 6, especially problematic if some dimensions have a high background intensity.

Let  $\mathcal{P}[T^{\text{train}}, T^{\text{test}}) = \bigcup_{i=1}^{P-1} [o_i, o_{i+1})$ , where  $o_1 = T^{\text{train}}$  and  $o_P = T^{\text{test}}$ , be a partition of  $[T^{\text{train}}, T^{\text{test}})$ . A computationally efficient scheme to predict expected counts can be done with the following three-step approach.

1. Sample only the  $E^c$  dimensions on  $[T^{\text{train}}, T^{\text{test}})$ .

2. For each sample, compute expected counts on  $\mathcal{P}[T^{train}, T^{test}]$  as  $\{\Xi_E(o_{i+1}) - \Xi_E(o_i) | i \in 1 \cdots P - 1\}$ .
3. Compute the average of  $\{\Xi_E(o_{i+1}) - \Xi_E(o_i) | i \in 1 \cdots P - 1\}$  across samples.

This approach relies on two properties of the PCMHP( $d, e$ ) process. First,  $\xi_E(t)$  and  $\Xi_E(t)$  only depends on the  $E^c$  dimensions, and so we only need to actually sample these dimensions to calculate the intensity and compensator as these are independent of events that occurs in the  $E$  dimensions. Second, similar to what is stated in Remark 2 for the Hawkes process, the compensator  $\Xi_E(t)$  of a PCMHP( $d, e$ ) process can be interpreted as the expected count of events on  $[0, t)$  given event sequences  $\bigcup_{j \in E^c} \mathcal{H}_{t-}^j$ . Given a sample event sequence  $\bigcup_{j \in E^c} \mathcal{H}_{o_{i+1}}^j$ , the difference  $\Xi_E(o_{i+1}) - \Xi_E(o_i)$  then represents the expected count of events in  $[o_i, o_{i+1})$ . By averaging over samples, we are averaging over histories  $\bigcup_{j \in E^c} \mathcal{H}_{o_{i+1}}^j$ , and so we get expected counts on  $\mathcal{P}[T^{train}, T^{test}]$ .

Note that there is a subtle difference between the two approaches. The first approach returns event sequences in each dimension, which we then count and average over to get expected values. On the other hand, the second approach directly estimates the expected counts as it uses the compensator of the process.

Fig. 3 shows a comparison of the two methods over 1000 samples. We assume here that we observe data up until  $T^{train} = 10$  and we wish to get expected counts on  $\mathcal{P}[10, 20) = [10, 11), \dots, [19, 20)$ . The solid lines show the estimate of the expected count. It is evident that there is very good agreement between the two approaches. The uncertainty clouds around the lines mean different things. Since the second approach directly estimates the expected counts, the cloud around the blue line represents the variance of the expected counts, whereas the red cloud represents the variance of the counts across different histories.

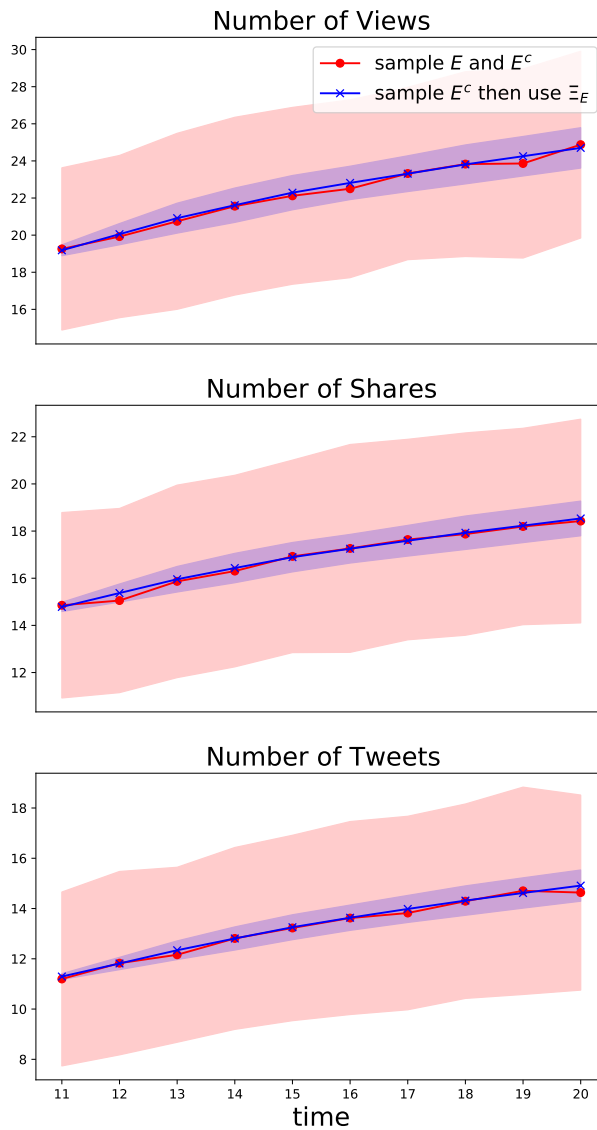


Figure 3: Comparing the two ways of predicting expected counts with  $\text{PCMHP}(d, e)$ . The first method samples all dimensions, while the second method samples only the Hawkes dimensions and uses the compensator of the process to estimate expected counts. In the figure, we observe data until  $T^{\text{train}} = 10$  and compute event counts over  $[10, 11), \dots, [19, 20)$ .

## 14 Additional Results for Section III

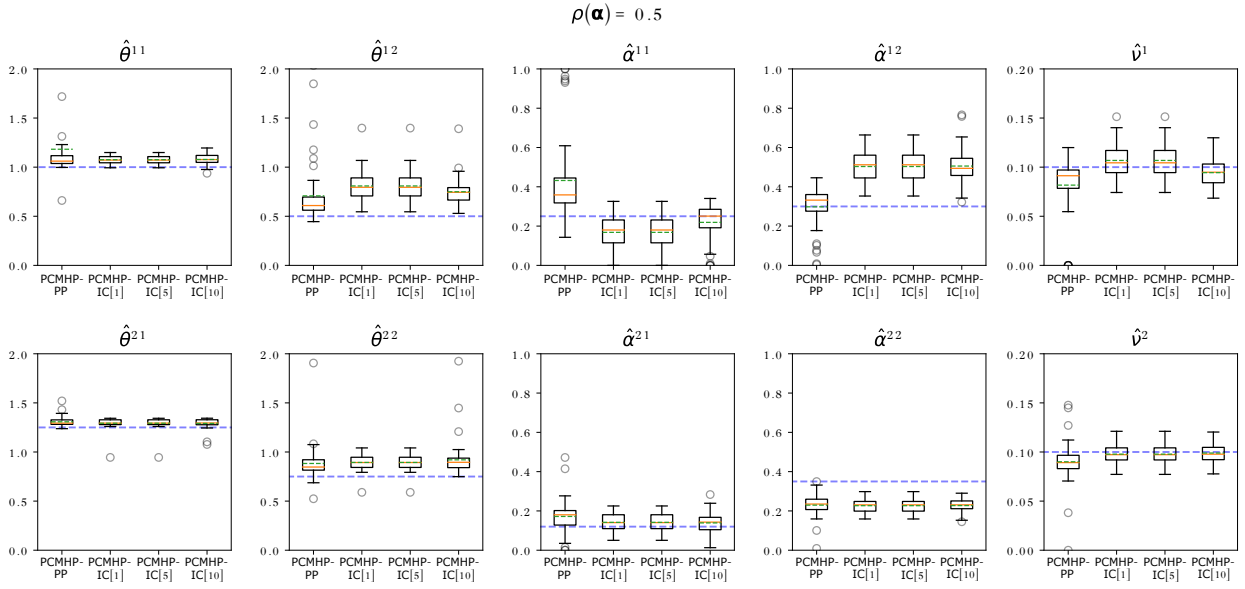


Figure 4: *The MHP model parameters can be reliably estimated with the PCMHP model. Parameter recovery results for  $\rho(\boldsymbol{\alpha}) = 0.5$ . In each subplot we show the parameter estimates obtained from the PCMHP(2, 1) model fitted on samples from a 2-dimensional MHP model using PCMHP-PP and PCMHP-IC. We consider three variants of interval censoring (observation window lengths 1, 5, and 10). The mean and median estimates are indicated by the dashed green lines and solid orange lines, respectively. The dashed blue lines show the original parameters of the MHP model.*

## 14.1 Individual Parameter Estimates

Here we present individual parameter fits of the PCMHP(2, 1) model on 2-dimensional MHP data. Table 1 lists the parameters for three considered values of the spectral radius:  $\rho(\boldsymbol{\alpha}) \in \{0.5, 0.75, 0.9\}$ . The  $\rho(\boldsymbol{\alpha}) = 0.5$  indicates a clearly subcritical MHP; the  $\rho(\boldsymbol{\alpha}) = 0.9$  corresponds to a MHP approaching the critical regime; and  $\rho(\boldsymbol{\alpha}) = 0.75$  corresponds to an intermediate case between these two.

Fig. 4, Fig. 5 and Fig. 6 show the PCMHP(2, 1)-estimated  $\{\boldsymbol{\theta}, \boldsymbol{\alpha}, \boldsymbol{\nu}\}$  for the parameter sets corresponding to  $\rho(\boldsymbol{\alpha}) = 0.5$ ,  $\rho(\boldsymbol{\alpha}) = 0.75$  and  $\rho(\boldsymbol{\alpha}) = 0.9$  in Table 1.

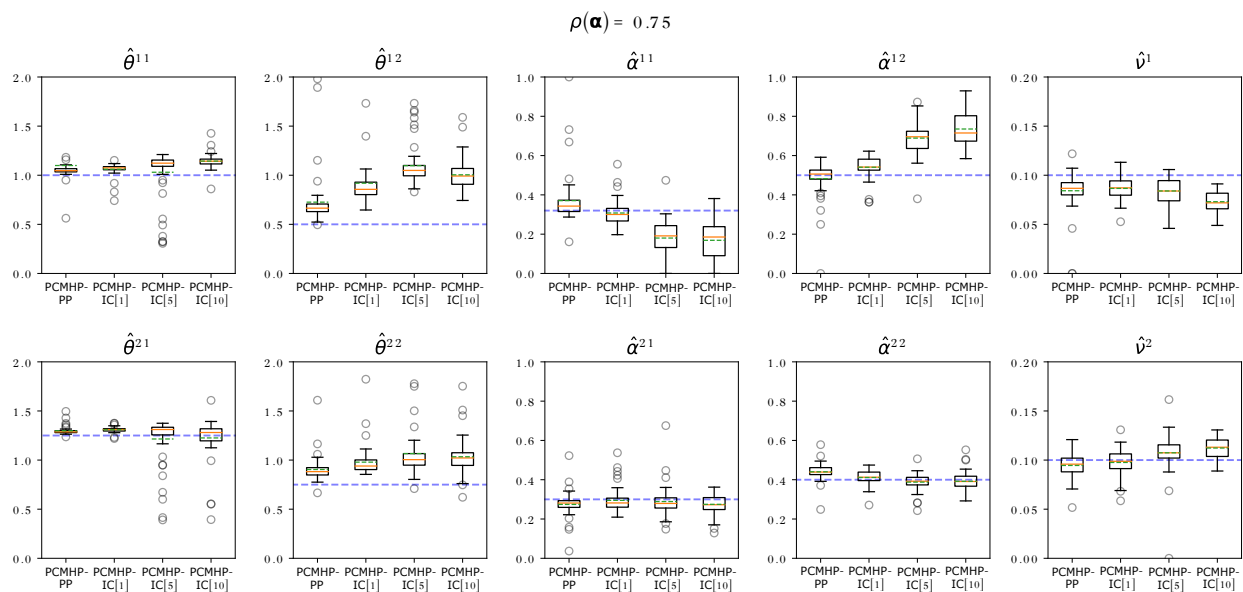


Figure 5: *The MHP model parameters can be reliably estimated with the PCMHP model. Parameter recovery results for  $\rho(\boldsymbol{\alpha}) = 0.75$ . In each subplot we show the parameter estimates obtained from the PCMHP(2,1) model fitted on samples from a 2-dimensional MHP model using PCMHP-PP and PCMHP-IC. We consider three variants of interval censoring (observation window lengths 1, 5, and 10). The mean and median estimates are indicated by the dashed green lines and solid orange lines, respectively. The dashed blue lines show the original parameters of the MHP model.*

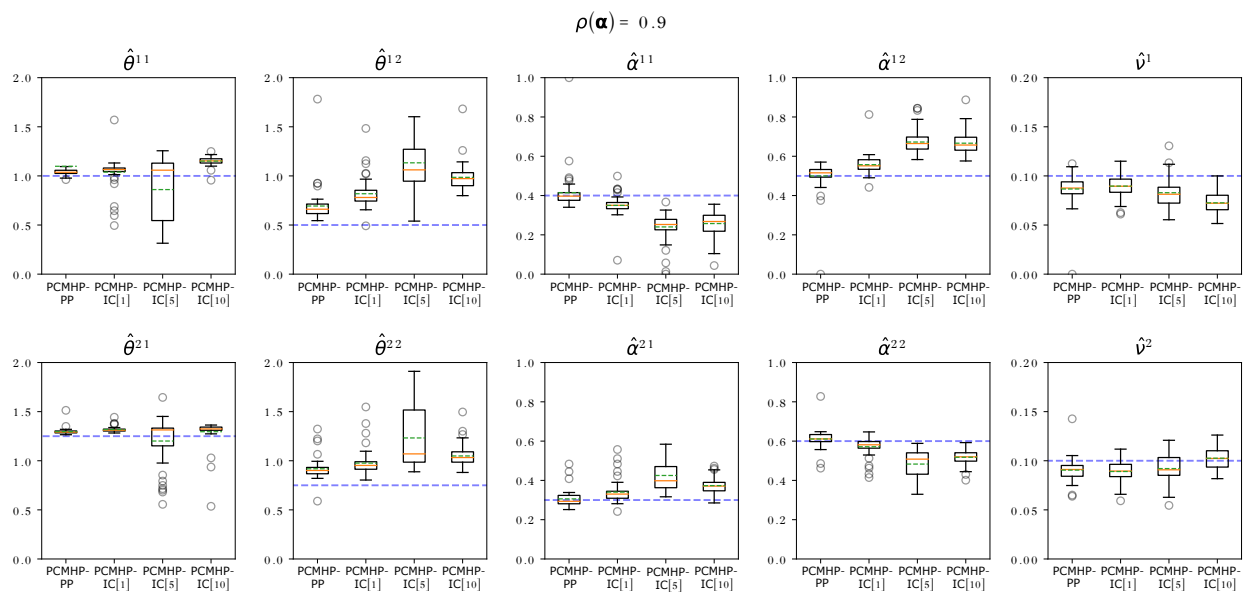


Figure 6: *The MHP model parameters can be reliably estimated with the PCMHP model. Parameter recovery results for  $\rho(\boldsymbol{\alpha}) = 0.9$ . In each subplot we show the parameter estimates obtained from the PCMHP(2, 1) model fitted on samples from a 2-dimensional MHP model using PCMHP-PP and PCMHP-IC. We consider three variants of interval censoring (observation window lengths 1, 5, and 10). The mean and median estimates are indicated by the dashed green lines and solid orange lines, respectively. The dashed blue lines show the original parameters of the MHP model.*

**Parameter recovery.** Below we discuss results for the case  $\rho(\boldsymbol{\alpha}) = 0.75$  (Fig. 5). Results for  $\rho(\boldsymbol{\alpha}) = 0.5$  and  $\rho(\boldsymbol{\alpha}) = 0.9$  are similar. The horizontal dashed blue lines show the values used for generating the data. For each parameter, we plot four boxplots. The leftmost boxplot is the PCMHP-PP fit (*i.e.*, the fit on the timestamp dataset). The next three are the PCMHP-IC[1], PCMHP-IC[5], and PCMHP-IC[10] fits.

We see that the PCMHP-PP estimates are tight around the generating MHP parameters for all parameters. This indicates that the model mismatch information loss (*i.e.*, of type (1)) appears to have a small impact on fitting quality. Arguably, we observe a slight overestimation for  $\theta^{12}$  and  $\theta^{22}$ , and a clear overestimation of  $\alpha^{11}$  and underestimation of  $\alpha^{22}$ . The  $\nu^i$  parameters appear tightly recovered by PCMHP on the timestamp dataset.

On the partially interval-censored dataset, we continue to observe good fits. This indicates that PCMHP can successfully recover the generating MHP parameters even after interval-censoring. However, we see that the  $\theta^{ij}$  parameters become increasingly overestimated as the observation window widens, particularly for  $\theta^{12}$  and  $\theta^{22}$ . Similarly,  $\alpha^{12}$  is overestimated, and  $\alpha^{11}$  is underestimated. The approximation quality degrades as the observation window widens, indicating an increasing information loss of type (2).

**Recovery of the spectral radius.** We see in Fig. 7 that the estimated spectral radius  $\rho(\hat{\boldsymbol{\alpha}})$  is close to the actual value regardless of the model mismatch and interval-censoring. The recovered spectral radius is estimated close to the original MHP spectral radius for all considered cases.

## 14.2 Convergence Analysis

We study the error convergence of the PCMHP(2, 1)-estimated parameters  $\{\hat{\boldsymbol{\theta}}, \hat{\boldsymbol{\alpha}}, \hat{\boldsymbol{\nu}}\}$  and spectral radius  $\rho(\hat{\boldsymbol{\alpha}})$  under different settings of (1) the time window  $T$  over which we fit the



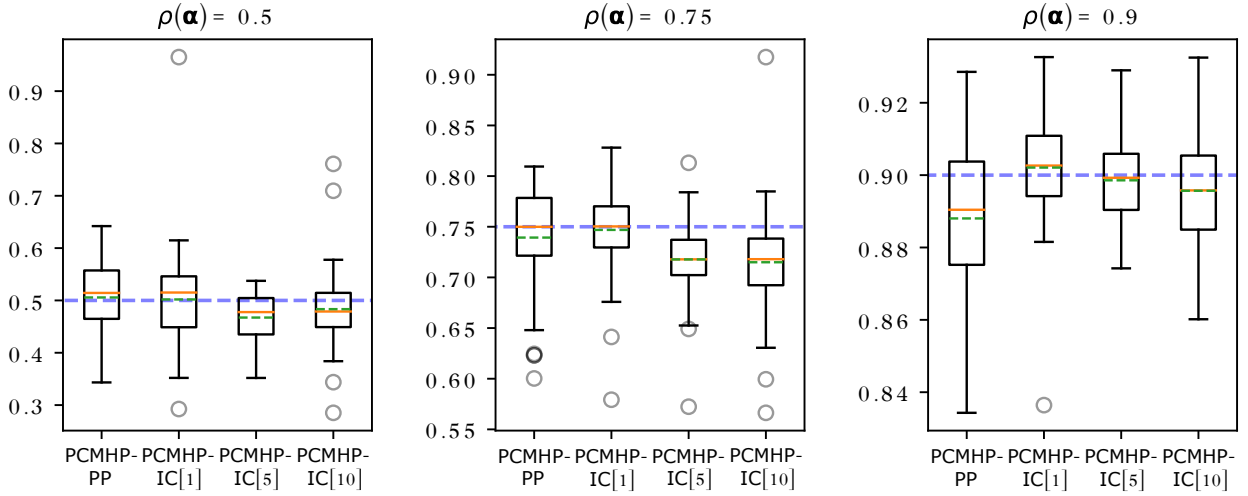


Figure 7: *The spectral radius estimated by the PCMHP model approximates well the spectral radius of the generating MHP.* In each column we show the spectral radius estimated from the PCMHP(2, 1) model fitted on samples from a 2-dimensional MHP model (see parameters in Table 1). Dashed lines show the spectral radii of the MHP model.

model and (2) the number of sequences used for joint fitting (see Remark 17). Next, we fix  $T$  and investigate spectral radius recovery of the underlying MHP by fitting PCMHP(2, 1) over datasets of increasing spectral radii.

**Varying  $T$  and  $N_{sequences}$ .** Fig. 8a, Fig. 8c, Fig. 8e and Fig. 8g show  $\text{RMSE}(\alpha)$ ,  $\text{RMSE}(\theta)$ ,  $\text{RMSE}(\nu)$  and  $\Delta\rho$  as a function of the fitting window length  $T$ , respectively. Meanwhile, Fig. 8b, Fig. 8d, Fig. 8f and Fig. 8h show  $\text{RMSE}(\alpha)$ ,  $\text{RMSE}(\theta)$ ,  $\text{RMSE}(\nu)$  and  $\Delta\rho$  as a function of the number of sequences in the joint fit, respectively. Both sets of plots correspond to the case  $\rho(\alpha) = 0.75$  parameter set in Table 1. We see in Figs. 8a and 8g that  $\text{RMSE}(\alpha)$  and  $\Delta\rho$  both converge to stable values as we increase the length of the fitting time window and the number of sequences in the joint fit.

**Varying the spectral radius.** In Fig. 9a we evaluate how well our different models recover the MHP spectral radius. We fix  $T = 100$ ,  $N_{sequences} = 50$  and we plot the

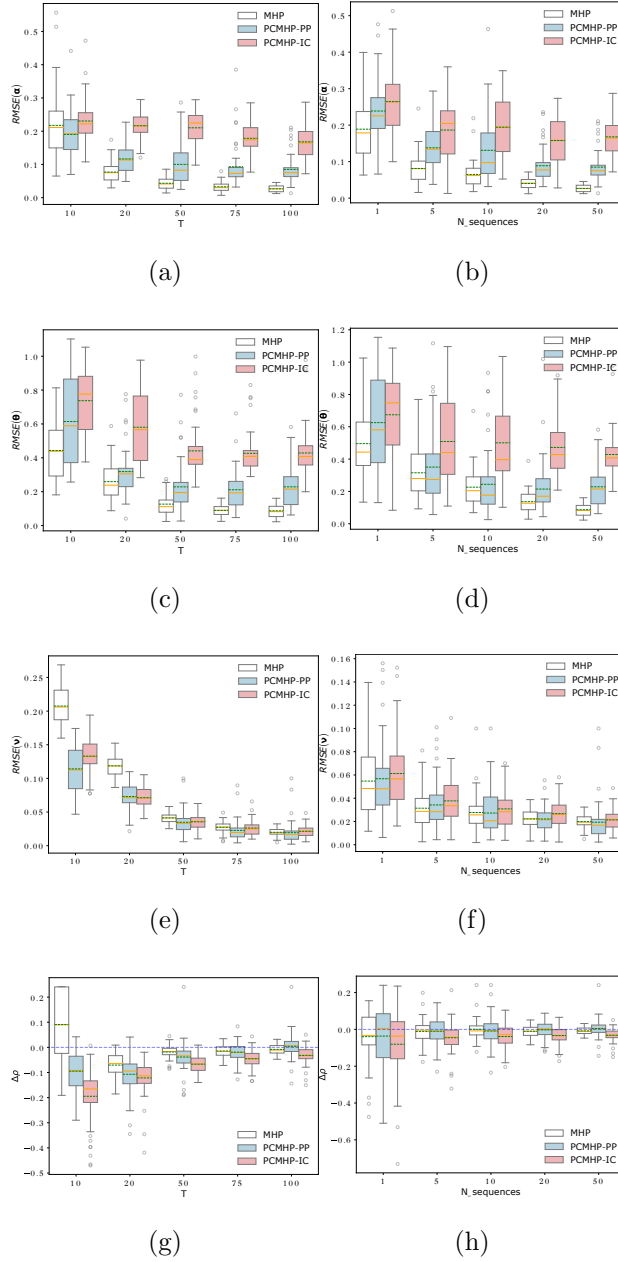
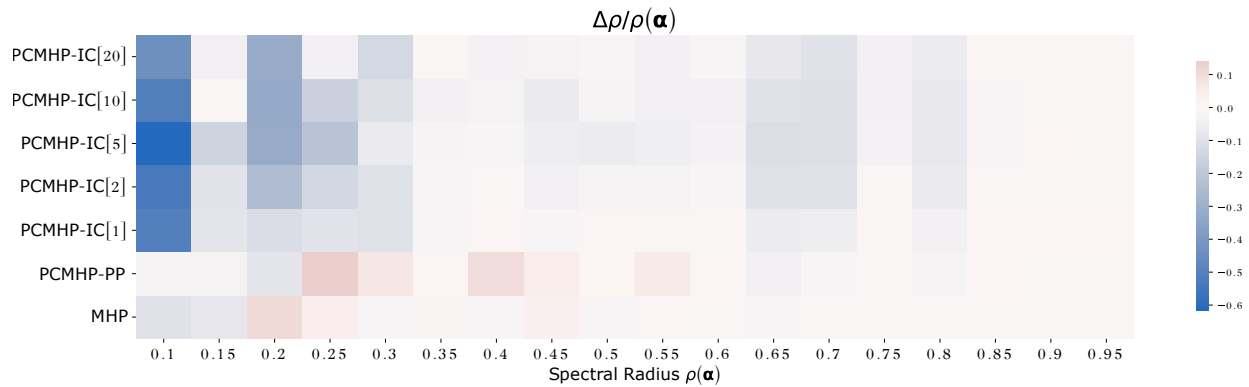


Figure 8: The error of  $\hat{\alpha}$  (first row),  $\hat{\theta}$  (second row),  $\hat{\nu}$  (third row) and recovered spectral radius (fourth row) are plotted vs. varying  $T$  (left column) and  $N_{sequences}$  (right column). Samples are drawn from a 2D MHP with  $\rho(\alpha) = 0.75$  and parameters in Table 1. Default hyperparameters are  $T = 100$ ,  $N_{sequences} = 50$  and interval size = 5. In each plot we compare performance for three model fits: MHP, PCMHP-PP and PCMHP-IC as three boxplots. The mean and median estimates are indicated by the dashed green lines and solid orange lines, respectively.

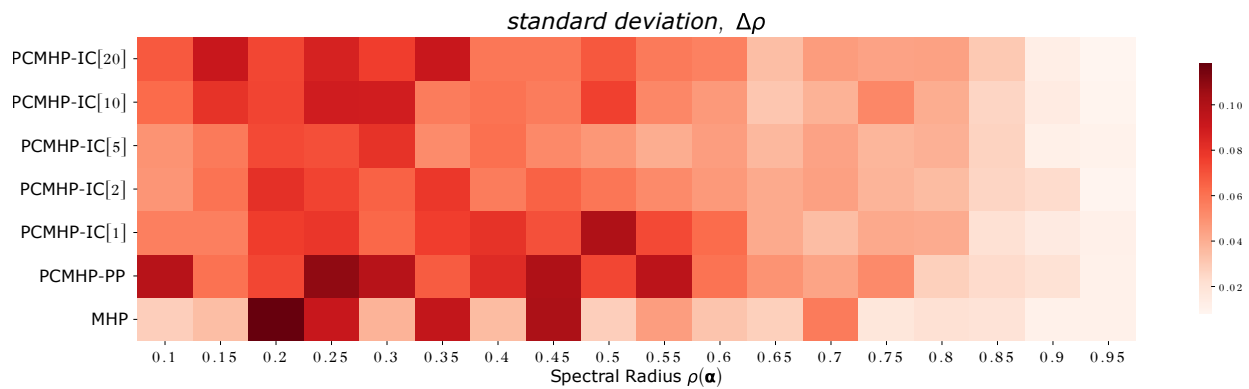
spectral radius deviation  $\Delta\rho$  as a function of the generating MHP spectral radius  $\rho(\boldsymbol{\alpha})$ . We generate samples from 2D MHPs with increasing  $\rho(\boldsymbol{\alpha}) \in \{0.1, 0.15, \dots, 0.9, 0.95\}$  and we fit MHP, PCMHP-PP, and PCMHP-IC[ $k$ ] for  $k \in \{1, 2, 5, 10, 20\}$ . We see that when the spectral radius is not too small, it is recovered well. This is intuitive since for small spectral radius, the MHP generates only a few events to fit on. We also notice that fitting with partially interval-censored data (*i.e.* the PCMHP-IC fits) tends to underestimate the spectral radius. In Fig. 9b we plot the standard deviation of the estimated  $\Delta\rho$  when fitted to MHP samples of different spectral radii for different model configurations.

**Varying the number of MBP dimensions  $e$ .** Here, we consider the PCMHP(5,  $e$ ) and vary  $e \in \{0, 1, 2, 3, 4, 5\}$ . We fix  $T = 100$  and  $\rho(\boldsymbol{\alpha}) = 0.92$ . We plot the parameter recovery error for  $\boldsymbol{\alpha}$  (Fig. 10a),  $\boldsymbol{\theta}$  (Fig. 10b) and  $\boldsymbol{\nu}$  (Fig. 10c). We see in Figs. 10a and 10c that  $\text{RMSE}(\boldsymbol{\alpha})$  and  $\text{RMSE}(\boldsymbol{\nu})$  increase with  $e$ , while in Fig. 10b that  $\text{RMSE}(\boldsymbol{\theta})$  plateaus for intermediate  $e$ . The behavior for  $\boldsymbol{\alpha}$  and  $\boldsymbol{\nu}$  is not surprising since a higher  $e$  implies more MHP dimensions are replaced with MBP, increasing the model mismatch information loss.

**On the consistency of the PCMHP estimator.** The convergence of  $\text{RMSE}(\boldsymbol{\alpha})$  and  $\Delta\rho$  of the PCMHP-PP (Figs. 8a and 8g) for high  $T$  and number of sequences provide evidence of the consistency of the PCMHP MLE estimator for the MHP. Similar to (Rizoïu et al. 2022), we perform numerical experiments in lieu of an analytical treatment to study limiting behavior since – as far as we are aware – there is no previous literature on the asymptotic theory (consistency and asymptotic normality) of the MLE for multivariate nonstationary MHPs (which the PCMHP falls under). Previous work has focused on the consistency of the univariate stationary (Ogata 1978), multivariate stationary (Chornoboy et al. 1988, Guo et al. 2018) and univariate nonstationary (Chen & Hall 2013) cases. The



(a)



(b)

Figure 9: (a) The deviation of recovering the spectral radius by our various approaches, as a function of the spectral radius itself. The x-axis shows a wide array of spectral radius values and the y-axis presents the different models used for fitting. The color shows the mean deviation  $\Delta\rho/\rho(\boldsymbol{\alpha})$  over multiple fittings. (b) Standard deviation of  $\Delta\rho$  vs. the spectral radius of the generating MHP. Rows correspond to the spectral radius  $\rho(\boldsymbol{\alpha})$  of the MHP samples used for data generation, while the columns represent the different models used for fitting.

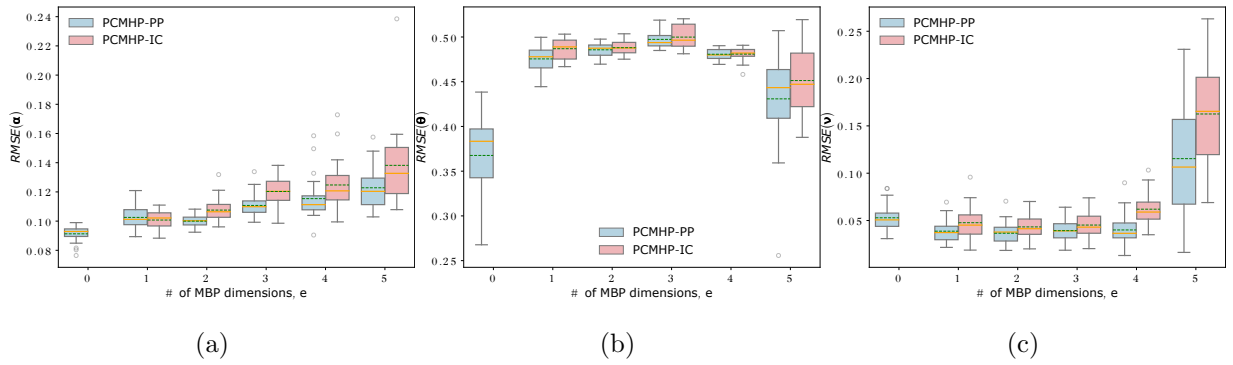


Figure 10: *Recovery error increases with the number of MHP dimensions we replace with MBP.* Error of  $\hat{\alpha}$ ,  $\hat{\theta}$  and  $\hat{\nu}$  are plotted as functions of the number of MBP dimensions  $e$ . Samples are drawn from a 5-dimensional MHP with spectral radius  $\rho(\alpha) = 0.92$ . Hyperparameters are  $T = 100$ ,  $N_{sequences} = 20$  and interval size = 1. We compare the PCMHP-PP, and PCMHP-IC model fits in each column. The mean and median estimates are indicated by the dashed green lines and solid orange lines, respectively.

asymptotic theory of MLE for multivariate nonstationary MHPs and the partially interval-censored case are both open topics and fruitful directions for future work.

## 15 Additional Details for Section IV

In this section, we provide additional details on the fitting procedure for the PCMHP(3,3) and PCMHP(3,2) models on the online video popularity task and the filtering procedure we performed on ACTIVE to identify dynamic videos for performance evaluation.

### 15.1 Technical Details for Fitting

We present here details on fitting PCMHP(3,3) and PCMHP(3,2) models on the ACTIVE dataset of views/shares/tweets. Specifically, we discuss four points:

1. assigning weights to each dimension’s contribution to  $\mathcal{L}(\Theta; T)$ ,
2. regularizing the exogenous parameter  $\nu$ ,
3. hyperparameter tuning, and
4. the optimization algorithm.

**Assigning weights to each dimension’s contribution to  $\mathcal{L}(\Theta; T)$ .** For the first point, recall that the negative log-likelihood for a PCMHP process given a mix of event sequences and interval-censored data is defined as the sum of the likelihood contribution in each dimension. Recall for the PCMHP that

$$\mathcal{L}(\Theta; T) = \sum_{j \in E} \mathcal{L}_{\text{IC-LL}}^j(\Theta; T) + \sum_{j \in E^c} \mathcal{L}_{\text{PP-LL}}^j(\Theta; T).$$

A problem that we encountered with this formulation is that it treats the dimensions equally, but the scale of each dimension’s values could differ largely from one another. For instance, in the online video popularity case study, view counts are orders of magnitudes higher than share counts and tweet counts, which would then cause the likelihood contribution of views to dominate the total likelihood, prioritizing fit on the views over the tweets and shares. This is problematic, in particular, for the PCMHP(3, 2) model as we want to fit the tweets dimension well, as it drives the self- and cross-exciting behavior of the process. To solve this, we assign a dimension weight hyperparameter  $w^j$  to each dimension  $j \in D$  which we multiply to the log-likelihood contribution of dimension  $j$ . Instead of  $\mathcal{L}(\Theta; T)$ , we use a dimension-weighted version  $\mathcal{L}(\Theta; T, \mathbf{w})$ , given by

$$\mathcal{L}(\Theta; T, \mathbf{w}) = \sum_{j \in E} w^j \mathcal{L}_{\text{IC-LL}}^j(\Theta; T) + \sum_{j \in E^c} w^j \mathcal{L}_{\text{PP-LL}}^j(\Theta; T). \quad (103)$$

The corresponding gradients for this dimension-weighted version can be obtained by a trivial adjustment of Section 11.

**Regularizing the exogenous parameter  $\nu$ .** For the PCMHP models we fit in the online popularity case study in Main Text Section IV and COVID-19 case study in Main Text Section V, we optimize the parameter set  $\Theta = \{\theta, \alpha, \nu\}$ . To reduce the size of the parameter space, the initial impulse parameters  $\gamma$  are fixed as hyperparameters. Similar to Bessy-Roland et al. (2021), we found that adding a term that regularizes the exogenous parameter  $\nu$  on the dimension-weighted likelihood  $\mathcal{L}(\Theta; T, \mathbf{w})$  in Eq. (103) further improves performance. We introduce another hyperparameter  $w^\nu$  that controls the level of regularization on the  $\mathcal{L}^1$  norm  $\|\nu\|_1$ . Intuitively, using a higher  $w^\nu$  is equivalent to biasing the model optimization to avoid taking on high values for the baseline intensities  $\nu$ , thereby resulting to larger values in  $\alpha$ . The regularized version of Eq. (103), where  $\mathbf{w} = \{w^1, \dots, w^d, w^\nu\}$ , is then given by

$$\mathcal{L}(\Theta; T, \mathbf{w}) = \sum_{j \in E} w^j \mathcal{L}_{\text{IC-LL}}^j(\Theta; T) + \sum_{j \in E^c} w^j \mathcal{L}_{\text{PP-LL}}^j(\Theta; T) + w^\nu \|\nu\|_1. \quad (104)$$

This is the version of the log-likelihood that we use to fit the models in Main Text Section IV and Main Text Section V. The parameter set that we optimize for is  $\Theta = \{\theta, \alpha, \nu\}$ .

**Hyperparameter tuning.** The hyperparameters that we tune in our model are shown in Table 2. There are three different types of hyperparameters we consider. The first two types are the dimension weights  $\{w^j\}$  and the  $\nu$  regularization weight  $w^\nu$  we discussed above. The third hyperparameter is how we fix the  $\gamma$  parameter. We consider two different modes: (1) max, where we fix  $\gamma$  for a particular video to be fitted to the maximum value of the daily view, share, and tweet count on days 1-10, and (2) start, where we fix  $\gamma$  to the video’s initial daily view, share, and tweet count. The candidate hyperparameters we sweep over are also shown in Table 2. Note that we have different candidate hyperparameters for PCMHP(3, 2) and PCMHP(3, 3), which we selected based on heuristics.

We use days 1-90 to perform hyperparameter tuning and fitting. Specifically, we use

days 1-75 as the training set for hyperparameter selection, and use days 76-90 as the validation set. Once we determine the best-performing hyperparameter set for a video, we refit the model on days 1-90. Lastly, the performance of the tuned model is evaluated on the test set, days 91-120.

**Optimization algorithm.** To optimize  $\mathcal{L}(\Theta; T, \mathbf{w})$  over  $\Theta$ , we use IPOPT, a nonlinear optimization solver for large-scale problems (Wächter & Biegler 2006). The solver requires the gradient of the objective and the Hessian of the Lagrangian. We wrap the procedure in Section 11 as a function to compute the gradient iterately. For the Hessian of the Lagrangian, we use the limited-memory quasi-Newton approximated provided by IPOPT.

## 15.2 Filtering for Dynamic Videos

In our performance evaluation and baseline comparison in Main Text Section IV, we filtered the ACTIVE dataset for YouTube videos that have rich dynamics on days 21–90. We showed that PCMHP(3, 2) performs best on these dynamic videos.

We present here the filtering procedure we implemented to arrive at the evaluation dataset in Main Text Figure 4.

1. Filter ACTIVE for videos that have a mean daily tweet count on days 20-90 of at least 1. This ensures that the videos we consider have minimal activity on days 20-90.
2. Filter for videos that have less than 1000 tweets on days 1-90, as we only fit PCMHP(3, 2) on this set to avoid computational explosion, as discussed in the main text.
3. Compute the standard deviation of the daily view count, daily share count and daily tweet count on days 20-90. Filter for videos that have higher than median standard deviation for each measure.



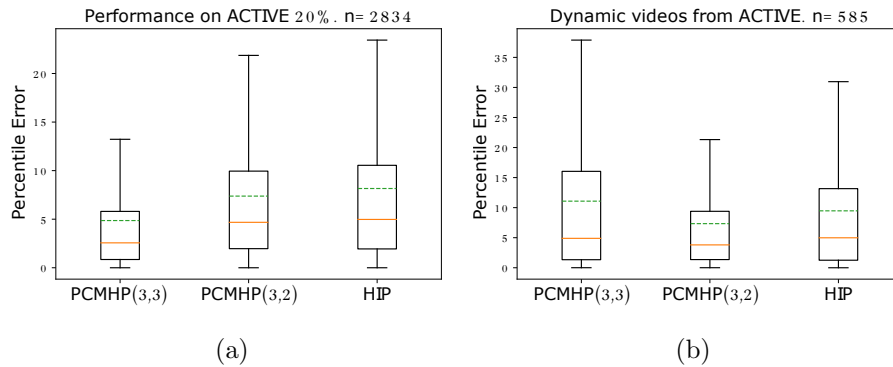


Figure 11: Performance comparison of PCMHP(3,3), PCMHP(3,2) and HIP on (a) a random sample that comprises 20% of the videos in ACTIVE, and (b) the set of dynamic videos from ACTIVE. The dashed line and solid line indicate the mean and median estimates, respectively.

### 15.3 Performance Comparison of PCMHP and HIP

Fig. 11 shows a comparison of the performance of PCMHP(3,3), PCMHP(3,2), and HIP on ACTIVE 20% (Fig. 11a) and DYNAMIC VIDEOS (Fig. 11b).

## 16 Additional Results for Section V

In this section, we (1) elaborate on the goodness-of-fit tests we perform on the model fit of PCMHP(2,1) on the COVID-19 daily case count and news article dataset and (2) present an interpretation of PCMHP-fitted parameters for each country in our global sample.

### 16.1 Goodness-of-Fit Tests

To check model fit of PCMHP(2,1) on the cases-news data in Main Text Section V, we perform separate goodness-of-fit tests for the news dimension and the case dimension. We found that the PCMHP(2,1) fits are statistically significant for 9 out of 11 countries on

the news dimension and 5 out of 11 countries on the cases' dimension. For UK, Italy, and Brazil, the model fits are significant on both dimensions.

Observations in the news dimension are in the form of event timestamps  $t_1^2, \dots, t_{n^2}^2$ , where  $n^2$  is the number of news articles. The time-rescaling theorem (Brown et al. 2002) says that

$$\Xi^2(t_{j+1}^2) - \Xi^2(t_j^2) \sim \text{Exp}(1), \quad (105)$$

where  $j \in 1 \dots n^2 - 1$ . Applying the previous formula on the observed data gives us  $n^2$  samples from  $\text{Exp}(1)$ . Fig. 12 shows the  $Q - Q$  plots for  $\{\Xi^2(t_{j+1}^2) - \Xi^2(t_j^2)\}$ , comparing the samples to the theoretical distribution for  $\text{Exp}(1)$ . We can also use the Kolmogorov-Smirnov (KS) test to check the significance of Eq. (105), which we show in Table 3.

Observations in the case dimension are in the form of daily case counts  $C_1^1, \dots, C_{120}^1$ , corresponding to counts in  $[0, 1), \dots, [119, 120)$ . Under the PCMHP(2, 1) process, the dimension 1 subprocess is a Poisson process, and so

$$C_j^1 \sim \text{Poi}(\Xi^1(j) - \Xi^1(j - 1)). \quad (106)$$

To convert the  $C_j^1$  observations to samples from a single distribution, we use the Anscombe transform (Anscombe 1948). Given  $x \sim \text{Poi}(m)$ , the transformation

$$A : x \rightarrow 2\sqrt{x + \frac{3}{8}} \quad (107)$$

approximately yields standard normal samples:  $A(x) \sim \mathcal{N}\left(2\sqrt{m + \frac{3}{8}}, 1\right)$  given large  $m$ .

Combining Eq. (106) and Eq. (107) then subtracting the Gaussian mean, we see that

$$2\left(\sqrt{C_j^1 + \frac{3}{8}} - \sqrt{\Xi^1(j) - \Xi^1(j - 1) + \frac{3}{8}}\right) \sim \mathcal{N}(0, 1). \quad (108)$$

Fig. 13 shows the  $Q - Q$  plots for  $\{2\left(\sqrt{C_j^1 + \frac{3}{8}} - \sqrt{\Xi^1(j) - \Xi^1(j - 1) + \frac{3}{8}}\right)\}$ , comparing the samples to the theoretical distribution for  $\mathcal{N}(0, 1)$ . We can then apply the Skew-Kurtosis (SK) test for normality to check significance of Eq. (108), which we show in Table 3.

We also introduce a sampling-based score to measure quality of fit of PCMHP(2, 1) to the daily case count. For each day  $j$ , we sample  $N_i$  observations from  $\text{Poi}(\Xi^1(j) - \Xi^1(j-1))$ . We then check whether the actual case count  $C_j^1$  is within the [2.5%, 97.5%] band of the distribution of the  $N_i$  samples. We do this for each day  $j \in 1 \dots 120$  and average the result. In summary, we calculate

$$\frac{1}{120} \sum_{j=1}^{120} \mathbb{I}[C_j^1 \in [2.5\%, 97.5\%] \text{ interval of } \text{Poi}(\Xi^1(j) - \Xi^1(j-1))], \quad (109)$$

The metric is simply the percentage of days where the actual count falls within the interval predicted by the model. The fit scores are tabulated in Table 3.

## 16.2 Interpreting Individual Country Fits

Table 4 contains the PCMHP(2, 1) parameter estimates  $\{\boldsymbol{\theta}, \boldsymbol{\alpha}, \boldsymbol{\gamma}\}$  for each country. Fig. 14 shows the PCMHP(2, 1) fits for UK, USA, Brazil, China, France, Germany, Spain, Sweden, Philippines.

The PCMHP(2, 1) model parameters shown in Table 4 are interpretable. Here, we discuss them in the order  $\theta^{ij}$ ,  $\alpha^{ij}$ , and finally  $\nu^i$ . We treat the parameters as approximations of the corresponding MHP parameters, similar to Main Text Section III.

The parameter  $\theta^{ij}$  encodes the *speed of influence decay from dimension  $j$  to  $i$* . Small values of  $\theta^{ij}$  indicate that  $j$  influences  $i$  over a longer period, whereas large values imply a short half-life of the influence of  $j$  on  $i$ . From Table 4 we see that India has the smallest  $\theta^{11}$  (self-excitement of case numbers), which indicates the slow, consistent progression of COVID in India during the early phase. Brazil has the smallest  $\theta^{12}$  (influence of news on cases); this indicates that Brazil cases did not immediately spike once Brazil made its way into the English-speaking news but instead steadily increased over an extended period. Similar interpretations can be made for  $\theta^{21}$  and  $\theta^{22}$ .

The parameter  $\alpha^{ij}$  measures the *strength of influence from  $j$  to  $i$*  – it captures the expected number of  $i$  events triggered by a single  $j$  event. The multivariate Hawkes process, and consequently the PCMHP process, assumes  $\alpha^{ij} > 0$  for all  $i$  and  $j$ ; this implies that events can only self- or cross-excite other events but not inhibit. This is a modeling assumption that can be relaxed in future work. We can see from Table 4 that Brazil, India, and the Philippines all have  $\alpha^{11} > 1$ , implying that COVID was highly contagious in these countries during the early stage (every infection generated more than one infection in average). We interpret  $\alpha^{12}$  as how strong news preempts an increase in cases. Given that Brazil has the largest  $\alpha^{12}$  in our sample, the news was particularly preemptive of cases there during the early stage. Conversely,  $\alpha^{21}$  measures the expected number of news articles published after a single case. In countries with high  $\alpha^{21}$ , news serves a reactionary role to an increase in cases. Among the countries considered, China has the highest  $\alpha^{21}$ , probably because it was the first country in which COVID-19 has spread at a nation level.

The exogenous parameters  $\nu^1$  and  $\nu^2$  represent the *exogenous rates for cases and news*, respectively. These parameters capture external factors that cannot be accounted by the self- and cross-excitation of cases and news.  $\nu^1$  is a measure of imported cases from other countries, while  $\nu^2$  captures the base level of reporting. India has the highest importation of cases among the countries considered as it has the highest  $\nu^1$ , whereas Brazil, given its high  $\nu^2$ , has the highest base reporting.

We remind our readers that these are English-speaking news (based mostly in English-speaking countries), indicating that Brazil had privileged coverage by news media. We hypothesize that it is probably due to its government’s skepticism of the very existence of COVID-19 in the early days.

## References

- Anscombe, F. J. (1948), ‘THE TRANSFORMATION OF POISSON, BINOMIAL AND NEGATIVE-BINOMIAL DATA’, *Biometrika* **35**(3-4), 246–254.
- Bessy-Roland, Y., Boumezoued, A. & Hillairet, C. (2021), ‘Multivariate Hawkes process for cyber insurance’, *Annals of Actuarial Science* **15**(1), 14–39.
- Brémaud, P. & Massoulié, L. (1996), ‘Stability of nonlinear Hawkes processes’, *The Annals of Probability* **24**(3), 1563 – 1588.
- Brown, E. N., Barbieri, R., Ventura, V., Kass, R. E. & Frank, L. M. (2002), ‘The Time-Rescaling Theorem and Its Application to Neural Spike Train Data Analysis’, *Neural Computation* **14**(2), 325–346.
- Chen, F. & Hall, P. (2013), ‘Inference for a nonstationary self-exciting point process with an application in ultra-high frequency financial data modeling’, *Journal of Applied Probability* **50**(4), 1006–1024.
- Chornoboy, E. S., Schramm, L. P. & Karr, A. F. (1988), ‘Maximum likelihood identification of neural point process systems’, *Biological Cybernetics* **59**(4-5), 265–275.
- Folland, G. B. (1999), *Real analysis: Modern techniques and their applications*, Wiley, New York.
- Guo, X., Hu, A., Xu, R. & Zhang, J. (2018), ‘Consistency and Computation of Regularized MLEs for Multivariate Hawkes Processes’. arXiv:1810.02955 [math, stat].
- Hubbard, J. H. & Hubbard, B. B. (2002), *Vector Calculus, Linear Algebra, and Differential Forms: A Unified Approach*, second edn, Prentice Hall.

- Kamont, Z. (2012), *Hyperbolic functional differential inequalities and applications*, Vol. 486, Springer Science & Business Media.
- Maleknejad, K., Mollapourasl, R. & Mirzaei, P. (2014), ‘Numerical solution of volterra functional integral equation by using cubic b-spline scaling functions’, *Numerical Methods for Partial Differential Equations* **30**(2), 699–722.
- Ogata, Y. (1978), ‘The asymptotic behaviour of maximum likelihood estimators for stationary point processes’, *Annals of the Institute of Statistical Mathematics* **30**(2), 243–261.
- Ogata, Y. (1981), ‘On Lewis’ simulation method for point processes’, *IEEE Transactions on Information Theory* **27**(1), 23–31.
- Ogata, Y. (1988), ‘Statistical Models for Earthquake Occurrences and Residual Analysis for Point Processes’, *Journal of the American Statistical Association* **83**(401), 9–27.
- Pintér, J. D. (1996), *Global Optimization in Action*, Vol. 6 of *Nonconvex Optimization and Its Applications*, Springer US, Boston, MA.
- Rasmussen, J. G. (2018), ‘Lecture Notes: Temporal Point Processes and the Conditional Intensity Function’, *arXiv:1806.00221 [stat]*. arXiv: 1806.00221.
- Rizoiu, M.-A., Soen, A., Li, S., Calderon, P., Dong, L., Menon, A. K. & Xie, L. (2022), ‘Interval-censored Hawkes processes’, *Journal of Machine Learning Research* **23**(338), 1–84.
- Rizoiu, M. A., Xie, L., Sanner, S., Cebrian, M., Yu, H. & Van Henteryck, P. (2017), ‘Expecting to be HIP: Hawkes intensity processes for social media popularity’, *26th International World Wide Web Conference, WWW 2017* pp. 735–744.

Wächter, A. & Biegler, L. T. (2006), ‘On the implementation of an interior-point filter line-search algorithm for large-scale nonlinear programming’, *Mathematical Programming* **106**(1), 25–57.

Xie, H., Zhang, R. & Brunner, H. (2011), ‘Collocation methods for general volterra functional integral equations with vanishing delays’, *SIAM Journal on Scientific Computing* **33**(6), 3303–3332.

---

**Algorithm 1:** Simulating a  $d$ -dimensional Hawkes Process on  $[0, T)$  with Thinning(Ogata 1981)

---

**Input:** kernel matrix  $\varphi(t)$ , background intensity  $\boldsymbol{\mu}$ , time horizon  $T > 0$ **Output:**  $\mathcal{H}_T^j = \{t_k^j\}$  for  $j = 1 : d$ **initialize**  $t = 0; \mathcal{H}_T^1 = \dots = \mathcal{H}_T^d = \emptyset;$ **while**  $t < T$  **do**

$$\bar{\lambda} = \sum_{i=1}^d \lambda^m(t^+) = \sum_{i=1}^d \left[ \mu^i + \sum_{j=1}^d \sum_{t_k^j \leq t} \varphi^{ij}(t - t_k^j) \right];$$

 $u \sim \text{uniform}(0, 1);$ 

$$w = -\log \frac{u}{\bar{\lambda}};$$

$$t = t + w;$$

 $U \sim \text{uniform}(0, 1);$ **if**  $U\bar{\lambda} \leq \sum_{i=1}^d \lambda^m(t)$  **then**

$$j = 1;$$

**while**  $U\bar{\lambda} \leq \sum_{i=1}^j \lambda^m(t)$  **do**

$$j = j + 1;$$

**end**

$$t_k^j = t;$$

$$\mathcal{H}_T^j = \mathcal{H}_T^j \cup \{t_k^j\};$$

**end****end****if**  $t_{k^j}^j < T$  **then****return**  $\mathcal{H}_T^j$  for  $j = 1 : d;$ **else****return**  $\mathcal{H}_T^1, \dots, \mathcal{H}_T^j \setminus \{t_k^j\}, \dots, \mathcal{H}_T^d;$ **end**

---



---

**Algorithm 2:** Approximation of  $\xi_E(t)$  by Discrete Convolution and Infinite Series

---

Truncation

---

**Input:** kernel  $\varphi(t)$ , kernel integral  $\Phi(t)$  exogenous input function  $\mu(t)$ , partition

$\mathcal{P}[0, T] = [0 : T]$  with increment  $\Delta^{\mathcal{P}} > 0$ , observed  $E^c$  data points in  $[0, T)$

$\{\mathcal{H}_T^j = \{t_k^j\} \mid j \in E^c, t_k^j < T\}$ , threshold  $\gamma^h > 0$

**Output:**  $\xi_E[0 : T]$

**initialize**  $P = \frac{T}{\Delta^{\mathcal{P}}}$ ;

$\xi_E[0 : T] = \mathbf{a}[0 : T] = \mathbf{0}^{d \times (P+1)}$ ;  $\mathbf{h}_E[0 : T] = \mathbf{\Delta}[0 : T] = \varphi_E[0 : T]$ ;

**do**

$\mathbf{\Delta}[0 : T] = \text{conv}(\mathbf{\Delta}, \varphi_E, [0 : T])$ ;

$\mathbf{h}_E[0 : T] = \mathbf{h}_E[0 : T] + \mathbf{\Delta}[0 : T]$ ;

**while**  $\max_{p=0:P} (\|\mathbf{\Delta}[t_p]\|_{\max}) \geq \gamma^h$ ;

$\mathbf{H}_E[0 : T] = \Phi[0 : T] + \text{conv}(\mathbf{h}_E, \Phi, [0 : T])$ ;

**for**  $j \in E^c$  **do**

**for**  $t_k^j \in \mathcal{H}_t^j$  **do**

**for**  $t_p \in [0 : T]$  **do**

**if**  $t_k^j < t_p$  **then**

$\mathbf{a}[t_p] = \mathbf{a}[t_p] + \varphi_{E^c}^j(t_p - t_k^j)$ ;

**end**

**end**

**end**

**end**

$\xi_E[0 : T] = \mu[0 : T] + \mathbf{a}[0 : T] + \text{conv}(\mathbf{h}_E, \mu + \mathbf{a}, [0 : T])$ ;

**return**  $\xi_E[0 : T]$

---

---

### Algorithm 4: Computing the Negative Log Likelihood of a Partial MBP Process

---

**Input:** kernel matrix  $\varphi(t)$ , kernel integral matrix  $\Phi(t)$ , exogenous input function  $\mu(t)$ , exogenous input integral  $\mathbf{S}(t)$ , points-of-interest set  $\tilde{\mathcal{T}} = \{(t_i, (r_j, d_j))\} = \mathcal{T} \cup \left(\bigcup_{j \in E} \mathcal{O}^j\right) \cup \mathcal{P}$ , censored counts  $\{C_k^j\}$  for  $j \in E$ , threshold  $\gamma^h > 0$

**Output:** NLL, the negative log likelihood of the partial MBP process

**initialize**  $\mathbf{h}_E[t_0 : t_P] = \mathbf{0}^{d \times d \times (P+1)}$ ;  $\Delta[t_0 : t_P] = \varphi_E[t_0 : t_P]$ ;  $\mathbf{a}[t_0 : t_{|\tilde{\mathcal{T}}|}] = \mathbf{A}[t_0 : t_{|\tilde{\mathcal{T}}|}] = \mathbf{0}^{d \times (|\tilde{\mathcal{T}}|+1)}$ ;  $\tilde{\mathbf{H}}_E[t_0 : t_{|\tilde{\mathcal{T}}|+1}] = \mathbf{0}^{d \times d \times (|\tilde{\mathcal{T}}|+1)}$ ;  $l^j = 0$ ,  $\omega^j = \mathbf{0}^{|\mathcal{O}^j| \forall j \in E}$ ; PPLL = ICLL = 0;

**do**

- $\Delta[t_0 : t_P] = \text{conv}(\Delta, \varphi_E, [t_0 : t_P])$ ;
- $\mathbf{h}_E[t_0 : t_P] = \mathbf{h}_E[t_0 : t_P] + \Delta[t_0 : t_P]$ ;

**while**  $\max_{p=0:P} (\|\Delta[t_p]\|_{\max}) \geq \gamma^h$ ;

$\mathbf{H}_E[t_0 : t_P] = \Phi[t_0 : t_P] + \text{conv}(\mathbf{h}_E, \Phi, [t_0 : t_P])$ ;

**for**  $k = 0 : |\tilde{\mathcal{T}}|$  **do**

- for**  $j \in E^c$  **do**
  - for**  $t_l \in \mathcal{H}_{t_k}^j$  **do**
    - $\mathbf{a}[t_k] = \mathbf{a}[t_k] + \varphi_{E^c}^j(t_k - t_l)$ ;
    - $\mathbf{A}[t_k] = \mathbf{A}[t_k] + \Phi_{E^c}^j(t_k - t_l)$ ;
  - end**
- end**
- for**  $r_j, d_j \in C_k$  **do**
  - if**  $r_j = ts$  **then**
    - $\xi_E = \mu(t_k) + \mathbf{a}[t_k]$ ;
    - if**  $|E| \neq 0$  **and**  $k \neq 0$  **then**
      - $\xi_E = \xi_E + \text{conv}(\mathbf{h}_E, \mu + \mathbf{a}, [t_0 : t_k])$ ;
    - end**
    - PPLL = PPLL +  $\log \xi_E^{d_j}$
  - end**
  - if**  $r_j = o$  **then**
    - $\Xi_E = \mathbf{S}(t_k) + \mathbf{A}[t_k]$ ;
    - if**  $|E| \neq 0$  **and**  $k \neq 0$  **then**
      - $\Xi_E = \Xi_E + \text{conv}(\mathbf{h}_E, \mathbf{S} + \mathbf{A}, [t_0 : t_k])$ ;
    - end**
    - $\omega^j[l] = \Xi_E^{d_j}$ ;
    - $l^j = l^j + 1$ ;
  - end**
- end**
- if**  $k = |\tilde{\mathcal{T}}|$  **then**
  - $\Xi_E = \Xi_E + \text{conv}(\mathbf{h}_E, \mathbf{S} + \mathbf{A}, [t_0 : t_k])$ ;
  - for**  $j \in E^c$  **do**
    - PPLL = PPLL -  $\Xi_E^j$ ;
  - end**
- end**

**end**

**for**  $j \in E$  **do**

- $\text{diff}[1 : |\mathcal{O}^j|] = \omega^j[1 : |\mathcal{O}^j|] - \omega^j[0 : |\mathcal{O}^j| - 1]$ ;
- ICLL = ICLL +  $\sum_{k=1}^{|\mathcal{O}^j|} (C_k^j \cdot \log \text{diff}[k] - \text{diff}[k])$ ;

**end**

NLL =  $-(\text{PPLL} + \text{ICLL})$ ;

**return** NLL

---

Table 1: Hawkes spectral radii and model parameters used in the parameter recovery synthetic experiment. We fix the initial impulse parameters  $\gamma^0 = \gamma^1 = 0$  in our simulations.

$\rho(\boldsymbol{\alpha})$	$\theta^{11}$	$\theta^{12}$	$\theta^{21}$	$\theta^{22}$	$\alpha^{11}$	$\alpha^{12}$	$\alpha^{21}$	$\alpha^{22}$	$\nu^1$	$\nu^2$
0.5	1.0	0.5	1.25	0.75	0.25	0.3	0.12	0.35	0.1	0.1
0.75	1.0	0.5	1.25	0.75	0.32	0.5	0.3	0.4	0.1	0.1
0.9	1.0	0.5	1.25	0.75	0.4	0.5	0.3	0.6	0.1	0.1

Table 2: Hyperparameters of the PCMHP( $d, e$ ) models considered in the YouTube popularity prediction experiment

Hyperparameter	Description	( $d, e$ ): Values
$w^1 \dots w^d$	dimension weights in $\mathcal{L}(\boldsymbol{\Theta}; T, \mathbf{w})$	(3, 3) : {[1000, 1, 1]} (3, 2) : {[1, 1, 1], [1, 1, 1000]}
$w^\nu$	weight of the $\ \boldsymbol{\nu}\ _1$ term in $\mathcal{L}(\boldsymbol{\Theta}; T, \mathbf{w})$	(3, 3) : {10, 1000} (3, 2) : {1000}
$\gamma^{init}$	value of exogenous impulse at $t = 0$	{max, start}

Table 3: Goodness-of-fit measures on the PCMHP(2, 1) models fitted on the COVID-19 daily case count and news article timestamp dataset.

Country	News KS p-value	Cases SK p-value	Cases Fit Score
UK	<b>0.47</b>	<b>0.09</b>	0.60
USA	0.04	<b>0.33</b>	0.48
Brazil	<b>0.18</b>	<b>0.22</b>	0.79
China	<b>0.17</b>	0	0.60
France	<b>0.33</b>	0	0.51
Germany	<b>0.99</b>	0	0.36
India	0	<b>0.09</b>	0.97
Italy	<b>0.09</b>	<b>0.24</b>	0.61
Spain	<b>0.15</b>	0.04	0.28
Sweden	<b>0.24</b>	0	0.72
Philippines	<b>0.96</b>	0	0.73

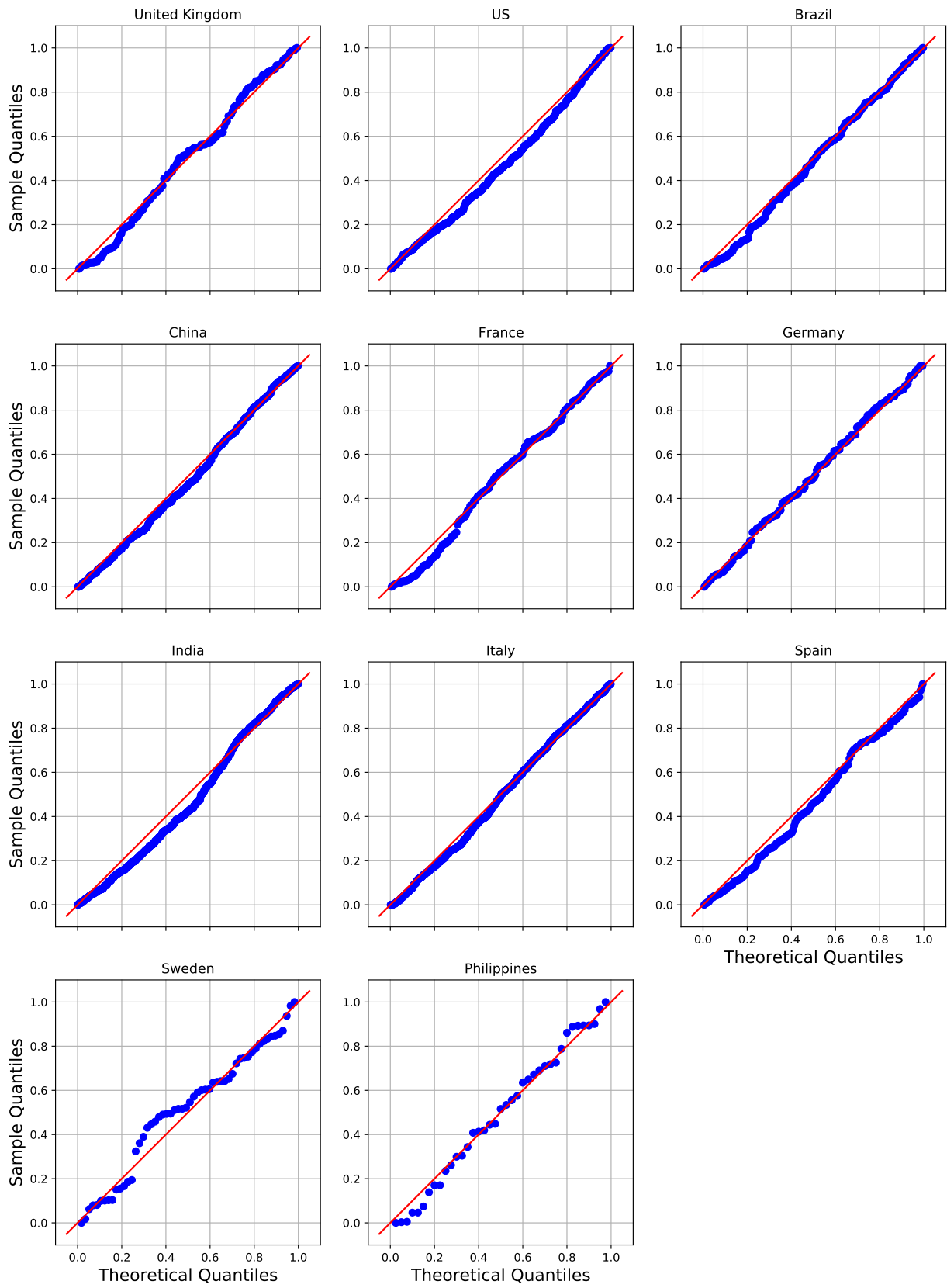


Figure 12: Q-Q plots for observations in the news dimension in the COVID-19 country PCMH $P(2, 1)$  fits

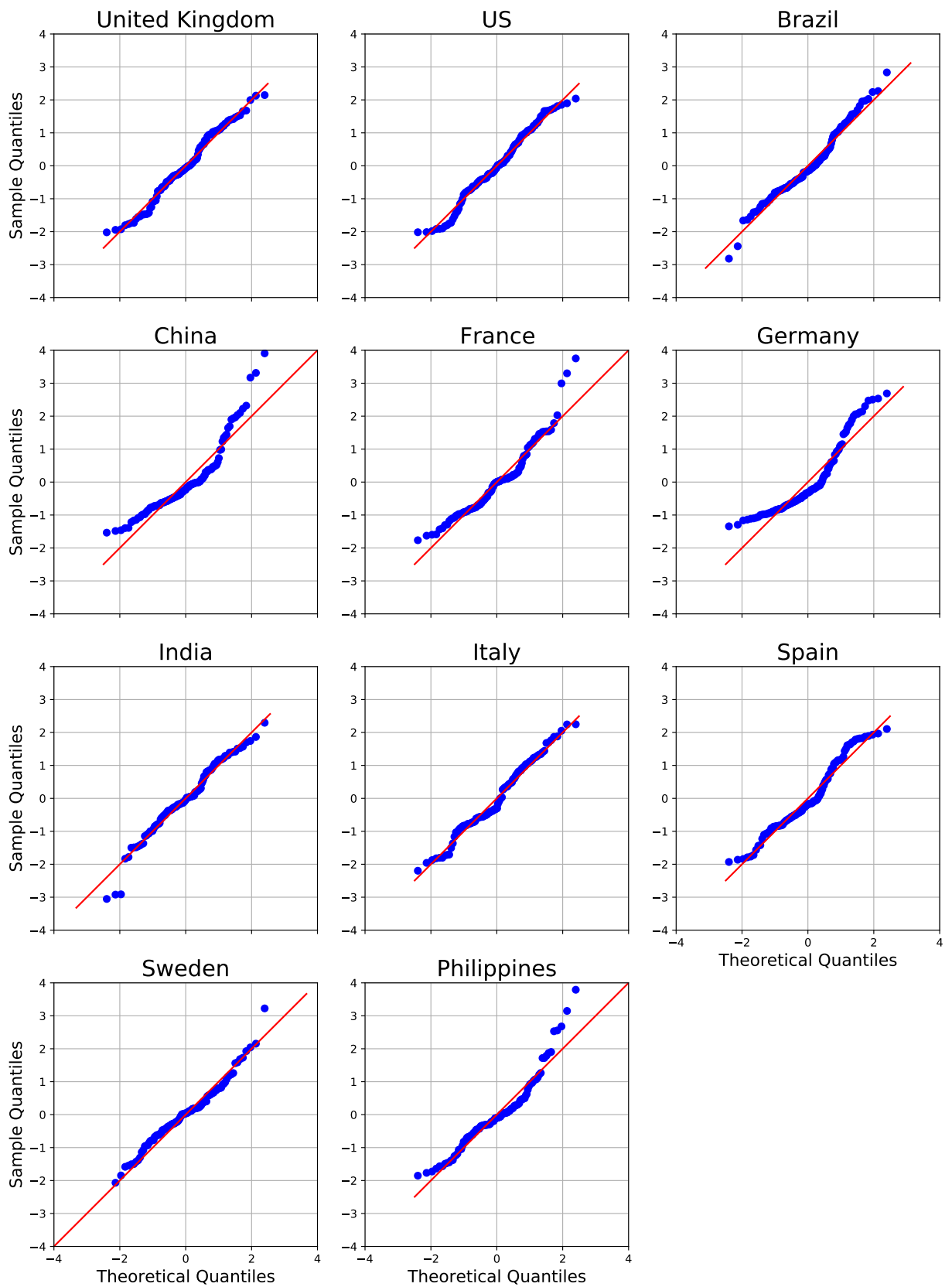


Figure 13: Q-Q plots for observations in the cases dimension in the COVID-19 country PCMHP(2, 1) fits.

Table 4: Parameters of the PCMHP(2, 1) models fitted on daily COVID-19 case counts and COVID-19 news article timestamps for the 11 countries we consider.

Country	$\theta^{11}$	$\theta^{12}$	$\theta^{21}$	$\theta^{22}$	$\alpha^{11}$	$\alpha^{12}$	$\alpha^{21}$	$\alpha^{22}$	$\nu^1$	$\nu^2$
UK	0.89	0.11	1.84	1.98	0.89	145.27	0.0004	0.29	1.99	0.36
USA	0.76	0.03	0.88	0.44	0.93	419.8	0	0.71	0.0054	0.85
Brazil	0.13	0.01	1.89	2.46	1.08	2198.7	0	0.38	0.24	1.47
China	0.93	4	1.39	4	0.59	0.1	0.012	0.39	0.0001	0.02
France	0.31	4	2.01	3.1	0.77	86.89	0.0015	0.38	0.025	0.07
Germany	0.98	0.18	2.05	1.9	0.75	247.16	0.0005	0.36	1.75	0.3
India	0.06	2.02	1.98	1.82	1.6	8.75	0	0.76	28.52	1.14
Italy	0.79	0.08	1.95	2.21	0.88	38.55	0.0002	0.91	0.11	0.62
Spain	0.4	0.08	1.57	1.62	0.73	316.27	0.0001	0.61	2.69	0.19
Sweden	0.48	0.53	2	1.89	0.98	2.13	0.0005	0.32	11.11	0.28
Philippines	0.18	2.54	2.31	1.94	1.11	14.6	0	0.4	0.04	0.19

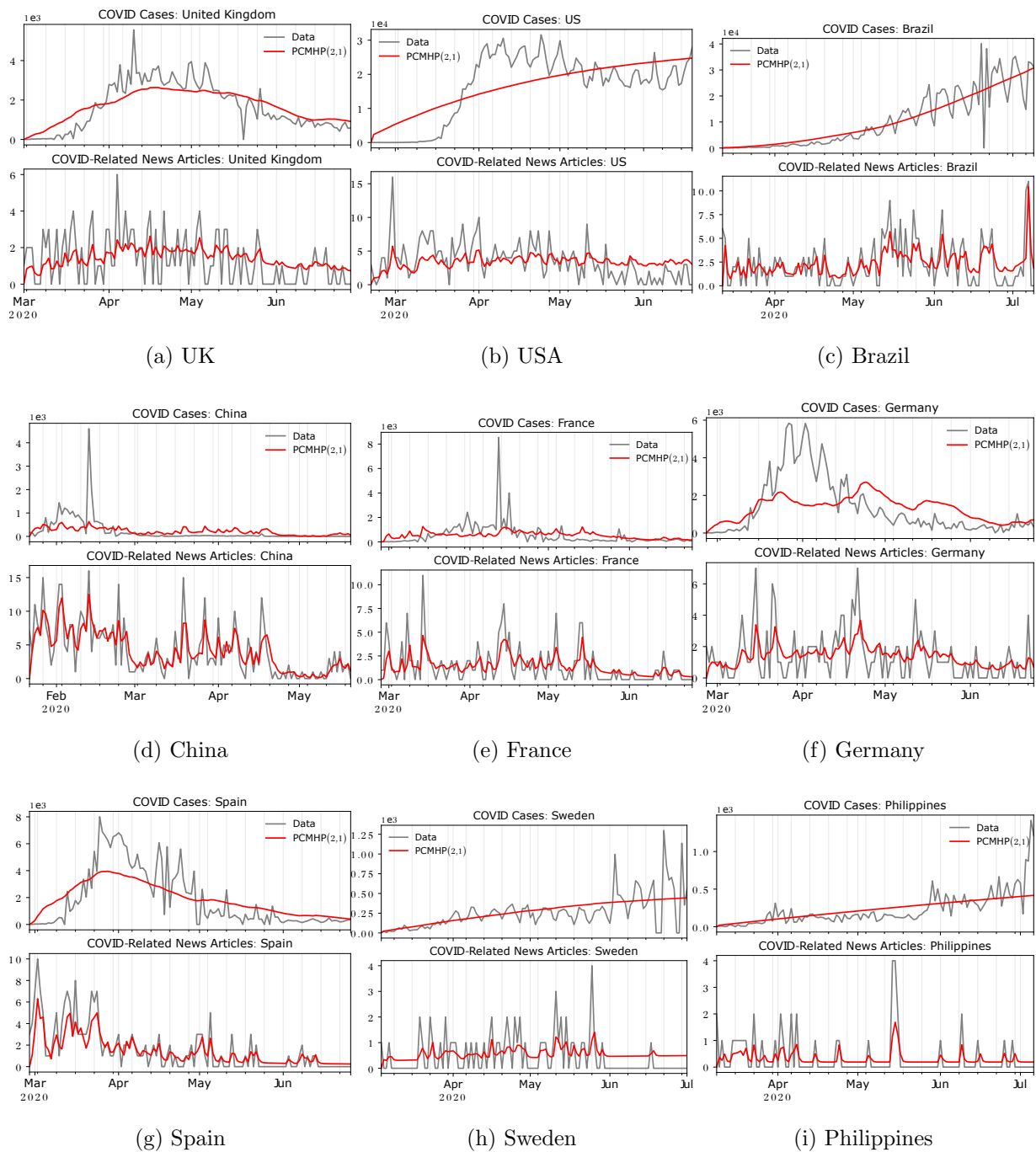


Figure 14: Fit of the PCMHP(2,1) model on the daily COVID-19 case count and COVID-19-related news articles, for the other countries in the global sample.